Electrophysiological Characterization of Mesenchymal Stem Cells Differentiating into Tenocytes via Dielectrophoresis

A Thesis
Presented in Partial Fulfillment of the Requirements for the
Degree of Master of Science
with a
Major in Chemical Engineering
in the
College of Graduate Studies
University of Idaho
by
Anthony Tushar Giduthuri

Major Professor: Soumya K. Srivastava, Ph.D.
Committee Members: D. Eric Aston, Ph.D.; Matthew Bernards, Ph.D.; Nathan R. Schiele, Ph.D.
Department Administrator: Ching-An Peng, Ph.D.

August 2020

Authorization to Submit Thesis

This thesis of Anthony Tushar Giduthuri, submitted for the degree of Master of Science with a Major in Chemical Engineering and titled "Electrophysiological Characterization of Mesenchymal Stem Cells Differentiating into Tenocytes via Dielectrophoresis," has been reviewed in final form. Permission, as indicated by the signatures and dates below, is now granted to submit final copies to the College of Graduate Studies for approval.

Major Professor: _____ Date: _____
Soumya K. Srivastava, Ph.D.

Committee Members: _____ Date: _____
D. Eric Aston, Ph.D.

_____ Date: _____
Matthew Bernards, Ph.D.

_____ Date: _____
Nathan R. Schiele, Ph.D.

Department Administrator: _____ Date: _____
Ching-An Peng, Ph.D.

Abstract

Tenocytes or tendon cells are the primary cells of a tendon that are responsible for holding a muscle and a bone and are found throughout the body from head to the feet at several muscle bone joints such as collar bone, hip joint, knee, etc. It is also a major component of the musculoskeletal system. Tendons are susceptible to injuries such as tendinitis, tendon rupture due to the effects of aging and stress. Stem cell based therapies offer alternative methods to treat such conditions. Among various types of stem cells, mesenchymal stem cells (MSCs), a type of multipotent stem cell, are known for their ability to regenerate and differentiate to tendon lineages. Undifferentiated MSCs derived from the bone marrow of a mouse, are characterized to obtain dielectric properties (i.e., conductivity and permittivity) of their outer membrane and cytoplasm using the dielectrophoretic crossover frequency technique. Undifferentiated MSCs are then treated with growth factors to induce differentiation (tenogenesis) into tenocytes and are dielectrically characterized at several time points. In this thesis, we chose to explore the day-3 time point of differentiation to detect changes in the membrane and cytoplasm along with undifferentiated cells aged to day-3 as control samples. Experimental results are statistically analyzed for their reproducibility and are modeled using a single shell model to quantify the dielectric properties.

It is observed that the electrical nature of the cells significantly varied through their course of differentiation, which will be utilized to serve as a label-free biomarker for sorting the differentiated MSCs from the undifferentiated ones. Sorted differentiated cells can then be used in stem cell based therapy without resulting in post-treatment complications such as tumors. The designed stem cell sorter via dielectrophoresis (DEP) in a label-free way avoids complications involved in the current separation techniques such as FACS and MACS.

Acknowledgements

I cannot thank my Major Professor, Dr. Soumya K. Srivastava enough for her immense efforts in mentoring, shaping, laying the foundation for this project, and for her profound belief in my ability. Her unwavering support throughout the project was commendable. I am grateful to the entire MESA lab research group, Courtney Molvig, Sahara Waymire, Sierra Knowles, Kendall Reeder, Rebecca Kelley, for their contribution in helping to accomplish this thesis. Special thanks to Dr. Eric Aston, Dr. Matthew Bernards, and Dr. Nathan Schiele for taking their time and supporting me by serving as my committee members. I want to thank my co-graduate students Sophia K. Theodossiou and Jonathan Counts, for helping me at various levels. My special thanks to Sophia K. Theodossiou for her relentlessly working with me and providing guidance and stem cells required to succeed in this research. Completing my thesis would not have been possible without the support Dr. Ezekiel O. Adekanmbi, an alumnus of the MESA group, for his guidance and support since I began my graduate studies at UI and for constantly providing valuable insights through conversation.

I am indebted to Dr. Eric Aston, who supported me in every way possible in accomplishing this thesis work, especially providing access to his Olympus IX71 Inverted microscope for carrying out the experiments in this thesis.

I wish to express my gratitude to Gail Bergman, Margaret Baker, and Dr. Dave MacPherson for being available all the time to address every need since 2018.

Additionally, I would like to thank Dr. Suat U. Ay, Professor in Electrical Engineering at the University of Idaho, for lending the high-frequency generator, without which this work would not have been accomplished.

I am grateful to the National Science Foundation for providing the fund [NSF/CBET #1500815] to execute the projects reported in this thesis over summer 2019, IDeA Network of Biomedical Research Excellence (INBRE) and Graduate and Professional Student Association (GPSA) for awarding travel grants to present the research work at various conferences across the country at different stages of this thesis work.

Dedication

I dedicate this work to my maternal grandmother and her siblings for their immense commitment and work in the field of education, who inspired most of my family members to be teachers.

Table of Contents

List of Tables

List of Figures

Statement of Contribution

Chapters 3 and 4 are collaborative efforts of Drs. Soumya K. Srivastava and Nathan Schiele and authored by me and Sophia K. Theodossiou, who contributed in getting the chapter revised to be submitted as an article for publishing.

_____

Nathan R. Schiele, Ph.D.

Chapter 5 is a collaborative effort of Drs. Soumya K. Srivastava and James Moberly that is currently under review in the *Electrophoresis* Journal.

_____

James G. Moberly, Ph.D.

Chapter 1: Introduction

1.1 Background of stem-cell research

Stem cell based therapies offer a promising cure for several injuries such as cardiovascular diseases, musculoskeletal disorders, retinal disorders, and autoimmune diseases [1]. Stem cell research is of great interest due to their characteristic of inducing repair of damaged tissue in regenerative medicine and also towards aiding in wound healing, cell therapy, and drug therapies, along with their ability to differentiate into different cell types which finally form into a mature cell thereby resulting in the formation of its respective organ [2]. Out of various types of stem cells available, Mesenchymal stem cells (MSCs), which are multipotent, have the ability to develop into specific cell types closely related to their lineage [3]. Several researchers in the biomedical field study these due to their self-renewal property.

As the stem cells are cultured and differentiated artificially, it is essential to make sure prior to use in a clinical setting, that the cell culture is viable, fully differentiated [4, 5], and does not have any non-viable cell mass to ensure no complications, such as tumors, arise post-treatment [4, 6]. Current challenges to clinically utilize the sorted differentiated stem cells by commercially available cell sorter systems such as fluorescent activated cell sorting (FACS) [7] and magnetic activated cell sorting [8] is that the cell preparation is tedious [2], requires expensive raw materials and is labor intensive [9]. These processes also involve labeling of cells, which alters cellular function [9].

This thesis focuses on characterizing differentiating MSCs into tenocytes over the course of time via an electrokinetic technique, called Dielectrophoresis (DEP). Subsequently, fully developed tenocytes can be potentially used to treat tendon injuries such as tendonitis and tendon tears, which are very common in athletes and older population. The use of developed tendon cells for treating injuries will substantially decrease the healing time in contrast to self-healing or other methods [10, 11].

Dielectrophoresis is a simple, powerful technique and effective in terms of cost and detecting subtle changes in the cells caused due to the physiological changes induced on the membrane and cytoplasm. There is a lack of a proper technique that can identify and sort cells without the need for tagging or labeling cells. DEP was first introduced by Herbert A. Pohl in the 1960's to separate live and dead cells [12, 13]. Over time, in the past fifty years since its inception, DEP has emerged as a powerful cell separation technique [14]. Hence DEP is an appropriate technique to be implemented in the current scenario to address the challenges.

Microfluidics is a multidisciplinary field combining engineering, physics, chemistry, and microscale dimensions with practical applications designed to handle small volumes ranging from 10^{-9} to 10^{-18} liters. Microfluidics has several advantages: the ability to use a minimal volume of regents, less sample volume, highly effective and sensitive, low cost, and short times ranging from seconds to minutes [15] based on the application of analysis on a miniaturized device. Microfluidics became popular and emerged [15] as an interdisciplinary field combining with other sciences. Microfluidics, when combined with DEP, evolves as a powerful microfluidic technique with advantages such as high-throughput, efficient yet economical, which can be applied for various applications such as isolation, enrichment, trapping, separation, characterization, and several other biological applications. The primary focus of this thesis is to characterize MSCs for the changes associated with membrane and cell's interior on differentiation into tenocytes using DEP and microfluidics.

1.2 Research goal and objectives

The principle goal of this thesis is to characterize the mesenchymal stem cells for their electrophysiological properties on their course of differentiation to tenocytes, primary cells of a tendon using dielectrophoresis, which will subsequently lead into designing a high throughput, economical, and efficient sorter to separate the differentiating tenocytes and the undifferentiated MSCs. The objectives are listed below**:**

Objective 1: Characterizing the dielectric behavioral changes associated with the membrane of both the primary bone marrow derived MSCs and the tenogenesis induced MSCs.

Objective 2: Characterizing the intracellular (cytoplasm) changes in terms of their electrophysiology of both the primary bone marrow derived MSCs and the tenogenesis induced MSCs.

Objective 3: Simulate and design an efficient DEP aided microfluidic sorter to sort cells in a label freeway.

1.3 Thesis layout

This thesis is divided into five chapters. Chapter 1 introduces the motivation behind the current research study and how DEP emerged as a promising technique. Chapter 2 discusses the theory behind DEP. Often many novice researchers confuse with the terms: electrophoresis and Dielectrophoresis, hence a brief discussion comparing them is included as well. Chapter 3 is a detailed literature review based on previously published research and review pertaining to stem cell research using DEP. Chapter

4 focuses on characterizing MSCs and their differentiated progeny (tenocytes) using DEP and results associated with objectives 1 and 2, by using dielectric parameters as label free cell markers. Chapter 5 focuses on developing a stem-cell sorter, based on previous work through modeling and simulation using COMSOL 5.5a based on the dielectric parameters of *Cupriavidus necato*r determined through experiments. Though simulation presented in Chapter 5 does not employ the dielectric properties of MSCs, this chapter serves as a model in achieving a final optimized device design for sorting, thereby validating the simulated device platform. Finally, this thesis concludes with Chapter 6, illustrating the challenges related to experimenting with mesenchymal stem cells in particular related to their heterogeneity and sampling time. This chapter also provides a brief discussion of the future direction of applying DEP in a clinical setting to use stem cells for regenerative medicine.

References

[1] K. Nawab, D. Bhere, A. Bommarito, M. Mufti, and A. Naeem, "Stem Cell Therapies: A Way to Promising Cures," (in eng), *Cureus,* vol. 11, no. 9, p. e5712, Sep 20 2019, doi: 10.7759/cureus.5712.

[2] N. Abd Rahman, F. Ibrahim, and B. Yafouz, "Dielectrophoresis for Biomedical Sciences Applications: A Review," *Sensors (Basel),* vol. 17, no. 3, 2017/02/24/ 2017, doi: 10.3390/s17030449.

[3] S. B. Hima Bindu A, "Potency of Various Types of Stem Cells and their Transplantation " *Journal of Stem Cell Research & Therapy* vol. 1, no. 3, p. 115, 2011.

[4] N. A. Willoughby *et al.*, "A scalable label-free approach to separate human pluripotent cells from differentiated derivatives," *Biomicrofluidics,* vol. 10, no. 1, p. 014107, 2016, doi: 10.1063/1.4939946.

[5] N. S. Hwang, S. Varghese, and J. Elisseeff, "Controlled differentiation of stem cells," (in eng), *Adv Drug Deliv Rev,* vol. 60, no. 2, pp. 199-214, 2008, doi: 10.1016/j.addr.2007.08.036.

[6] S. Ikehara, "Grand challenges in stem cell treatments," (in eng), *Front Cell Dev Biol,* vol. 1, pp. 2-2, 2013, doi: 10.3389/fcell.2013.00002.

[7] Z. Hewitt, N. R. Forsyth, M. Waterfall, D. Wojtacha, A. J. Thomson, and J. McWhir, "Fluorescence-activated single cell sorting of human embryonic stem cells," (in eng), *Cloning Stem Cells,* vol. 8, no. 3, pp. 225-34, Fall 2006, doi: 10.1089/clo.2006.8.225.

[8] P. Korkusuz, S. Köse, N. Yersal, and S. Önen, "Magnetic-Based Cell Isolation Technique for the Selection of Stem Cells," (in eng), *Methods Mol Biol,* vol. 1879, pp. 153-163, 2019, doi: 10.1007/7651_2018_151.

[9] T. N. G. Adams, P. A. Turner, A. V. Janorkar, F. Zhao, and A. R. Minerick, "Characterizing the dielectric properties of human mesenchymal stem cells and the effects of charged elastin-like polypeptide copolymer treatment," (in eng), *Biomicrofluidics,* vol. 8, no. 5, p. 054109, 2014/09// 2014, doi: 10.1063/1.4895756.

[10] S. Thomopoulos, W. C. Parks, D. B. Rifkin, and K. A. Derwin, "Mechanisms of tendon injury and repair," *J Orthop Res,* vol. 33, no. 6, pp. 832-839, 2015.

[11] F. Wu, M. Nerlich, and D. Docheva, "Tendon injuries: Basic science and new repair proposals," (in eng), *EFORT Open Rev,* vol. 2, no. 7, pp. 332-342, Jul 2017, doi: 10.1302/2058-5241.2.160075.

[12] H. A. Pohl, "The Motion and Precipitation of Suspensoids in Divergent Electric Fields," *Journal of Applied Physics,* vol. 22, no. 7, pp. 869-871, 1951/07/01/ 1951, doi: 10.1063/1.1700065.

[13] H. A. Pohl and I. Hawk, "Separation of Living and Dead Cells by Dielectrophoresis," (in en), *Science,* vol. 152, no. 3722, pp. 647-649, 1966/04/29/ 1966, doi: 10.1126/science.152.3722.647-a.

[14] M. P. Hughes, "Fifty years of dielectrophoretic cell separation technology," *Biomicrofluidics,* vol. 10, no. 3, 2016/06/30/ 2016, doi: 10.1063/1.4954841.

[15] D. Mark, S. Haeberle, G. Roth, F. von Stetten, and R. Zengerle, "Microfluidic lab-on-a-chip platforms: requirements, characteristics and applications," *Chemical Society Reviews,* 10.1039/B820557B vol. 39, no. 3, pp. 1153-1182, 2010, doi: 10.1039/B820557B.

Chapter 2: Theory of Dielectrophoresis

2.1 Introduction

Biological cells when subjected to AC or DC electric currents, respond with a distinct electrical stimulus, which is classified to be passive and active electrical response [1].

a) Passive electrical response

Passive electrical response is produced when an electric current is forced across a biological membrane due to the virtue of the membrane's dielectric properties, such as capacitance and conductance.

b) Active electrical response

Active electrical response often termed as membrane excitation, is found in excitable tissues such as nerve, muscles, and sensory receptors that occur as a result of the response to a stimulus.

DEP can be applied using alternating current (AC) or direct current (DC) [3] to analyze and separate cells by estimating the passive electrical properties of cells[4]. From the AC response, dielectric properties such as capacitance, cell's ability to store electrical energy; permittivity, cell's ability to resist electrical field; and conductance, cell's ability to conduct electric current can be quantified [5]. From the cells' response under DC, electrokinetic mobility of cells can be quantified, which is a key deterministic property to detect subtle changes in cells [6]. DC based DEP, also known as insulator DEP (iDEP) is commonly achieved using external electrodes, while non-uniformity in introduced through insulating hurdles and obstacles within the channel, the reason for the need of non-uniformity is discussed in the next paragraph. Since external electrodes are employed, DC-DEP needs high voltages to generate sufficient DEP force that may lead to Joule heating within the channel, disturbing the functioning of cells and affecting the cell's viability [7]. DC-DEP is preferred with applications pertaining to cell sorting due to advantages such as avoiding metal electrodes within channel, thus no chance of electrode fouling [8]. DC-DEP is also known to induce electrokinetic particle transport while simultaneously performing DEP based separation [8], unlike AC-DEP, where pressure driven flow is necessary to transport particles within the channel. Recently DC-DEP is being exploited in applications pertaining to characterization [6]. This thesis employs usage of the AC electric field to characterize biological cells (mammalian) to obtain dielectric properties relating to their physiology.

DEP is a phenomenon that describes the force acting on the particles suspended in a medium subjected to non-uniform electric field. The force experienced is based on the polarizability between the particles and the suspending medium [9, 10].

In the case of a uniform electric field, the force experienced by the particles results in motion based on the polarity of the applied electric field and the charges carried by the particle. This phenomenon of particle motion in the uniform electric current (usually DC) is termed as electrophoresis (EP) [11]. Since uniform electric field is applied, the net force experienced by the particle is zero, and the motion of particles is purely due to the charges possessed, signified by electrophoretic mobility. Thus, particles need to possess a charge to be manipulated by a uniform DC electric field.

However, in the case of DEP, it is based on the polarization of the particles due to the non-uniform electric field and does not require the particles to be charged. Hence non-uniformity is a primary characteristic [1], which is introduced using electrodes, such as the pin and plate electrode setup, as shown in Figure 2.1. As AC is frequency dependent, the DEP force experienced by the particles varies based on the intrinsic electrical properties of the particle and the frequency of the applied field. At a particular frequency, when the polarizability of the particle is greater than the suspending medium, the particles experience force termed as positive dielectrophoresis (pDEP), leading to the movement of the particle towards the high electric field and when the polarizability of the particle is less than the suspending medium, particles experience a force termed as negative dielectrophoresis (nDEP), leading to movement of particles away from the high electric field. As the frequency is tuned, the net DEP force experienced is altered, switching the particle's behavior from nDEP to pDEP at a specific frequency, termed as crossover frequency, which can be used to dielectrically characterize particles. At the crossover frequency point, the polarizability of the medium and the particles are equal, and hence the particles do not experience any DEP force, causing no motion of the particles [2].

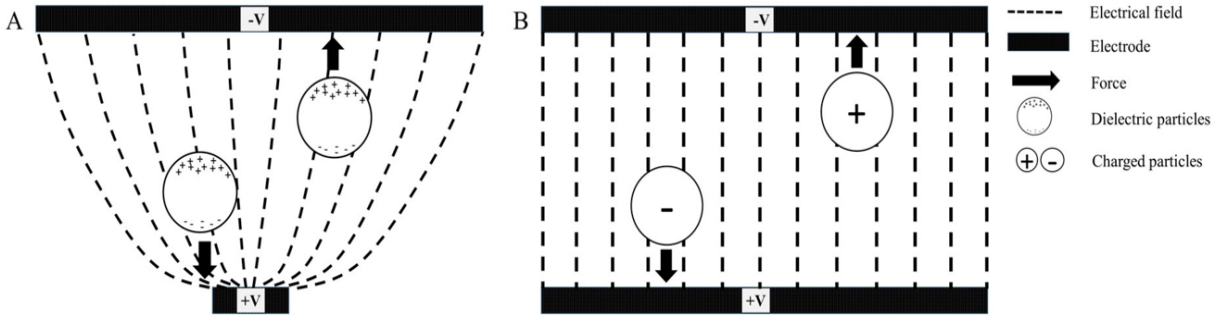

Figure 2.1: Diagram describing dielectrophoresis (DEP) and electrophoresis (EP). A) illustrates DEP where particles experience pDEP and nDEP, i.e., particles travel towards high electric field (pin electrode at the bottom) and away from the high electric field towards low electric field (plate electrode at the top). B) illustrates EP where anions and cations move towards positive and negative electrodes respectively in a uniform electric field. (Image adapted from [11]).

To better understand the polarizability of a particle, Figure 2.2 is shown to demonstrate polarization of a dielectric particle in a uniform electric field, where the charges arrange, in response to the electric field but experiences no movement owing to the uniformity of the electric field.

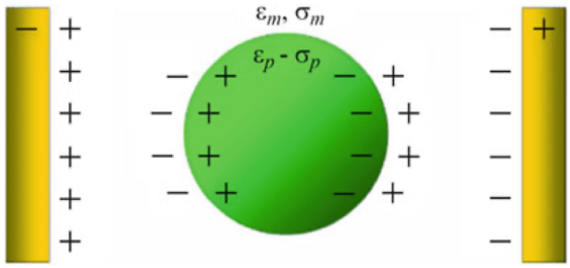

Figure 2.2: Illustrating the polarization of a dielectric spherical particle in a uniform electric field, where ε and σ refer to the permittivity and conductivity, the key dielectric properties. Subscript 'm' and 'p' refer to the properties of the medium and the particle respectively.(Reproduced with permission [2]).

In Figure 2.3, a dielectric particle suspended in a medium is subjected to a non-uniform electric field, demonstrating its polarizability. Figure 2.3a shows the polarization of the particle when the particles' polarizability is greater than that of the suspending medium, due to which more charges accumulate inside the interface than on the outside depicting the behavior of conducting particle in insulating medium (pDEP behavior). Figure 2.3b shows the polarization of the particle when particles' polarizability is less than that of the suspending medium, reversing the direction of net dipole due to which the particle behaves as an insulator in a conductive medium (nDEP behavior).

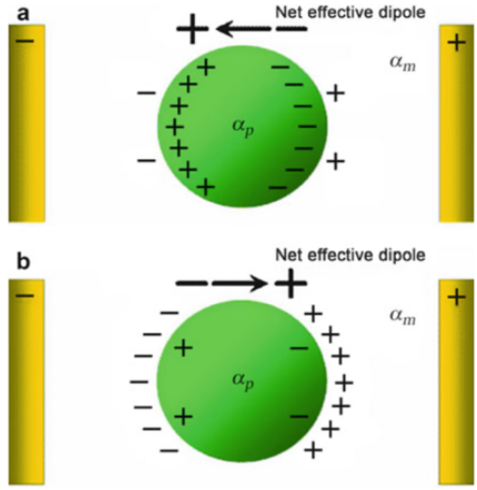

Figure 2.3: Illustrating the polarization of dielectric spherical particle in non-uniform electric field, where α is the polarizability and the subscripts 'm' and 'p' refer to the property of the medium and the particle. (Reproduced with permission [2]).

Figure 2.4 shows the imaginary electric field lines based on the particles' polarizability. Figure 2.4a shows when the particle is more polarizable than the medium, i.e., the particle is conducting, and the dipole is aligned with the applied field. Figure 2.4b refers to the case when the particle is less polarizable than the medium, where the electric field lines do not align with the particle (insulating particle).

This chapter provides a brief theory related to the behavior of the particle under DEP force based

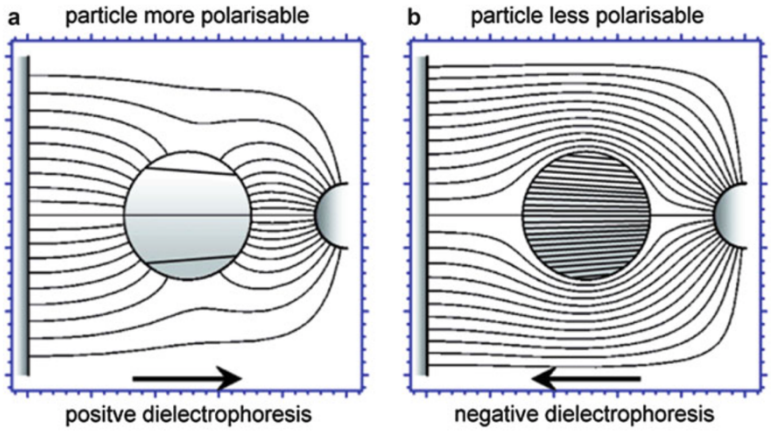

Figure 2.4: Electric field lines for a dielectric spherical particle under nonuniform electric field. a) particle is more polarizable than the medium, b) particle is less polarizable than the medium. (Reproduced with permission [2]).

on the particles' polarizability. DEP theory in detail, including the equations, are further discussed in the relevant chapters. Chapter 3 covers theory related to the derivation of the DEP force equation and Clausius-Mosotti (CM) Factor, an important parameter that evaluates particles polarizability and equations correlating crossover frequency to cells' membrane capacitance, size, and relative permittivity. Chapter 4 includes the theory behind first (low) and second (high) crossover frequencies, correlating experimental crossover frequencies to dielectric properties of the cell and single shell model to evaluate complex permittivity of a cell based on its membrane and cytoplasmic conductivity and permittivity and curve fitting to estimate the best-fit properties using non-linear regression minimizing the sum of squares error between experimental and theoretical values. Chapter 5 focuses on second (high) crossover frequency and modeling of a microdevice to simulate separation using AC-DEP using COMSOL *Multiphysics 5.5a* and talks about all the physics used in modeling such as creeping flow, wall conditions, AC electric current, particle tracing for fluid flow, and all the equations relevant to the respective physics.

References

[1] R. R. Pethig, *Dielectrophoresis: Theory, Methodology and Biological Applications*. 2017.

[2] H. Morgan and N. Green, "Dielectrophoresis," in *Encyclopedia of Microfluidics and Nanofluidics*, D. Li Ed. Boston, MA: Springer US, 2008, pp. 350-357.

[3] U. V. Devi, P. Puri, N. N. Sharma, and M. Ananthasubramanian, "Electrokinetics of Cells in Dielectrophoretic Separation: A Biological Perspective," *BioNanoScience,* vol. 4, no. 3, pp. 276-287, 2014/09/01 2014, doi: 10.1007/s12668-014-0140-y.

[4] S. A. Faraghat *et al.*, "High-throughput, low-loss, low-cost, and label-free cell separation using electrophysiology-activated cell enrichment," *Proceedings of the National Academy of Sciences,* vol. 114, no. 18, pp. 4591-4596, 2017, doi: 10.1073/pnas.1700773114.

[5] T. N. G. Adams, A. Y. L. Jiang, P. D. Vyas, and L. A. Flanagan, "Separation of neural stem cells by whole cell membrane capacitance using dielectrophoresis," (in en), *Methods,* vol. 133, pp. 91-103, 2018/01/15/ 2018, doi: 10.1016/j.ymeth.2017.08.016.

[6] Y. Liu *et al.*, "Identification of neural stem and progenitor cell subpopulations using DC insulator-based dielectrophoresis," (in en), *Analyst,* vol. 144, no. 13, pp. 4066-4072, 2019/06/24/ 2019, doi: 10.1039/C9AN00456D.

[7] B. Cetin and D. Li, "Dielectrophoresis in microfluidics technology," (in eng), *Electrophoresis,* vol. 32, no. 18, pp. 2410-27, Sep 2011, doi: 10.1002/elps.201100167.

[8] K. H. Kang, Y. Kang, X. Xuan, and D. Li, "Continuous separation of microparticles by size with direct current-dielectrophoresis," (in eng), *Electrophoresis,* vol. 27, no. 3, pp. 694-702, 2006/02// 2006, doi: 10.1002/elps.200500558.

[9] P.-Y. Weng, I. A. Chen, C.-K. Yeh, P.-Y. Chen, and J.-Y. Juang, "Size-dependent dielectrophoretic crossover frequency of spherical particles," *Biomicrofluidics,* vol. 10, no. 1, 2016/02/11/ 2016, doi: 10.1063/1.4941853.

[10] B. Yafouz, N. A. Kadri, and F. Ibrahim, "Dielectrophoretic Manipulation and Separation of Microparticles Using Microarray Dot Electrodes," *Sensors (Basel),* vol. 14, no. 4, pp. 6356-6369, 2014/04/03/ 2014, doi: 10.3390/s140406356.

[11] N. Abd Rahman, F. Ibrahim, and B. Yafouz, "Dielectrophoresis for Biomedical Sciences Applications: A Review," *Sensors (Basel),* vol. 17, no. 3, 2017/02/24/ 2017, doi: 10.3390/s17030449.

Chapter 3: Dielectrophoresis as a tool for electrophysiological characterization of stem cells: A Review

Anthony T. Giduthuri[1], Sophia K. Theodossiou[1], Nathan R. Schiele[1], Soumya K. Srivastava[1, *]

[1]Department of Chemical & Biological Engineering, University of Idaho, Moscow, ID. 83844-1021 USA.

Abstract

Dielectrophoresis (DEP), an electrokinetic technique, is a powerful cell manipulation technique used widely for various applications such as enrichment, trapping, and sorting of heterogenous cell populations. While conventional methods require tagging or labeling of cells, DEP offers a label-free way of achieving heterogeneous cell separation efficiently and affordably. There is renewed interest in applying DEP to characterize and sort stem cells, which have widespread potential applications in the field of tissue engineering and regenerative medicine. This review summarizes recent, significant research findings regarding the electrophysiological characterization of stem cells, with a focus on cellular dielectric permittivity and conductivity, and on studies that have obtained these measurements using techniques that preserve cell viability, namely electro-rotation or crossover frequency.

Keywords: Dielectrophoresis, electrokinetics, stem cells, mesenchymal stem cells.

3.1 Introduction

Dielectrophoresis (DEP), an electrokinetic technique, is widely used for characterizing biological cells. DEP was first utilized for sorting stem cells in the 1990s [4-6]. There has been renewed interest in using DEP for characterizing different types of stem cells via their dielectric properties for applications in tissue engineering and regenerative medicine [8-13]. Since the inception of DEP in the 1950s [14], its widespread use has refined it into a powerful tool for applications ranging from separation of live and dead cells [15, 16] to separation of cells in various stages of differentiation [8, 17]. Recent advances in the technique, such as using non-uniform electric fields, have significantly improved DEP accuracy and utility for characterizing and separating cells. DEP has now been applied to separate various biological components such as proteins [18], bacteria [19], and stem cells [8, 10, 20] for various applications such as trapping, sorting, and characterization.

This technique evolved as a powerful cells sorting tool as it eliminates the necessity of labeling the cells, instead exploiting the differences in the cellular dielectric properties and being sensitive to slight changes within the cell or its membrane which is known to affect the dielectric properties [17, 21, 22]. Thus, DEP has several advantages over traditional cell sorting methods such as fluorescence activated cell sorting (FACS), as it relies on less tedious preparation and results in improved cell viability following separation [23, 24]. Additionally, the experimental setup for DEP is relatively simple [25] compared to other methods of cell sorting such as flow cytometry, making it an attractive tool for distinguishing between cell populations based on small variations in physical properties. Because of the high accuracy and simple setup of DEP compared to the other microfluidic separation techniques, DEP is also utilized on lab-on-a-chip for trapping, separating, and manipulating cells based on free surface charge distributions [26]. DEP technology has also been extensively tested and refined to provide high

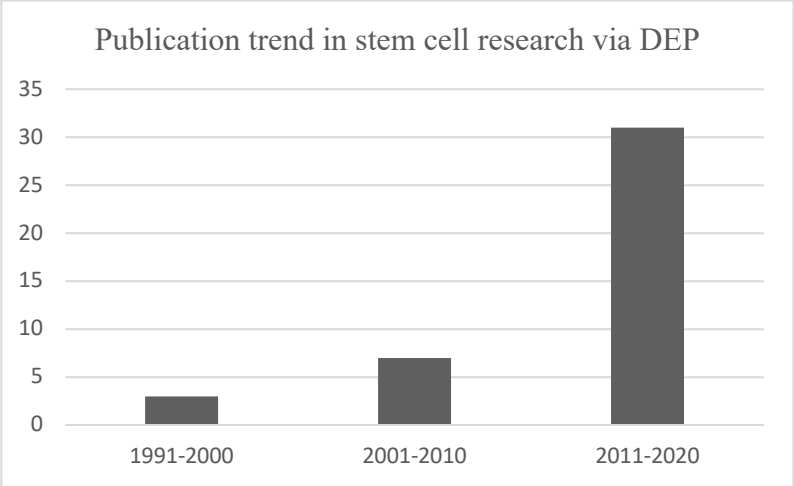

Figure 3.1: An increase in trend of number of DEP related experiments on stem cells, reported by researchers across the globe over the past three decades.

levels of accuracy, even compared to other microfluidic techniques [27]. Based on these recent advances and potential applications, this review briefly summarizes the theory that enables dielectrophoresis, significant research findings regarding the electrophysiological characterization of stem cells, with a focus on cellular dielectric permittivity and conductivity, and on studies that have obtained these measurements using techniques that preserve cell viability, namely electro-rotation or crossover frequency. The first stem cell studies using DEP were reported in 1995 [6], 1996 [5], 1999 [4] that studied the hematopoietic stem cells (CD34+). In the subsequent years of 2001-2010 the number of studies doubled to at least 7 and increased to at least 10 times in the current decade (2011-2020). The number of studies subsequently increased and by 2018, roughly 30 projects were investigating the

potential of DEP for stem cell research [22]. There has been an addition of about 2 or more studies in the recent years after 2018.

The potential of DEP as a stem cell sorting and diagnostic tool has been explored in several recent reviews [3, 23, 28, 29], though it has not been investigated as extensively in the context of generating homogeneous cell populations for applications in musculoskeletal tissues. Therefore, the utility and future needs for DEP with a particular focus on musculoskeletal tissues are also discussed.

3.2 Theory of dielectrophoresis

DEP is a non-invasive, label-free technique which induces motion of particles relative to its medium due to the gradient of a non-uniform electric field, based on the polarizability and the dielectric properties (permittivity and conductivity) of the cell membrane and cell interior (cytoplasm & organelles) [9, 14]. DEP was later used to separate live and dead cells [15]. In the first decade since its inception, the applications of DEP have been extended to several processes such as enrichment, trapping, and sorting [30]. Briefly, when a biological cell (by virtue non-polar) is subjected to non-uniform electric field, an induced dipole moment (m_{eff}) occurs within the cell. The dipole magnitude can be derived as follows [3], considering the cell to be spherical in shape of radius r:

$$m_{eff} = 4\pi\varepsilon_m r^3 pE \quad (1)$$

where ε_m is dielectric permittivity, E is the applied electric field, p is the effective polarizability (per unit volume) signified by the Clausius-Mossotti (CM) factor, which is expressed as [23]:

$$p = \frac{\varepsilon_p^* - \varepsilon_m^*}{\varepsilon_p^* + 2\varepsilon_m^*} \quad (2)$$

where ε_p^* and ε_m^* are the complex permittivity of the particle and the medium, respectively. Complex permittivity of the particle and the medium can be calculated using the relation below:

$$\varepsilon^* = \varepsilon - j\frac{\sigma}{\omega} \quad (3)$$

where $j = \sqrt{-1}$, σ is conductivity of the material and ω is the angular frequency.

The net DEP force acting is proportional to the product of the induced dipole moment and the field gradient, which can be expressed as [23]:

$$F_{DEP} = \quad (m_{eff}.\nabla)E \quad (4)$$

Combining (1) and (4), we have the following equation after substituting (1) in (4):

$$F_{DEP} = 4\pi\varepsilon_m r^3 p(E.\nabla)E \quad (5)$$

where ∇ is the gradient operator, which mathematically represents $i\frac{\partial}{\partial x} + j\frac{\partial}{\partial y} + k\frac{\partial}{\partial z}$. This result considers a depolarization factor of 1/3 to account for the fact that a spherical body distorts an external applied field, and that the electric field inside the sphere differs from the external field.

Equation (5) can also be represented by neglecting the imaginary part of *p* and considering the real part alone as:

$$F_{DEP} = 4\pi\varepsilon_m r^3 Re[p](E.\nabla)E \quad (6)$$

Equation (6) is analogous to equation (7), which is another widely used expression with vector transformation on electric field [12, 31]:

$$F_{DEP} = 2\pi\varepsilon_m r^3 Re[p]\nabla E^2 \quad (7)$$

Dielectrophoretic force can also be commonly written as [32]:

$$F_{DEP} = \frac{3}{2}\upsilon Re(p)\,\nabla E^2 \quad (8)$$

where υ is volume i.e., $\frac{4}{3}\pi r^3$. Substituting volume in equation (8) results in equation (7).

Mathematically, p is bound within the limits $-0.5 \leq p \leq 1.0$. The dielectric properties of the suspending medium (DEP buffer) and the cells determine the value of *p*, based on the angular frequency. In general, the medium properties are standardized, and altering the frequency of the applied electric field results in motion of the suspended cells towards the high and low electric field regions. Cells move towards the high electric field (i.e., towards the electrodes) when $p > 0$, termed positive dielectrophoresis (pDEP). Cells move towards the low electric field (i.e., away from electrodes) when $p < 0$, termed negative dielectrophoresis (nDEP). Finally, there exists a frequency at which $p = 0$, where there is no noticeable motion of the cells. This is termed the crossover frequency (f_{x1}) or the zero-force frequency, at which the acting DEP force is zero. This crossover frequency indicates that the real part of the effective polarizabilities of the cell and the medium are equal to each other.

Utilizing f_{x1}, i.e., the transition from nDEP to pDEP or vice versa (determined experimentally), the properties of the membrane can be estimated using [9]:

$$C_{mem} = \frac{\sqrt{2}\sigma_{med}}{2\pi r f_{x1}} \quad (9)$$

where C_{mem} is the capacitance of the membrane, σ_{med} is the electrical conductivity of the medium, *r* is

the radius of the cell, and f_{x1} is the first crossover frequency. f_{x1} typically occurs in the radio frequency band due to β-dispersion (i.e., frequencies between 0.010 – 0.1 MHz). Biological cells produce three types of dispersions under wide frequency bandwidth, based on which they are classified into α, β, and γ [33]. These cells are characterized for dielectric properties based on α-dispersion at low frequencies (Hz – kHz), β-dispersion in the radio frequency band (kHz – MHz) and γ-dispersion in the microwave frequency region (> GHz) [34]. Estimated C_{mem} can be extended to determine the permittivity of the membrane, which is proportional to its capacitance and is given by:

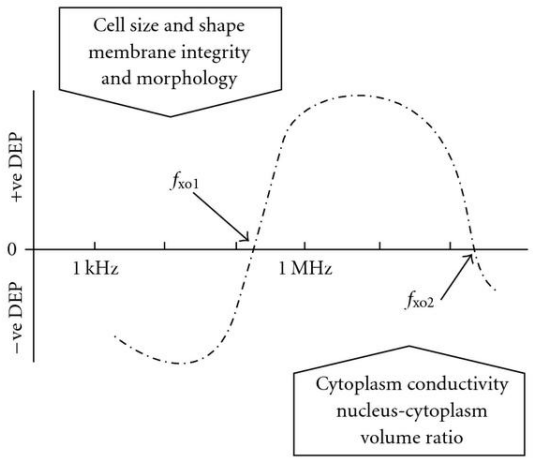

Figure 3.2: DEP response exhibited by a viable cell indicating the first and the second crossover frequencies with the respective dependence on parameters. (Image adapted from [3]).

$$\varepsilon_{mem} = \frac{C_{mem} d}{4\pi r^2 \varepsilon_0} \qquad (10)$$

where ε_{mem} is the permittivity of the membrane, d is the thickness of the membrane, and ε_0 is the permittivity of a vacuum.

At frequencies >10 MHz, i.e., high frequency range (10 MHz – 1 GHz), contents of a cell's interior (e.g., cytoplasm) play a significant role in determining the second crossover frequency (f_{x2}). Properties of the cytoplasm (conductivity & permittivity), nuclear envelope permittivity, and nucleus-cytoplasm (N/C) volume ratio play significant role in determining f_{x2} [3]. Though DEP is sensitive to detect subtle changes within cell, one of the disadvantages of exposing cell to stronger electric fields i.e. > 10 V_{pp} for longer durations of >30 min. alters cell's properties and decreases viability [35-38].

3.3 Applications of DEP on stem cell research

Overall, stem cells have the potential to greatly enhance tissue engineered regenerative therapies due to their ability to differentiate into multiple tissue types. However, stem cells require further characterization to improve their clinical potential. DEP is an appealing separation technique due to its demonstrated ability to sort cells with a high degree of accuracy and based on minute electrical differences, while also preserving cell viability. DEP sorting also takes advantage of the electrical properties of cells, which can serve as label free biophysical markers and may be distinct at different stages of differentiation. We briefly discuss types of stem cells before examining the existing, but limited examples of DEP-based stem cell characterization. The current article's focus is limited to a basic classification of stem cells only before discussing the DEP characterization technique for stem cells. Hence, further discussion of stem cells developmental biology and classification is out of the scope for this current article.

3.4 Types of stem cells

Stem cells are undifferentiated cells that can differentiate into multiple cell lineages with the potential to self-renew [39], and exist both in embryos and adults. Stem cells are classified based on their origin and potency, as summarized in Tables 1 and 2. "Potency" refers to a stem cell's ability to differentiate into different cell types. Totipotent stem cells have the highest potency and can differentiate into both embryonic (cells found in an embryo) and extraembryonic (placental cells) cell types. During the early stages of embryonic development, primary cell layers are formed. Early embryos consist of three layers: the endoderm (inner layer), the ectoderm (outer layer), and the mesoderm (middle layer) [40]. Any primary cell layer is called as a 'germ layer' [40]. These cells are usually termed based on their origin or their potency (ability to regenerate). The ability to regenerate varies based on the origin of the cell. Based on potency, totipotent stem cells have the highest potential of differentiating into cells of any kind, followed by the pluripotent stem cells (PSCs). PSCs are descendants of totipotent cells and can differentiate into cells derived from any of the germ layers, but not the placenta [41]. Multipotent stem cells have a narrower spectrum of differentiation, compared to pluripotent stem cells. Multipotent stem cells can differentiate into cells that are closely related in their cell lineage. For example, bone marrow contains multipotent stem cells that can give rise to all the cells of blood, (e.g. Hematopoietic (blood) stem cells – HSCs) [41], but no other cell types. Oligopotent stem cells have the ability to differentiate into only a few cells, for example lymphoid or myeloid stem cells that can only replenish other lymph of myeloid cells. Unipotent cells can divide repeatedly to produce only their own cell type,

are usually able to proliferate rapidly, but have the least differentiation capacity [39, 41]. Muscle stem cells are a representative unipotent cell in the human body [42, 43].

Table 3.1: Classification of stem cells based on potency (regenerative potential). (Adapted from book chapter [39] with permission).

Classification of stem cells based on potency	
Type of cell	**Characteristic**
Totipotent	Ability to differentiate into cell lineages derived from all three germ layers: mesoderm, endoderm, ectoderm (including placental cells).
Pluripotent	Ability to differentiate into cell lineages derived from all three germ layers: mesoderm, endoderm, ectoderm (excluding placental cells).
Multipotent	Ability to differentiate into a limited number of types from germ layer of origin.
Oligopotent	Ability to differentiate into few types of cells with related functions.
Unipotent	Ability to produce cells of their own type exclusively.

In addition to their potency, stem cells are broadly classified into three categories based on their original source: embryonic stem cells, adult stem cells, and infant stem cells, a larger grouping that includes induced pluripotent stem, fetal stem cells, skeletal stem cells, and cord blood stem cells [43]. Embryonic stem cells can differentiation into any fully developed cell of the body [44]. In the initial stages of embryonic development, the cells of the zygote are totipotent [7, 43]. Once the zygote forms a blastocyst (approximately 7 days following fertilization), these cells become pluripotent [43]. Adult stem cells (also known as somatic stem cells) are harvested from mature tissues. MSCs, hematopoietic, neural, hepatic, epidermal, and pancreatic stem cells are commonly utilized somatic stem cells [43]. Induced-pluripotent stem cells are programmed embryonic stem cells with pluripotent characteristics, and are widely used in drug development and disease modeling applications [43].

Table 3.2: Classification of stem cells based on their source. (Adapted from book chapter [39] with permission).

Classification of stem cells based on source	
Stem cells	**Source; Characteristic**
Embryonic Stem cells	Blastocysts; Pluripotent
Adult Stem cells	Adipose tissue/bone marrow/ peripheral blood; Multipotent
Induced pluripotent stem cells (iPS)	Any somatic cell, most commonly fibroblasts, keratinocytes, peripheral blood mononuclear cells; Pluripotent
Mesenchymal stem cells	Bone marrow/adipose tissue/skin/ peripheral blood, Perinatal tissue: umbilical cord blood, amniotic fluid, membrane and placenta; Multipotent, Non-hematopoietic
Hematopoietic stem cells	Bone marrow/ hepatic tissue; Multipotent/bipotent
Skeletal stem cells	Bone marrow and local periosteum; Multipotent

Next, we examine existing uses of DEP in stem cell research and discuss ongoing investigation areas in which expanded DEP use may have a positive impact.

3.5 Applications of DEP on stem cell research

Experimental studies using DEP for stem cell sorting are still at their nascent stages [3], but have received renewed interest throughout the last three decades. The first stem cell studies utilizing DEP studied the CD34+ hematopoietic stem cells [4-6].

Major unmet needs in stem cell research include selecting specific cells of interest from a cell population (e.g., isolation and separation), identifying when cells have differentiated (e.g., characterization), and increasing the number of cells of interest (e.g., enrichment). DEP has the potential to address these major unmet needs in stem cell research, and DEP has been applied to characterize, separate, enrich, isolate, and sort different types of stem cells (Table 3.3). In the following section, we discuss the recent characterizations of the dielectric properties stem cells, which can be used to further advance DEP to characterize, separate, enrich, isolate, and sort different types of stem cells and progress towards addressing these unmet needs in stem cell research [45].

Table 3.3: Application of dielectrophoresis (DEP) in studying stem cells for various applications such as isolation, characterization, separation, etc.

DEP application	**Types of stem cells**	**References**
Isolation	Cancer (Glioblastoma) stem cells	[31]
Characterization	Human mesenchymal stem cells	[9]
Separation	Neural stem cells, BM-MSCs, NSPCs, ADSCs	[46], [47]
Trapping	Mouse NSPCs	[48]
Enrichment	BM-MSCs, ADSCs	[46], [49]

BM-MSCs – Bone Marrow derived Mesenchymal Stem Cells

NSPCs – Neural Stem/Progenitor Cells

ADSCs – Adipose tissue derived Stem Cells

3.5.1 Adipose-derived Stem cells (ADSCs)

ADSCs are promising for stem cell-based therapies due to their availability and relatively easy procurement from adipose tissue [50]. ADSCs have not previously been characterized using DEP, and their dielectric parameters have not been established. However, one prior study explored the potential use of dielectric properties in monitoring ADSC differentiation into osteoblasts and mature adipocytes. The cell membrane capacitance of undifferentiated human ADSCs was reported as 1.65 ± 0.07 μF/cm^2, while the membrane capacitance of osteo-induced and adipose-induced cells (4 days after induction) was found to be 1.72 ± 0.10 μF/cm^2 and 2.25 ± 0.27 μF/cm^2 respectively, representing significant differences in their membrane and cytoplasmic structures. The capacitance values were measured using electric cell-substrate impedance system by monitoring time and frequency dependent complex impedance at the cell-electrode interface [51]. Alterations in membrane capacitance present a mechanism by which DEP might be useful for selecting ADSCs from more differentiated progeny. In a different study, human undifferentiated ADSCs had a mean radius of 15.4 μm, while the differentiated adipocyte cells (7 day) exhibited a slightly larger mean radius of 18.8 μm. 14 days after induction, cells were further enlarged, with a mean radius of 20.3 μm [52]. These changes in size also indicate the DEP might be able to detect undifferentiated and differentiated ADSCs.

Another recent study assessed the electrokinetic adaptability, the virtue of no-response to induced electric fields by repeated stimulation. Due to their adaptive nature of ADSCs, they had higher resistance to oxidative stress as examined using oxidative stress-induced senescence and β-galactosidase (SA-β-Gal) assay by staining. Oxidative stress was induced by treating cells with hydrogen peroxide (H_2O_2). This induced oxidative stress was utilized to simulate decline in organ function and cellular

aging. After treatment, ADSCs and MSCs did not show any morphological changes (Figure 3.3). However, the BM-MSC proliferation rate decreased and 90% of BM-MSCs tested positive for cellular senescence as measured by 3-(4,5-dim ethylthiazol-2-yl)-2,5-diphenyltetrazolium bromide (MTT) assay described in [7], whereas ADSCs remained more potent. Therefore, ADSCs were resistive to induced oxidative stress, and displayed a higher capability to adapt to the electric field when exposed to repeated electric stimulation. This adaptative potential to electric fields was characterized by measuring electrical properties using DEP traveling wave technique i.e., traveling wave speed and rotational speed were measured at 10 V_{pp} and 8 MHz. Overall, ADSCs displayed slower velocity movement at lower frequency and higher speed at higher frequency compared to BM-MSCs which almost remained constant throughout the frequency sweep measurements from 1 kHz to 8 MHz at a fixed voltage of 10 V_{pp} [7].

Taken together, previous studies suggest that ADSCs are a promising alternative to MSCs for studies using stem cells. ADSCs display better adaptive potential to electric fields and higher regenerative potential compared to bone-marrow derived MSCs [7]. Additionally, the viability of using DEP to separate cells for clinical uses is higher in ADSCs, compared to MSCs, and ADSCs are considered safe for human use [47]. DEP has also been evaluated for enrichment of stem cells from adipose tissue using field flow fractionation technique, by subjecting the cells to AC electric field of

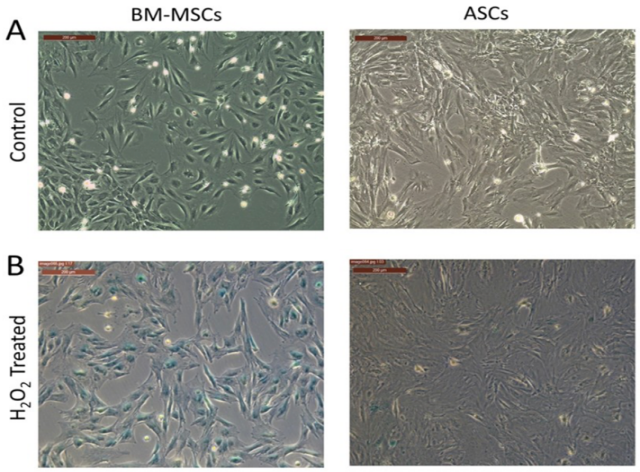

Figure 3.3: A) Control group – BM-MSCs and ADSCs; B) Hydrogen peroxide treated BM-MSCs and ADSCs to induce oxidative stress which is known to cause cellular aging and deteriorates organ functioning. It is observed that ADSCs had higher proliferation to that of BM-MSCs, after treatment. BM-MSCs – Bone marrow derived mesenchymal stromal cells; ADSCs – Adipose stem cells. (Image adapted from [7]).

200 kHz frequency and linearly decreasing the frequency to 60 kHz over 40 min at a processing volume of 1500 µL/min. At 200 kHz frequency, intact cells experienced pDEP which resulted in trapping, while the damaged cells and cell debris are not retained in the fractionating chamber. Further decrease in

frequency over time, resulted in nDEP behavior of intact cells and achieved satisfactory results with up to 14 fold enrichment from initial <2% of NG2-positive cells, highlighting their potential use in clinical trials [49].

3.5.2 Hematopoietic stem cells

Hematopoietic stem cells (HSCs) were the first stem cells successfully sorted by DEP. Sorting was based on separation and enrichment of CD34+ cells (a marker for human HSCs). These initial studies in HSCs found that DEP was effective for enriching and separating HSCs from a heterogenous cell population, which consisted of HSCs as well as bone marrow and peripheral blood stem cells [5, 6]. Another study showed DEP was able to isolate human breast cancer cells from HSCs, while also characterizing CD34+ stem cells (HSCs) to obtain their dielectric properties. The values reported [4] are provided in Table 3.4. A pDEP regime has also been successfully used to create DEP-based artificial micro-environments for developing hematon-like structures (a compact, three-dimensional spheroid complex from central adipocytes, fibroblastoid cells, and resident macrophages that compartmentalize progenitor cells), while maintaining cell viability [53]. A hematon consists of at least two distinct structures, an inner core to support cells and an outer layer of blood producing cells. In this study mouse stromal cells were used as support cells, layered on the top using Jurkat cells (human T lymphocytes) that produce blood cells. Frequency of 1 MHz at 20 V_{pp} was used to first layer the bottom with stromal cells using pDEP followed by adding Jurkat cells to aggregate on the top layer until desired height was attained, which usually took about few minutes to a maximum of 15 min. Cell diameter of human HSCs is estimated to be 8.2 ±1.1 μm and 8.7 ± 1.7 μm using Coulter electronic counter method and image analysis method respectively [54].

Table 3.4: Reported dielectric properties of membrane and cytoplasm of human CD34+ cells (HSCs)[4].

Cell type	**Specific membrane capacitance (C_{mem}) (mF/m^2)**	**σ_{int} (S/m)**	**ε_{int}**
CD34+	10.2 ±1.2	0.71±0.11	141.2±28.0

3.5.3 Mesenchymal stem cells

Mesenchymal stem cells (MSCs), the multipotent progenitors of muscle, tendon, bone, and cartilage, are especially promising for musculoskeletal tissue engineering applications due to their ability to undergo differentiation into several musculoskeletal tissue lineages [55-61]. However, the inherent heterogeneity of cell populations presents a unique challenge for tissue engineering

applications, where precise stem cell's fate is crucial to the function of the engineered construct. Cells that are not differentiating into the exact tissue can result in aberrant tissue formation, including ectopic ossification when used in tendon repairs [62], or form malignant tumors [63].

Human MSCs (h-MSCs) express a range of biomarkers on their membrane, challenging characterization efforts. Nevertheless, undifferentiated h-MSCs membrane permittivity and capacitance have been characterized to obtain the dielectric properties [9], which are summarized in Table 3.5. This initial characterization also suggested that treatment of the cells with polymer (polypeptide) skewed the electrical properties significantly compared to the untreated cells, showing that pre-DEP treatment (such as adding polymers) i.e., ELP-PEI treated group in Table 3.5 should be accounted for when using cell-surface biomarkers to characterize cells.

Table 3.5: Dielectric properties of undifferentiated human mesenchymal stem cells as a function of medium conductivity [9].

Human MSCs		
Cell treatment (suspending medium conductivity – S/m)	***Membrane permittivity***	***Membrane capacitance (pF)***
Untreated (0.03 S/m)	2.0	2.2
Untreated (0.10 S/m)	4.1	4.5
ELP-PEI Treated (0.10 S/m)	0.050	>0.13

MSCs can be isolated from several sources, including bone marrow (BM-MSCs). A DEP assisted platform was used to separate and enrich BM-MSCs from a heterogenous cell population consisting of MSCs and human promyelocytic leukemia cells. Using AC voltage of 5 V_{pp} and 30 kHz of applied frequency for 5 min resulted in separation of BM-MSCs with purity, recovery, and enrichment rates of 83.5±7.1%, 29.1±4.1% and 2.3, respectively, while the viability of cells remained above 90% [46]. h-MSCs and their differentiation products (osteoblasts) were also assessed after continuous flow sorting using DEP to separate undifferentiated human mesenchymal stem cells (h-MSCs) from MSCs that had differentiated into osteoblasts, and was able to achieve 84% purity for h-MSCs and 87% purity for osteoblasts, respectively [12]. Cells were viable after sorting and collecting, and followed distinct trajectories during separation based on their differentiation state (h-MSCs or osteoblasts) [12]. Finally, the collection efficiency for h-MSCs was high (92%), while 67% was achieved for osteoblasts [12]. Overall, this study showed that DEP can separate osteoblasts from their parent stem cells, although due to the concern of ectopic ossification during tenogenic differentiation [62, 64], a higher collection efficiency would be desirable for musculoskeletal tissue engineering applications. DEP is also capable of separating mature musculoskeletal cell populations from stem cells. A recent study used DEP to

distinguish between two osteosarcoma cell lines (MG-63 and SAOS-2) and an immunoselected enriched skeletal stem cell fraction (STRO-1 positive cell) of human bone marrow [11]. By using DEP to develop a model that generated the membrane and cytoplasmic properties of the cell populations, significant differences were observed in the cytoplasmic conductivity and specific membrane capacitance of each cell type (MG-63, SAOS-2 and STRO-1), which allows further sorting of populations [11]. This study demonstrates the ability of DEP to separate both mature and stem cell populations, even from heterogeneous human bone marrow cell population. The ability to detect and separate musculoskeletal cell populations will greatly accelerate the clinical application of stem cell-based therapies. Characterization of cells using DEP is impacted by the cell shape and size, especially the first crossover frequency when using the DEP crossover technique. Hence the cell size and its effect should be well understood, since variance in size is thought to be a significant cause of severe vascular obstructions when MSCs are injected in large and small animal models [65]. MSCs had an average cell size (diameter) of 17.2 ± 1.2 µm, and remained small and spherical until 4 days of culture before increasing to over 30 µm in diameter by day 7 [66]. Discussing the morphology, h-MSCs which are cryopreserved has spindle shaped morphology one day after plating and it is observed that MSCs derived from different sources such as adipose tissue, amniotic tissue, bone marrow, chorionic tissue, liver and umbilical cord are not the same [2]. Based on the derived site, MSCs displayed varying differentiation potentials, even though at 1 d in culture cells from most sources had similar, spindle-like morphology [2] (Figure 3.4).

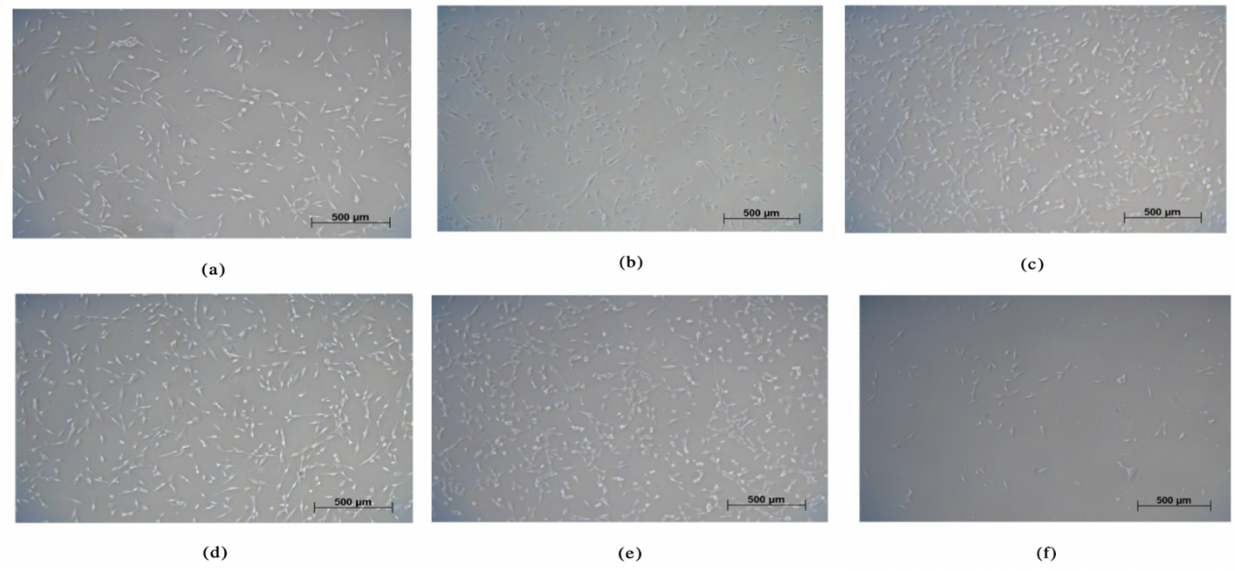

Figure 3.4: Phase contrast images of one day old plated human mesenchymal stem cells in culture (a) Adipose tissue derived (b) amniotic tissue-derived (c) bone marrow-derived (d) chorionic tissue-derived (e) liver-derived (f) umbilical cord-derived. (Image adapted from [2]). (Scale bar – 500 µm)

The above reported cell sizes also match prior work reporting the average cell diameter of fractionated MSCs based on the culturing method. Cells cultured in monolayer for six passages had cell diameters ranging from 17.9 μm (small) to 30.4 μm (large) [65]. Passage 6 MSCs varied significantly in size, from 15-50 μm with an average of 26.5 μm diameter. Clinical applications require homogenous populations of MSCs to order to avoid further post-treatment complication such as progression of the site of treatment using MSCs into a cancerous microsite[67], heterogeneity is thought to be one of the causes for such behavior of MSCs [67, 68]. Sorting MSCs into homogenous cells is challenging to isolate in large numbers rapidly, owing to the heterogeneity of differentiated products, using traditional label-based cell separation and sorting techniques due to great diversity of MSCs based on the primary tissue of origin, age of donor, method of isolation and culture conditions [69] especially since source and number of passages is an important consideration in regenerative medicine[69]. Adding on these challenges is the behavior of individuality of MSCs in spite being known for their heterogenous nature. This individuality of MSCs might result in a single cell of all the cell population used in clinical application to proliferate rapidly giving rise to new cells aiding recovery, or turn cancerous due, die due to nutrient deprivation, DNA and membrane damage etc. [70]. All the discussed parameters make sorting of stem cells more challenging than its' thought to be. Although most stem cells used in regenerative approaches are multipotent, the differentiation potential of MSCs derived from different sources varies. In one study, murine MSCs derived from bone marrow (BM), compact bone (CB), and adipose tissue (AT) were separated using FACS and cultured for three (3) passages. All cells retained fibroblastic morphology, but growth was stalled in the BM-derived MSCs [71]. Additionally, FACS analysis of cell markers revealed that the AT and CB derived MSCs were positive for CD29, CD44, CD105, and Sca-1, but negative for CD34, TER-119, CD45, and CD11b [71]. AT-derived cells appeared to have the most potential as a source of murine MSCs for future musculoskeletal tissue engineering uses based on their growth rate and ability to form colonies. While the distinctions detected by FACS are valuable, a method such as DEP that can separate cells based on characteristics other than membrane markers or tags, while maintaining cell viability, would improve predictions of which cell line is ideal for a specific musculoskeletal tissue application, such as tendon regeneration. In applications outside of tissue engineering, MSC contamination with hematopoietic stem cells during their isolation is a concern that is difficult to mitigate with traditional methods, such as FACS or cell labeling [72]. Future studies using DEP could enhance the homogeneity of isolated MSC populations and facilitate the isolation of MSCs from multiple sources. Overall, improved characterization of MSC differentiation will greatly enhance their potential use in regenerative therapies. More work is needed to elucidate the effects of cell

culture and differentiation on MSC morphology, size, and potency, and DEP is a promising tool for improving the clinical potential of MSCs.

3.5.4 Neural stem cells

The dielectric properties of neural stem cells (NSCs) have been characterized by using impedance measurement. The specific membrane capacitance and conductivity of cytoplasm of NSCs were studied as biophysical markers during the differentiation process at time points Day 0, 1, 3, and 7. [73]. The membrane capacitance and conductivity are found to serve as label free biophysical markers and are distinct for different stages of differentiation. Undifferentiated NSC's isolated from two different rats of same species are characterized for electrical properties at day 0 in culture media and days 1, 3 and 7 in the differentiating media. Specific membrane capacitance was obtained to be 1.71±0.45 $\mu F/cm^2$ and 1.74±0.66 $\mu F/cm^2$ for rats I and II respectively; cytoplasmic conductivity was estimated to be 3.21±2.05 S/m and 2.41±1.40 S/m for rats I and II respectively. further properties into differentiation at varying time points are tabulated in Table 3.6. Undifferentiated cells (Day 0) exhibited large differences in cytoplasmic conductivity, compared to the differentiating cells, possibly due to differences in culture medium signifying cellular heterogeneity. Throughout differentiation, specific membrane capacitance varied widely as a function of day in culture, signifying changing expression of the membrane proteins. The reported values include data for two different rats (Table 3.6).

Table 3.6: Dielectric properties of rat NSCs during their course of differentiation at day 0, 1,3 and 7 which depict significant difference in the properties at every time point. (Table adapted from [73]).

Dielectric properties of rat NSCs				
Time point	**Specific membrane capacitance ($\mu F/cm^2$)**		**Conductivity of cytoplasm (S/m)**	
	Rat I	*Rat II*	*Rat I*	*Rat II*
Day 0	1.71±0.45	1.74±0.66	3.21±2.05	2.41±1.40
Day 1	4.26±1.73	3.44±1.22	3.71±2.26	2.83±1.59
Day 3	2.80± 1.71	3.12±2.07	1.19±0.59	1.43±0.73
Day 7	2.65 ±1.50	3.70±1.81	1.40±0.65	1.22±0.64

Utilizing whole membrane capacitance i.e., cell's ability to store electrical energy, separation of rat NSCs using DEP was assessed, which yielded promising results of applying DEP to separate cells at

transplantation scale ~10^9 cells [8]. Results also suggest that whole membrane capacitance has the potential to serve as a biophysical marker to enrich and separate NSCs [8].

The dielectric properties can also be used to distinguish undifferentiated NSCs from differentiated cells, while also revealing heterogeneity in the cell population [10]. In another study, DC-iDEP (Direct current-insulator based Dielectrophoresis) was successfully employed to distinguish NSCs [74], which measures electrokinetic mobility ratio, a key biophysical property that can be measured using DC-iDEP which is observed to be distinct for NSPCs (Neural stem and progenitor cells). This opens the opportunity to apply DC-iDEP, which does not depend on the frequency of electric field in identifying and distinguishing cells successfully in heterogenous cell populations.

In addition to characterizing NSCs, DEP has been used to characterize the physical properties of differentiated neural cells. DEP is shown to accurately estimate the dielectric permittivity, cytoplasm conductivity, and specific membrane capacitance of mouse hippocampal neuronal and glial cells, providing novel information about these three physical properties in two understudied types of neural cells [25].

3.6 Recent advances in DEP for sorting stem cells

Owing to the characteristic of heterogeneity, stem cells which are extensively being studied to exploit their use in regenerative medicine is hurdled [74]. Another significant challenge is to identify cells accurately at high-throughput, since only a small percent of population can be of use in therapy [74]. In order to advance stem cell based studies, to better understand the functions at cellular level, DEP is seen as a powerful and successful technique in distinguishing and manipulating cells based on their morphological and physiological characteristics such as size, shape, ratio of cytoplasm to the nucleus volume, etc. [49].Recent modifications to DEP based devices, combined with hydrophoretic modules where in induced pressure gradient aids cell motion along with the non-uniformity in fluid flow caused by the embedded microstructures within the channel. These modifications have allowed high-throughput separation of stem cells at rates of ~240,000 cells per hour [20], which is much higher than any conventional DEP based platform (6000-100,000 per hour) as well as commercial techniques like FACS and MACS. A mean optimal sorting frequency of 184 kHz was reported based on trap and release mechanism that is operated as a DEP standalone platform using the differences in the dielectric behavior of neural stem cells [20]. To our knowledge, no therapeutic based evaluations were reported for NSCs using DEP. However, based on these existing studies, DEP offers a promising way of sorting NSCs for use in treating neurological disorders.

3.7 Potential future impact and application of DEP for musculoskeletal tissues

While all musculoskeletal tissues are active research objectives for regenerative therapies using stem cells, tendons have emerged as a previously understudied tissue that would benefit immensely from more effective regenerative treatment options. Tendons, the musculoskeletal tissues that transfer forces from muscle to bone to enable movement, are frequently injured and heal poorly, resulting in permanent loss of function. Tendons are especially challenging to imitate with *in vitro* tissue engineered approaches using stem cells, as they have low cellularity and the characteristics of tendon-specific cells are poorly understood. There are only a few distinguishing transcription factors that allow for differentiated tendon cells to be identified [75-77]. Therefore, using DEP to identify, isolate and enrich populations of stem cells primed for tenogenesis (differentiation towards tendon) would greatly enhance tissue engineering and regenerative approaches to treat tendon injuries.

A promising application of DEP is improved characterization of the cells involved in tendon differentiation and development. A recent study showed that, contrary to prior expectations, the make-up of tendon progenitor cell populations is heterogeneous. Single-cell analysis of tendon stem/progenitor cells (TSPCs) showed that some cells had active expression of nestin at specific stages of tendon development [78]. Nestin, an intermediate-filament protein commonly associated with nerve cells, was expressed by some TSPCs, and nestin+ TSPCs displayed enhanced tenogenic capacity and ability to self-renew, compared to nestin- cells [78]. When nestin's expression was knocked down using shRNA, TPSCs had suppressed clonogenic capacity and reduced tenogenic potential both in vitro and in vivo [78]. These results suggest that certain subpopulations of TSPCs may be more primed towards tenogenesis than others, despite all being tendon progenitors, and highlight a potential use for DEP in generating viable pools of nestin+ TPSCs. While nestin expression alone is unlikely to affect the physical properties that allow for DEP separation, it is possible that other variations exist between nestin+ and nestin- TPSCs that do allow for DEP-mediated distinction.

Variations between tenogenically differentiating cells may manifest as differences in the transmembrane cell-cell junction proteins, including cadherins and connexins [79]. Embryonic tendon contains an array of cell-cell junction proteins including cadherin-11, N-cadherin, connexin-43, and connexin-32 [80, 81]. These membrane-bound junctions are also potential mechanotransducers, or proteins that can convert mechanical signals into cellular responses [82], and are thought to modulate the tendon response to mechanical loading. Prior research suggests that connexin-32 and connexin-43 have opposite roles in either enhancing or suppressing collagen deposition, and may differ between energy-storing and positional tendons, or within regions of the same tendon (e.g. the midsubstance

versus the enthesis) [83, 84]. In addition to connexins, cadherin-11 and N-cadherin are altered during tenogenesis *in vitro* [85] and subtle changes in their cellular levels may distinguish tenogenic differentiation from the related and concurrent process of chondrogenesis [86]. Subtle differences in levels of membrane-bound cadherins and connexins would likely result in detectable changes to the membrane specific capacitance of the cells, allowing DEP to distinguish between populations based on their production of these cell-cell junctions. Taken together, the emerging role of cell-cell junction proteins during tenogenesis provides an additional marker that DEP can utilize to derive optimized cellular precursors for tendon tissue engineering applications.

Beyond cell sorting, DEP may be useful to tendon tissue engineering applications as a method of building and characterizing scaffolds. Aligned three-dimensional nanofibrous silk fibroin-chitosan (eSFCS) scaffolds were fabricated using DEP [87]. Silk fibroin and chitosan have several characteristics that make them a promising candidate for tissue engineering approaches, including biocompatibility and biomimicity. The percent aligned area of the scaffolds was increased by modulating the DEP frequency at 10 MHz resulting in the greatest scaffold alignment. Furthermore, as DEP frequency increased from 100 kHz to 10 MHz fibril sizes decreased significantly [87]. By tuning the DEP frequency and adding sodium chloride to the scaffolds, the elastic modulus was also tuned, and changing scaffold elastic modulus resulted in changes to the elastic modulus of seeded human umbilical vein endothelial cells (HUVECs). HUVECs also formed aligned and branched capillary-like vascular structures, indicating the parameters of the scaffold were favorable to vascularization. Overall, this study highlights the use of DEP beyond cell sorting, as a potential tool for customizing scaffolds to enhance differentiation towards a specific cell lineage, or promote vascularization, which is especially challenging for implantable tissue engineered tendon constructs.

In addition to sorting and selecting undifferentiated stem cells and enhancing the design of scaffolds, DEP has potential applications in characterizing the cells involved in musculoskeletal tissue injuries. In tendon, the ability to sort cells involved in the injury response may augment clinical treatments of tendinopathies. Tendons have limited healing capacity, and the inflammatory response involves distinct cell types. Embryonic tendon heals scarlessly [88], and postnatal tendon has been shown to retain some regenerative capacity [89], but this is lost in early postnatal stages. Several recent studies in mice have examined the roles of heterogeneous cell populations during both the injury and long-term healing responses in tendons. These studies highlight the application of DEP in sorting and potentially excluding cells that are detrimental to healing, as well as generating pure populations of embryonic or postnatal cells that are able to repair tendon scarlessly. To examine the roles of distinct

cell populations in scar formation, a recent study subjected postnatal days (P) 5 and 50 mice to an Achilles tendon transection. In the P5 mice, pools of scleraxis-positive cells infiltrated the wound and formed a “neo-tendon” that regained native mechanical function, as shown via the lack of scarring and the return to normal gait 28 days after the transection [89]. In the same study, P50 mice with Achilles transections did not have scleraxis-positive progenitors infiltrate the injury, and healing occurred with permanently altered gait and scarring [89]. These results suggest that simply isolating scleraxis-expressing cells for use in tissue engineered constructs to repair tendon injuries may enhance the healing response. The ability to separate and potentially exclude or enrich certain populations of cells *in vivo* following injury may improve the outcomes of tendon pathologies.

Injuries to the rotator cuff tendons are another significant clinical challenge [90], and a recent study showed heterogeneous cell populations are involved in the injury response of the rotator cuff enthesis (the progressively mineralized fibrocartilage of the rotator cuff). To identify the cell populations involved in this inflammatory response, partial and full detachment tears of the supraspinatus tendons were induced in adult mice [91]. While both injuries resulted in significant scarring, the amount of scarring following full detachment and repair led to permanent impairments in gait and disruption of enthesis architecture [91]. Lineage tracing showed cells with minimal scleraxis or Sox9 expression in the scar, while stem cell lineage cells were not found in the scar of the partial tear model, but were the majority of cells detected in the scar of the full tear [91]. Sox9-expressing cells were detected in the articular cartilage of the humeral head, the unmineralized enthesis fibrocartilage, and near the insertion following both the full and partial tear injuries. These results suggest that distinct cellular mechanisms may operate in response to partial or full tear injuries of the rotator cuff, and that minimizing the amount of resident stem cell-derived cells may prevent scarring. Maintaining cell viability during separation would be crucial for healing, making DEP an attractive separation method.

Following the initial injury response, it may be useful to separate cells during long-term healing. Different populations of cells participate in the healing process and, as the roles of each cell type are established, it may become desirable to separate cell populations when simulating the cellular injury response *in vitro*. A recent study demonstrated cell heterogeneity in adult mice after detachment of the central portion of their supraspinatus tendon. Following the injury, mice had distinct populations of cells on the distal versus proximal stump, with proteoglycan-4, smooth muscle actin, and aggrecan-expressing cells found in different locations within the injury [92]. The proximal stump showed enhanced healing compared to other areas, indicating that the cell population in this area may be optimized for healing [92]. Additionally, the distal stump of the injured tendon underwent minimal remodeling, but cells from

other areas (the bursal and articular surfaces) appeared to contribute to healing in the proximal stump [92]. Together, these data highlight a need for technologies that can recreate the natural healing response by sorting cells both *in vitro* and, ideally, *in vivo*.

Taken together, the above studies highlight the need to select for certain cell populations, as heterogeneous cell types are involved in the acute and long-term tendon injury response. *In vitro* models of tendon injuries that segregate cell types without more aggressive interventions, such as genetic knockouts or siRNA, can help determine the exact roles of each cell type, potentially leading to new clinical approaches that enhance the native healing response and suppress inflammation. DEP has the added advantage of detecting simple dielectric properties of cells (specific membrane capacitance, permittivity) and can thus be easily adapted to detect small changes that have recently been identified as markers of tenogenesis, such as drops in cadherins or increases in connexins [85]. The ability to separate cells based on tenogenic markers is highly desirable for tendon tissue engineering applications, and DEP is a promising method for accomplishing this separation. Overall, DEP has the potential to separate cells based on minute variations in physical properties, while preserving cell viability, making it an appealing technique for generating homogeneous populations of stem cells for tissue engineering and regenerative applications.

3.8 Potential application of DEP in microgravity environment for stem cells

Extended human space flight, such as the duration required for manned missions to Mars, is currently prohibited by the limited understanding of the effects of prolonged exposure to microgravity on the body, including on stem cells. Cells cultured in microgravity freely float and interact with each other to develop 3D structures [93]. Microgravity is known to induce significant changes in stem cells [94]. Exposure of mouse embryonic stem cells to microgravity resulted in retention of cellular self-renewal markers, and inhibited differentiation [94, 95]. Different mechanical devices are used to simulate microgravity-like conditions artificially. Clinostat systems are the most widely used method and reduce the impact of gravity by constantly changing orientation [1]. While more research is needed, clinorotation results in flattening in hMSCs due to changes in functional activity induced by the microgravity[93]. The effects of microgravity on living tissues and cells are of great interest to researchers attempting to understand the effects of microgravity on the human body. Continued space exploration depends on the development of effective ways to minimize the negative effects of microgravity on astronauts, as health problems such as bone loss, muscle atrophy, and cardiovascular and immune system changes are common following extended spaceflight [1]. 3D cell culture technique using stem cells better aids in maintaining the pluripotency thus benefits the formation of organs by

inducing differentiation [1]. Mammalian cells are cultured using high aspect ratio vessel (HARV) under µg conditions [96], there are several other types of equipment to simulate µg like conditions such as Random positioning machine (RPM) [97]. Figure 3.5 depicts osteoblast cells from Human fetus (hFOB) (Figs. 3.5A, B) and human mesenchymal stem cells (hMSCs) (Figs. 3.5C, D). h-FOB cells are grown on RPM and HARV (µg conditions), which resulted in the formation of spheroids from adherent cells, spheroids are stained with hematoxylin-eosin. hMSCs are cultured for seven days under normal gravity and microgravity using RPM, which resulted in the formation of 3D spheroids, as seen in Figure 5D. 3D spheroids, resulted from three-dimensional (3D) growth resembles tissue like environment found in living organisms, which can be achieved by negating the effect of gravitation field [93]. 3D cell culture techniques using stem cells are also known to maintain pluripotency improving the differentiation potential thereby aids formation of organoids [1] to be used in regenerative medicine. Hence these techniques are more sought over 2D monolayer culturing and is drawing attention of researchers and clinicians [93].

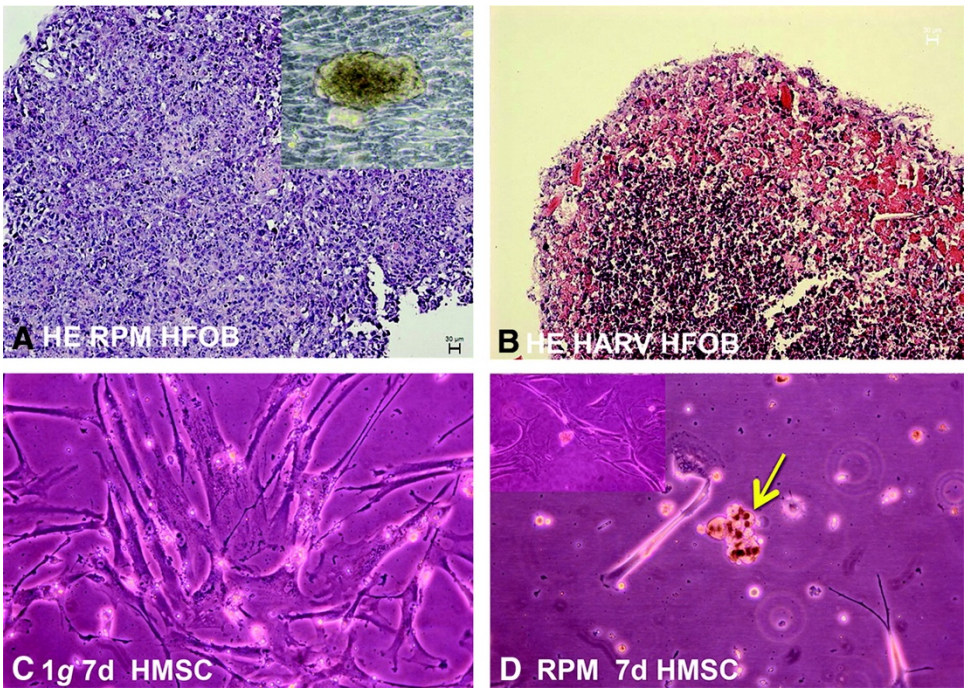

Figure 3.5: Images describing the effects of cell culturing at different conditions using HARV Bioreactor (High aspect ratio vessel) and RPM -Random Positioning Machine. A) Adherent cells and spheroids grown from human fetal osteoblasts (hFOB) cells cultured for 7days on RPM. Spheroids are stained with hematoxylin-eosin (HE) (insert: Phase contrast microscopy – adherent cells and spheroid). B) Similar 3D tissue grown from hFOB cells on HARV. C) hMSCs – 7d culture under standard gravity conditions D) hMSCs – 7d culture grown on RPM (microgravity) resulting in spheroids. (Insert: Adherent MSCs and spheroid) (Image adapted from [1]). (Scale bar - 30 µm)

3.9 Conclusions

Following its initial discovery, DEP has rapidly evolved as an efficient, accurate, and label-free technique for characterizing and sorting cells. Although DEP has been used in the field of stem cell research for some time, clinically satisfactory results have only recently been achieved, renewing the potential DEP use in tissue engineering applications. Dielectric properties, which serve as biomarkers for label-free sorting and enrichment purposes, are still being studied and recorded for large-scale characterization of many different types of cells. While the accuracy and reproducibility of DEP cell characterization require some improvement, DEP has already enhanced research in the field of regenerative medicine. DEP continues to be a promising, efficient, and low-cost technique that may revolutionize the field of stem cell science and advance regenerative medicine.

References:

[1] D. Grimm *et al.*, "Tissue Engineering Under Microgravity Conditions-Use of Stem Cells and Specialized Cells," (in eng), *Stem Cells Dev,* vol. 27, no. 12, pp. 787-804, Jun 15 2018, doi: 10.1089/scd.2017.0242.

[2] E. Schmelzer, D. T. McKeel, and J. C. Gerlach, "Characterization of Human Mesenchymal Stem Cells from Different Tissues and Their Membrane Encasement for Prospective Transplantation Therapies," *BioMed Research International,* vol. 2019, 2019.

[3] R. Pethig, A. Menachery, S. Pells, and P. De Sousa, "Dielectrophoresis: A Review of Applications for Stem Cell Research," (in en), *BioMed Research International,* Research article 2010 2010.

[4] Y. Huang, J. Yang, X. B. Wang, F. F. Becker, and P. R. Gascoyne, "The removal of human breast cancer cells from hematopoietic CD34+ stem cells by dielectrophoretic field-flow-fractionation," (in eng), *J Hematother Stem Cell Res,* vol. 8, no. 5, pp. 481-490, 1999, doi: 10.1089/152581699319939.

[5] M. Stephens, M. S. Talary, R. Pethig, A. K. Burnett, and K. I. Mills, "The dielectrophoresis enrichment of CD34+ cells from peripheral blood stem cell harvests," (in eng), *Bone Marrow Transplant,* vol. 18, no. 4, pp. 777-82, Oct 1996.

[6] M. S. Talary, K. I. Mills, T. Hoy, A. K. Burnett, and R. Pethig, "Dielectrophoretic separation and enrichment of CD34+ cell subpopulation from bone marrow and peripheral blood stem cells," *Med. Biol. Eng. Comput.,* vol. 33, p. 235, 1995.

[7] A. El-Badawy *et al.*, "Adipose Stem Cells Display Higher Regenerative Capacities and More Adaptable Electro-Kinetic Properties Compared to Bone Marrow-Derived Mesenchymal Stromal Cells," *Scientific Reports,* vol. 6, no. 1, p. 37801, 2016/11/24 2016, doi: 10.1038/srep37801.

[8] T. N. G. Adams, A. Y. L. Jiang, P. D. Vyas, and L. A. Flanagan, "Separation of neural stem cells by whole cell membrane capacitance using dielectrophoresis," *Methods,* vol. 133, pp. 91-103, 2018/01/15/ 2018, doi: https://doi.org/10.1016/j.ymeth.2017.08.016.

[9] T. N. G. Adams, P. A. Turner, A. V. Janorkar, F. Zhao, and A. R. Minerick, "Characterizing the dielectric properties of human mesenchymal stem cells and the effects of charged elastin-like polypeptide copolymer treatment," (in eng), *Biomicrofluidics,* vol. 8, no. 5, p. 054109, 2014/09// 2014, doi: 10.1063/1.4895756.

[10] L. A. Flanagan *et al.*, "Unique dielectric properties distinguish stem cells and their differentiated progeny," (in eng), *Stem Cells,* vol. 26, no. 3, pp. 656-665, 2008/03// 2008, doi: 10.1634/stemcells.2007-0810.

[11] A. Ismail, M. P. Hughes, H. J. Mulhall, R. O. Oreffo, and F. H. Labeed, "Characterization of human skeletal stem and bone cell populations using dielectrophoresis.," *J Tissue Eng Regen Med,* vol. 9, no. 2, pp. 162-168, 2015, doi: 10.1002/term.1629.

[12] H. Song *et al.*, "Continuous-flow sorting of stem cells and differentiation products based on dielectrophoresis," *Lab Chip,* vol. 15, p. 1320, 2015, doi: 10.1039/c4lc01253d.

[13] A. Y. L. Jiang *et al.*, "High-throughput continuous dielectrophoretic separation of neural stem cells," *Biomicrofluidics,* vol. 13, no. 6, p. 064111, Nov 2019, doi: 10.1063/1.5128797.

[14] H. A. Pohl, "The Motion and Precipitation of Suspensoids in Divergent Electric Fields," *Journal of Applied Physics,* vol. 22, no. 7, pp. 869-871, 1951/07/01 1951, doi: 10.1063/1.1700065.

[15] H. A. Pohl and I. Hawk, "Separation of Living and Dead Cells by Dielectrophoresis," (in en), *Science,* vol. 152, no. 3722, pp. 647-649, 1966/04/29/ 1966, doi: 10.1126/science.152.3722.647-a.

[16] B. H. Lapizco-Encinas, B. A. Simmons, E. B. Cummings, and Y. Fintschenko, "Dielectrophoretic Concentration and Separation of Live and Dead Bacteria in an Array of Insulators," *Anal. Chem.,* vol. 76, no. 6, pp. 1571-1579, 2004/03/01 2004, doi: 10.1021/ac034804j.

[17] Z. R. Gagnon, "Cellular dielectrophoresis: applications to the characterization, manipulation, separation and patterning of cells," *Electrophoresis,* vol. 32, no. 18, pp. 2466-87, Sep 2011, doi: 10.1002/elps.201100060.

[18] Z. Cao *et al.*, "Dielectrophoresis-Based Protein Enrichment for a Highly Sensitive Immunoassay Using Ag/SiO2 Nanorod Arrays," (in English), *Small,* Article vol. 14, no. 12, p. 10, Mar 2018, Art no. 1703265, doi: 10.1002/smll.201703265.

[19] B. H. Lapizco-Encinas, B. A. Simmons, E. B. Cummings, and Y. Fintschenko, "Dielectrophoretic concentration and separation of live and dead bacteria in an array of insulators," *Anal. Chem.,* vol. 76, p. 1571, 2004.

[20] A. Y. L. Jiang *et al.*, "High-throughput continuous dielectrophoretic separation of neural stem cells," *Biomicrofluidics,* vol. 13, no. 6, p. 064111, 2019/11/01 2019, doi: 10.1063/1.5128797.

[21] R. Pethig, "Review—Where Is Dielectrophoresis (DEP) Going?," (in English), *J Electrochem Soc,* vol. 164, no. 5, pp. B3049-B3055, 2016, doi: 10.1149/2.0071705jes.

[22] A. P. Lee, M. Aghaamoo, T. N. G. Adams, and L. A. Flanagan, "It's Electric: When Technology Gives a Boost to Stem Cell Science," *Current Stem Cell Reports,* vol. 4, no. 2, pp. 116-126, 2018/06/01 2018, doi: 10.1007/s40778-018-0124-x.

[23] N. A. Rahman, F. Ibrahim, and B. Yafouz, "Dielectrophoresis for Biomedical Sciences Applications: A Review," *Sensors,* vol. 17, p. 449, 2017, doi: 10.3390/s17030449.

[24] A. Thiel, A. Scheffold, and A. Radbruch, "Immunomagnetic cell sorting - pushing the limits," *Immunotechnology,* vol. 4, pp. 89-96, 1998.

[25] T. Zhou, Y. Ming, S. F. Perry, and S. Tatic-Lucic, "Estimation of the physical properties of neurons and glial cells using dielectrophoresis crossover frequency," *J. Biol. Phys.,* vol. 42, p. 571, 2016.

[26] P. Weng, I. Chen, C. Yeh, P. Chen, and J. Juang, "Size-dependent dielectrophoretic crossover frequency of spherical particles," *Biomicrofluidics,* vol. 10, p. 011909, 2016, doi: 10.1063/1.4941853.

[27] R. Pethig and D. B. Kell, "The passive electrical properties of biological systems: Their significance in physiology, biophysics and biotechnology," *Phys. Med. Biol.,* vol. 32, p. 933, 1987.

[28] B. Zhu and S. K. Murthy, "Stem Cell Separation Technologies," *Curr Opin Chem Eng,* vol. 2, no. 1, pp. 3-7, 2014, doi: 10.1016/j.coche.2012.11.002.

[29] J. Yang *et al.*, "Dielectrophoresis-Based Microfluidic Separation and Detection Systems," *Int J Adv Manuf Syst,* vol. 3, no. 2, pp. 1-12, 2000.

[30] E. O. Adekanmbi, A. T. Giduthuri, S. Waymire, and S. K. Srivastava, "Utilization of Dielectrophoresis for the Quantification of Rare Earth Elements Adsorbed on Cupriavidus necator," *ACS Sustainable Chemistry & Engineering,* vol. 8, no. 3, pp. 1353-1361, 2020/01/27 2020, doi: 10.1021/acssuschemeng.9b03878.

[31] N. Alinezhadbalalami, T. A. Douglas, N. Balani, S. S. Verbridge, and R. V. Davalos, "The feasibility of using dielectrophoresis for isolation of glioblastoma subpopulations with increased stemness," (in eng), *Electrophoresis,* vol. 40, no. 18-19, pp. 2592-2600, Sep 2019, doi: 10.1002/elps.201900026.

[32] H. Morgan and N. G. Green, *AC Electrokinetics Colloids and Nanoparticles*. 2003.

[33] Y. Feldman, I. Ermolina, and Y. Hayashi, "Time domain dielectric spectroscopy study of biological systems," *IEEE Trns. Dielectr. Electr. Insul.,* vol. 10, no. 5, pp. 728-753, 2003, doi: 10.1109/TDEI.2003.1237324.

[34] B. Bavnbek, B. Klösgen, J. Larsen, F. Pociot, and E. Renström, *BetaSys: Systems Biology of Regulated Exocytosis in Pancreatic Beta-Cells*. 2011.

[35] L. Yang, P. P. Banada, A. K. Bhunia, and R. Bashir, "Effects of Dielectrophoresis on Growth, Viability and Immuno-reactivity of Listeria monocytogenes," (in eng), *J Biol Eng,* vol. 2, pp. 6-6, 2008, doi: 10.1186/1754-1611-2-6.

[36] J. Zhang, Z. Song, Q. Liu, and Y. Song, "Recent advances in dielectrophoresis-based cell viability assessment," *ELECTROPHORESIS,* vol. 41, no. 10-11, pp. 917-932, 2020, doi: 10.1002/elps.201900340.

[37] V. Nerguizian, I. Stiharu, N. Al-Azzam, B. Yassine-Diab, and A. Alazzam, "The effect of dielectrophoresis on living cells: crossover frequencies and deregulation in gene expression," *The Analyst,* 10.1039/C9AN00320G vol. 144, no. 12, pp. 3853-3860, 2019, doi: 10.1039/C9AN00320G.

[38] J. Lu, C. A. Barrios, A. R. Dickson, J. L. Nourse, A. P. Lee, and L. A. Flanagan, "Advancing practical usage of microtechnology: a study of the functional consequences of dielectrophoresis on neural stem cells," (in eng), *Integr Biol (Camb),* vol. 4, no. 10, pp. 1223-1236, 2012, doi: 10.1039/c2ib20171b.

[39] M. J. Łos, A. Skubis, and S. Ghavami, "Chapter 2 - Stem Cells," in *Stem Cells and Biomaterials for Regenerative Medicine*, M. J. Łos, A. Hudecki, and E. Wiecheć Eds.: Academic Press, 2019, pp. 5-16.

[40] K. MacCord, ""Germ Layers"," ed. *Embryo Project Encyclopedia* 2013-09-17.

[41] W. Zakrzewski, M. Dobrzyński, M. Szymonowicz, and Z. Rybak, "Stem cells: past, present, and future," *Stem cell research & therapy,* vol. 10, no. 1, p. 68, 2019/02/26 2019, doi: 10.1186/s13287-019-1165-5.

[42] A. E. EL Barky AR, Mohamed TM, "Stem Cells, Classifications and their Clinical Applications," *American Journal of Pharmacology & Therapeutics,* vol. 1, no. 1, pp. 001-007, 2017.

[43] S. B. Hima Bindu A, "Potency of Various Types of Stem Cells and their Transplantation " *Journal of Stem Cell Research & Therapy* vol. 1, no. 3, p. 115, 2011.

[44] A. Biswas and R. Hutchins, "Embryonic stem cells," (in eng), *Stem Cells Dev,* vol. 16, no. 2, pp. 213-22, Apr 2007, doi: 10.1089/scd.2006.0081.

[45] R. Pethig, "Review Article—Dielectrophoresis: Status of the theory, technology, and applications," *Biomicrofluidics,* vol. 4, no. 2, p. 022811, 2010, doi: 10.1063/1.3456626.

[46] J. Yoshioka, Y. Ohsugi, T. Yoshitomi, T. Yasukawa, N. Sasaki, and K. Yoshimoto, "Label-Free Rapid Separation and Enrichment of Bone Marrow-Derived Mesenchymal Stem Cells from a Heterogeneous Cell Mixture Using a Dielectrophoresis Device," (in eng), *Sensors (Basel),* vol. 18, no. 9, 2018/09/08/ 2018, doi: 10.3390/s18093007.

[47] A. Y. Wu and D. M. Morrow, "Clinical use of Dieletrophoresis separation for live Adipose derived stem cells," *J Transl Med,* vol. 10, p. 99, 2012/05/17/ 2012, doi: 10.1186/1479-5876-10-99.

[48] L. A. Flanagan, J. Lu, L. Wang, S. A. Marchenko, and N. L. Jeon, "Unique dielectric properties distinguish stem cells and their differentiated progeny," *Stem Cells,* vol. 26, p. 656, 2008.

[49] J. Vykoukal, D. M. Vykoukal, S. Freyberg, E. U. Alt, and P. Gascoyne, "Enrichment of putative stem cells from adipose tissue using dielectrophoretic field-flow fractionation," *Lab Chip,* vol. 8, p. 1386, 2008.

[50] A. Bajek, N. Gurtowska, J. Olkowska, L. Kazmierski, M. Maj, and T. Drewa, "Adipose-Derived Stem Cells as a Tool in Cell-Based Therapies," (in eng), *Arch. Immunol. Ther. Exp. (Warsz.),* vol. 64, no. 6, pp. 443-454, 2016/12// 2016, doi: 10.1007/s00005-016-0394-x.

[51] P. O. Bagnaninchi and N. Drummond, "Real-time label-free monitoring of adipose-derived stem cell differentiation with electric cell-substrate impedance sensing," *Proc. Nat. Acad. Sci.,* vol. 108, p. 6462, 2011.

[52] "Rapid Analysis of Human Adipose- Derived Stem Cells and 3T3-L1 Differentiation Toward Adipocytes Using the Scepter™ 2.0 Cell Counter," *BioTechniques,* vol. 53, no. 2, pp. 109-111, 2012/08/01 2012, doi: 10.2144/000113910.

[53] G. H. Markx, L. Carney, M. Littlefair, A. Sebastian, and A. M. Buckle, "Recreating the hematon: microfabrication of artificial haematopoietic stem cell microniches in vitro using dielectrophoresis," (in eng), *Biomed Microdevices,* vol. 11, no. 1, pp. 143-50, Feb 2009, doi: 10.1007/s10544-008-9219-y.

[54] D. Y. Gao *et al.*, "Fundamental Cryobiology of Human Hematopoietic Progenitor Cells I: Osmotic Characteristics and Volume Distribution," *Cryobiology,* vol. 36, no. 1, pp. 40-48, 1998/02/01/ 1998, doi: https://doi.org/10.1006/cryo.1997.2060.

[55] A. I. Caplan, "Mesenchymal Stem Cells: Time to Change the Name!," *Stem Cells Translational Medicine,* vol. 6, pp. 1445-1451, 2017.

[56] S. D. Subramony *et al.*, "The guidance of stem cell differentiation by substrate alignment and mechanical stimulation," *Biomaterials,* Research Support, N.I.H., Extramural Research Support, Non-U.S. Gov't Research Support, U.S. Gov't, Non-P.H.S. vol. 34, no. 8, pp. 1942-53, Mar 2013, doi: 10.1016/j.biomaterials.2012.11.012.

[57] C. K. Kuo and R. S. Tuan, "Mechanoactive tenogenic differentiation of human mesenchymal stem cells," (in eng), *Tissue Eng Part A,* vol. 14, no. 10, pp. 1615-27, Oct 2008, doi: 10.1089/ten.tea.2006.0415.

[58] A. I. Goncalves *et al.*, "Understanding the Role of Growth Factors in Modulating Stem Cell Tenogenesis," *PLoS One,* vol. 8, no. 12, p. e83734, 2013.

[59] N. R. Schiele, J. E. Marturano, and C. K. Kuo, "Mechanical factors in embryonic tendon development: potential cues for stem cell tenogenesis," *Curr Opin Biotechnol,* Research Support, N.I.H., Extramural Research Support, Non-U.S. Gov't Review vol. 24, no. 5, pp. 834-40, Oct 2013, doi: 10.1016/j.copbio.2013.07.003.

[60] Y. H. Li *et al.*, "The Role of Scleraxis in Fate Determination of Mesenchymal Stem Cells for Tenocyte Differentiation," (in English), *Scientific Reports,* vol. 5, p. 13149, Aug 20 2015, doi: Artn 13149 10.1038/Srep13149.

[61] J. P. Brown, T. V. Galassi, M. Stoppato, N. R. Schiele, and C. K. Kuo, "Comparative analysis of mesenchymal stem cell and embryonic tendon progenitor cell response to embryonic tendon biochemical and mechanical factors," *Stem cell research & therapy,* vol. 6, no. 1, p. 89, 2015, doi: 10.1186/s13287-015-0043-z.

[62] M. T. Harris, D. L. Butler, G. P. Boivin, J. B. Florer, E. J. Schantz, and R. J. Wenstrup, "Mesenchymal stem cells used for rabbit tendon repair can form ectopic bone and express alkaline phosphatase activity in constructs," *J Orthop Res,* vol. 22, no. 5, pp. 998-1003, 2004.

[63] J. O. Jeong *et al.*, "Malignant tumor formation after transplantation of short-term cultured bone marrow mesenchymal stem cells in experimental myocardial infarction and diabetic neuropathy," *Circ Res,* vol. 108, no. 11, 2011.

[64] H. A. Awad, G. P. Boivin, M. R. Dressler, F. N. Smith, R. G. Young, and D. L. Butler, "Repair of patellar tendon injuries using a cell-collagen composite.," *J Orthop Res,* vol. 21, no. 3, pp. 420-31, 2003.

[65] J. Ge *et al.*, "The size of mesenchymal stem cells is a significant cause of vascular obstructions and stroke," (in eng), *Stem Cell Rev Rep,* vol. 10, no. 2, pp. 295-303, Apr 2014, doi: 10.1007/s12015-013-9492-x.

[66] L. Liu, L. Tseng, Q. Ye, Y. L. Wu, D. J. Bain, and C. Ho, "A New Method for Preparing Mesenchymal Stem Cells and Labeling with Ferumoxytol for Cell Tracking by MRI," *Scientific Reports,* vol. 6, no. 1, p. 26271, 2016/05/18 2016, doi: 10.1038/srep26271.

[67] S. M. Ridge, F. J. Sullivan, and S. A. Glynn, "Mesenchymal stem cells: key players in cancer progression," *Molecular Cancer,* vol. 16, no. 1, p. 31, 2017/02/01 2017, doi: 10.1186/s12943-017-0597-8.

[68] H. Y. Lee and I. S. Hong, "Double-edged sword of mesenchymal stem cells: Cancer-promoting versus therapeutic potential," (in eng), *Cancer Sci,* vol. 108, no. 10, pp. 1939-1946, Oct 2017, doi: 10.1111/cas.13334.

[69] U. Kozlowska *et al.*, "Similarities and differences between mesenchymal stem/progenitor cells derived from various human tissues," (in eng), *World J Stem Cells,* vol. 11, no. 6, pp. 347-374, 2019, doi: 10.4252/wjsc.v11.i6.347.

[70] M. F. Pittenger, D. E. Discher, B. M. Péault, D. G. Phinney, J. M. Hare, and A. I. Caplan, "Mesenchymal stem cell perspective: cell biology to clinical progress," *npj Regenerative Medicine,* vol. 4, no. 1, p. 22, 2019/12/02 2019, doi: 10.1038/s41536-019-0083-6.

[71] J. H. Sung *et al.*, "Isolation and characterization of mouse mesenchymal stem cells," (in eng), *Transplant. Proc.,* vol. 40, no. 8, pp. 2649-2654, 2008/10// 2008, doi: 10.1016/j.transproceed.2008.08.009.

[72] M. Baddoo *et al.*, "Characterization of mesenchymal stem cells isolated from murine bone marrow by negative selection.," *J Cell Biochem,* vol. 89, p. 1235, 2003, doi: 10.1002/jcb.10594.

[73] Y. Zhao *et al.*, "Electrical Property Characterization of Neural Stem Cells in Differentiation," *PLOS ONE,* vol. 11, no. 6, p. e0158044, 2016, doi: 10.1371/journal.pone.0158044.

[74] Y. Liu *et al.*, "Identification of neural stem and progenitor cell subpopulations using DC insulator-based dielectrophoresis," (in en), *The Analyst,* vol. 144, no. 13, pp. 4066-4072, 2019/06/24/ 2019, doi: 10.1039/C9AN00456D.

[75] R. Schweitzer *et al.*, "Analysis of the tendon cell fate using Scleraxis, a specific marker for tendons and ligaments," (in eng), *Development,* vol. 128, no. 19, pp. 3855-66, Oct 2001. [Online]. Available: http://www.ncbi.nlm.nih.gov/pubmed/11585810.

[76] Y. Ito *et al.*, "The Mohawk homeobox gene is a critical regulator of tendon differentiation," (in eng), *Proc Natl Acad Sci U S A,* vol. 107, no. 23, pp. 10538-42, Jun 8 2010, doi: 1000525107 [pii]10.1073/pnas.1000525107.

[77] K. Otabe *et al.*, "Transcription factor Mohawk controls tenogenic differentiation of bone marrow mesenchymal stem cells in vitro and in vivo," *J Orthop Res,* vol. 33, no. 1, pp. 1-8, Jan 2015, doi: 10.1002/jor.22750.

[78] Z. Yin *et al.*, "Single-cell analysis reveals a nestin+ tendon stem/progenitor cell population with strong tenogenic potentiality," *Science advances,* vol. 2, no. 11, p. e1600874, Nov 2016, doi: 10.1126/sciadv.1600874.

[79] S. K. Theodossiou, J. B. Murray, and N. R. Schiele, "Cell-cell junctions in developing and adult tendons," *Tissue Barriers,* vol. 8, no. 1, 2020, doi: https://doi.org/10.1080/21688370.2019.1695491.

[80] S. H. Richardson, T. Starborg, Y. Lu, S. M. Humphries, R. S. Meadows, and K. E. Kadler, "Tendon development requires regulation of cell condensation and cell shape via cadherin-11-mediated cell-cell junctions," (in English), *Mol Cell Biol,* vol. 27, no. 17, pp. 6218-28, 2007. [Online]. Available: <Go to ISI>://MEDLINE:17562872.

[81] R. L. Stanley, R. A. Fleck, D. L. Becker, A. E. Goodship, J. R. Ralphs, and J. C. Patterson-Kane, "Gap junction protein expression and cellularity: comparison of immature and adult equine digital tendons," *J Anat,* vol. 211, pp. 325-334, 2007.

[82] D. E. Leckband and J. de Rooij, "Cadherin adhesion and mechanotransduction," *Annual review of cell and developmental biology,* vol. 30, pp. 291-315, 2014, doi: 10.1146/annurev-cellbio-100913-013212.

[83] A. D. Waggett, M. Benjamin, and J. R. Ralphs, "Connexin 32 and 43 gap junctions differentially modulate tenocyte response to cyclic mechanical load," (in English), *Eur J Cell Biol,* vol. 85, no. 11, pp. 1145-1154, Nov 2006, doi: Doi 10.1016/J.Ejcb.2006.06.002.

[84] J. R. Ralphs, M. Benjamin, A. D. Waggett, D. C. Russell, K. Messner, and J. Gao, "Regional differences in cell shape and gap junction expression in rat Achilles tendon: relation to fibrocartilage differentiation," *J Anat,* vol. 193, pp. 215-222, 1998.

[85] S. K. Theodossiou, J. Tokle, and N. R. Schiele, "TGFbeta2-induced tenogenesis impacts cadherin and connexin cell-cell junction proteins in mesenchymal stem cells," *Biochemical and biophysical research communications,* vol. 508, no. 3, pp. 889-893, Jan 15 2019, doi: 10.1016/j.bbrc.2018.12.023.

[86] S. A. Oberlender and R. S. Tuan, "Expression and functional involvement of N-cadherin in embryonic limb chondrogenesis," *Development,* Research Support, Non-U.S. Gov't Research Support, U.S. Gov't, P.H.S. vol. 120, no. 1, pp. 177-87, Jan 1994. [Online]. Available: http://www.ncbi.nlm.nih.gov/pubmed/8119125.

[87] L. W. Dunne, T. Iyyanki, J. Hubenak, and A. B. Mathur, "Characterization of dielectrophoresis-aligned nanofibrous silk fibroin-chitosan scaffold and its interactions with endothelial cells for tissue engineering applications," *Acta Biomater,* vol. 10, no. 8, pp. 3630-3640, 2014, doi: 10.1016/j.actbio.2014.05.005.

[88] L. M. Galatz, L. Gerstenfeld, E. Heber-Katz, and S. A. Rodeo, "Tendon regeneration and scar formation: The concept of scarless healing," *J Orthop Res,* vol. 33, no. 6, pp. 823-31, Jun 2015, doi: 10.1002/jor.22853.

[89] K. Howell *et al.*, "Novel Model of Tendon Regeneration Reveals Distinct Cell Mechanisms Underlying Regenerative and Fibrotic Tendon Healing," *Sci Rep,* vol. 7, p. srep45238, 2017.

[90] S. Thomopoulos, W. C. Parks, D. B. Rifkin, and K. A. Derwin, "Mechanisms of tendon injury and repair," *J Orthop Res,* vol. 33, no. 6, pp. 832-839, 2015.

[91] H. L. Moser *et al.*, "Genetic lineage tracing of targeted cell populations during enthesis healing," *J Orthop Res,* vol. 36, pp. 3275-3284, 2018.

[92] R. Yoshida *et al.*, "Murine supraspinatus tendon injury model to identify the cellular origins of rotator cuff healing," *Connect Tissue Res,* vol. 57, no. 6, pp. 507-515, 2016.

[93] C. Ulbrich *et al.*, "The impact of simulated and real microgravity on bone cells and mesenchymal stem cells," (in eng), *Biomed Res Int,* vol. 2014, p. 928507, 2014, doi: 10.1155/2014/928507.

[94] D. Grimm *et al.*, "The effects of microgravity on differentiation and cell growth in stem cells and cancer stem cells," *STEM CELLS Translational Medicine,* vol. n/a, no. n/a, doi: 10.1002/sctm.20-0084.

[95] E. A. Blaber *et al.*, "Microgravity Reduces the Differentiation and Regenerative Potential of Embryonic Stem Cells," (in eng), *Stem Cells Dev,* vol. 24, no. 22, pp. 2605-21, Nov 15 2015, doi: 10.1089/scd.2015.0218.

[96] R. P. Schwarz, T. J. Goodwin, and D. A. Wolf, "Cell culture for three-dimensional modeling in rotating-wall vessels: an application of simulated microgravity," (in eng), *J Tissue Cult Methods,* vol. 14, no. 2, pp. 51-7, 1992, doi: 10.1007/bf01404744.

[97] S. L. Wuest, S. Richard, S. Kopp, D. Grimm, and M. Egli, "Simulated Microgravity: Critical Review on the Use of Random Positioning Machines for Mammalian Cell Culture," *BioMed Research International,* vol. 2015, p. 971474, 2015/01/14 2015, doi: 10.1155/2015/971474.

Chapter 4: Electrophysiological Characterization of Mesenchymal Stem Cells Differentiating into Tenocytes via Dielectrophoresis

Anthony T. Giduthuri[1], Sophia K. Theodossiou[1], Nathan R. Schiele[1], Soumya K. Srivastava[1,*]

[1]Department of Chemical & Biological Engineering, University of Idaho, Moscow, ID. 83844-1021 USA.

Abstract

Tenocytes or tendon cells are responsible for holding a muscle and a bone in mammals. It is also a major component of the musculoskeletal system. Tendons are susceptible to injuries such as tendonitis, Achilles tendon, etc., due to the effects of aging and stress. Stem cell-based therapies offer alternative methods to treat such conditions. Out of various types of stem cells, mesenchymal stem cells (MSCs), a type of multipotent cell, are known for their ability to regenerate and differentiate. Undifferentiated MSCs derived from the bone marrow of mouse, are characterized for dielectric properties (conductivity and permittivity) of their outer membrane and cytoplasm using the dielectrophoretic crossover technique. Undifferentiated MSCs (baseline) are then treated with growth factors to induce differentiation (tenogenesis) into tenocytes and are characterized for dielectric properties on day 3 of differentiation (3d-TGFβ2) to detect changes in the membrane and cytoplasm, along with undifferentiated cells and undifferentiated cells aged to day 3 (3d- control) as controls. Treated cell groups at time points Day 1 and Day 7 into differentiation are also studied for changes. Experimental results are statistically analyzed for their significance and modeled using a single shell model to quantify the dielectric properties, using which differentiation changes can be detected as early as 3 days of treatment . This difference in the dielectric properties at different time points Day 1, Day 3 and Day 7 enables the separation of cells in a label freeway avoiding complications involved with current separation techniques such as FACS and MACS. This work primarily focuses on characterizing the undifferentiated (day 0, 1 and 3) and differentiating cells (day 1 and 3).

Keywords: Dielectrophoresis, dielectric properties, mesenchymal stem cells, tendons, tenogenesis.

4.1 Introduction

Mesenchymal stem cells (MSCs) are multipotent cells that are known for their ability to differentiate and self-renew into various types of cells such as adipocytes [2], chondrocytes [3], osteoblasts [4, 5], myocytes [2, 6], tenocytes [7]. Since the discovery of MSCs in the 1960s [8], MSCs gradually established as standard cell line in the field of regenerative medicine [9]. Bone marrow is a predominant source of MSCs [10]. MSCs are also available by isolating from other sources such as adipose tissue, skin, peripheral blood, and perinatal tissues like umbilical cord blood, amniotic fluid, fetal membrane [11, 12] and placenta [13]. MSCs offer promising therapy to treat several conditions related to cardiovascular health [14-16] and other chronic conditions such as lupus, diabetes mellitus, liver cirrhosis, and Crohn's disease [17]. A study published in 2016 states that at least 493 MSC based clinical trials are completed or being investigated according to National Institutes of Health [18]. Like most stem cell populations, MSCs are heterogenous [17, 19] with diameters ranging widely from 15-30 μm, this considerable variance in size is also known to be the cause for severe vascular obstructions and stroke in animal models [20]. MSCs that are derived from different sources such as adipose tissue, amniotic tissue, bone marrow, chorionic tissue, liver, and umbilical cord had distinct differentiation potentials based on their source of origin which also should be considered for clinical applications [21]. Therefore, it is necessary to sort the heterogenous population of MSCs prior to clinical trials.

Current conventional stem cell separation techniques widely used and commercially available can be classified into two categories a) techniques based on physical parameters like size, density such as density gradient centrifugation, field-flow fractionation, etc., and b) techniques based on affinity-based on chemical, electrical or magnetic couplings such fluorescence-activated cell sorting (FACS) [22], magnet-activated cell sorting (MACS) [23]. Dielectrophoresis (DEP) [24] and flow cytometry [25] fall under the category of electrical affinity based techniques where DEP based sorting is much sought due its robustness and separation in label free way. . Size/density based separation techniques are time-consuming, expensive, and requires prior knowledge of the size/density parameter of the target cell type [24], Further, their inability to sort cells of same density and size regardless of them being distinct in their physiological make-up, is a major limitation. In order to overcome these limitations, affinity-based methods were developed, which include FACS and MACS. FACS is currently used for cell sorting [10] which involves labeling of cells with antibodies coated with fluorescent dyes and magnetic beads (for MACS). They require tedious cell preparation protocol, and are labor-intensive, expensive with high operating costs [24, 26]. This type of cell labeling technique also alters cellular function, which is not desirable [17].

In this thesis, we are exploring a possibility of utilizing DEP to sort the differentiated MSCs from their heterogenous population. DEP based methods are simple, cost-effective, label-free, accurate, and quick that overcomes all the limitations associated with the conventional cell separation methods. The application of DEP for stem cell research began in 1990's [27-29] and has significantly progressed over the past two decades. DEP was less explored to characterize stem cells and their differentiate progeny until the last decade [30]. Flanagan *et al.* in 2008 researched heavily on the dielectric properties of stem cells and their differentiated lineage[30]. DEP has a slight disadvantage of affecting cell viability when exposed to electric fields within the frequency range of 0.01- 1MHz for prolonged duration (5 – 30 min) [17], but is known that shorter exposure times of 30 s – 1 min does not affect cell viability and their metabolism substantially [31].

On the other hand, while FACS and MACS offer limited throughput of ~5000 cells/s and 280,000 cells/s respectively [32], DEP assisted sorting devices can progress to transplantation scale of ~10^9 cells, using at least four passages at 150,000 cells /hr of sorting throughput per passage. [32]. DEP was first applied in an clinical setting for hand atrophy correction by lipo-transfer using stromal vascular cells (SVF) that was successful and was found to be safe [33].

This work presented in Chapter 5 is the primary step towards developing a novel sorting technique for differentiated MSCs i.e., the dielectric characterization of both membrane and cytoplasm at cellular level using DEP crossover technique is critical and significant to separate stem cells from their differentiated tenogenic progeny.

4.2 Theory of DEP

DEP is the force observed on the dielectric particles when subjected to a non-uniform AC electric field as a result of the difference in the polarizability of the medium and the particles [34, 35]. For a spherical particle of radius *r*, the magnitude of DEP force is given as

$$\vec{F}_{DEP} = 2\pi r^3 \varepsilon_o \varepsilon_m Re[K(\omega)]\nabla E^2 \qquad (1)$$

where ε_o and ε_m are the permittivity of the free space and the relative permittivity of the surrounding medium respectively, $Re[K(\omega)]$ is the real part of the Clausius-Mosotti factor which is discussed below in equation (2) and ∇E^2 signifes the gradient of electric field. The force acting on the cells can be tuned by adjusting the frequency and magnitude of the electric field. Cell motion due to the force acting on the cell under electric field is defined by Clausius-Mossotti factor, $K(\omega)$ given by:

$$K(\omega) = \frac{\varepsilon^*_{cell} - \varepsilon^*_{med}}{\varepsilon^*_{cell} + 2\varepsilon^*_{med}} \quad (2)$$

where ε^*_{cell} and ε^*_{med} are complex permittivities of cell and the medium respectively. Complex permittivity, ε^* is defined as

$$\varepsilon^* = \varepsilon - j\frac{\sigma}{\omega} \quad (3)$$

where ε is permittivity, σ is conductivity, and ω is the angular frequency of the applied electric field. For spherical particles, $Re[K(\omega)]$ ranges between -0.5 and 1 accounting for the polarizability of the particle [34, 36]. Further estimation of dielectric properties using the determined complex permittivities of membrane and cytoplasm, to calculate ε^*_{cell} and thereby $K(\omega)$ using equation . requires an appropriate shell model. Biological shell models can be classified into single shell, double or multi shell models, ellipsoidal model whichh are discussed in detail[1, 37]. We modelled MSCs in this study using single shell model.

4.2.1 Single shell model

In here single shell model is considered. Stem cells' cytoplasm and its content i.e., nucleus, DNA, organelles etc., are considered as one homogenous sphere surrounded by a plasma membrane to reduce complexity (Figure 4.1). For a single-shell model, complex permittivity of a cell is given by [37, 38]:

$$\varepsilon^*_{cell} = \varepsilon^*_{mem}\left[\frac{\left(\frac{R}{R-d}\right)^3 + 2\left(\frac{\varepsilon^*_{cyt} - \varepsilon^*_{mem}}{\varepsilon^*_{cyt} + 2\varepsilon^*_{mem}}\right)}{\left(\frac{R}{R-d}\right)^3 - \left(\frac{\varepsilon^*_{cyt} - \varepsilon^*_{mem}}{\varepsilon^*_{cyt} + 2\varepsilon^*_{mem}}\right)}\right] \quad (4)$$

where R is the outer radius of the cell, d the thickness of the membrane, and the subscripts *mem*, *cyt* refer to the membrane and cytoplasm respectively.

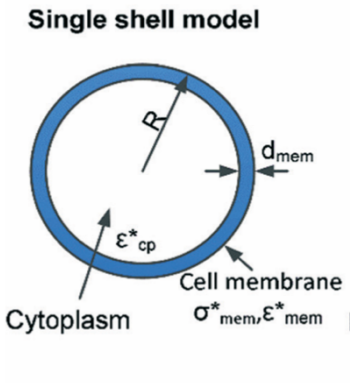

Figure 4.1: Single shell model of a cell where ε and σ denote permittivity and conductivity respectively. Subscripts mem, cp refer to the properties of membrane, and cytoplasm respectively[1]. (Reproduced with permission [1]).

DEP force is dependent on the frequency of the applied electric field. As frequency is tuned maintaining a fixed peak-to-peak voltage, cells exhibit distinct behavior based on their polarizability. When polarizability of the cell is greater than the medium in which it is suspended, the cell experiences attraction towards high field electrode termed as 'positive dielectrophoresis (pDEP)' and when the polarizability of the cell is less than that of the medium, cells move away from the high field electrode, thus experiencing a force termed as 'negative dielectrophoresis (nDEP)' [39]. There exists a certain frequency at which the cell experiences no net DEP force, which is termed as 'crossover frequency' [40]. Cells typically display two crossover frequencies, where the lower crossover frequency (f_{x1}), also refered as the first crossover frequency occurs in β region (kHz to several MHz) where cells transition from nDEP to pDEP, and signifies the cell's size, shape, and the outer membrane physiology [17]. The higher crossover frequency(f_{x2}), also referred as the second crossover frequency, occurs at frequencies above 10 MHz in low conductive medium [17], where cells transition from pDEP back to nDEP and is sensitive to the changes of the cell's interior physiology, especially with those associated with nucleus and the relative size of the nucleus to the cell's volume. It is also found that the changes in the conductivity of the suspending media did not effect the f_{x2} [41] but affects f_{x1}, where f_{x1} is directly proportional to the medium conductivity [42].

A direct relation correlating, the f_{x1} with the membrane capacitance, C_{mem} and medium conductivity is given by [17, 36]:

$$f_{x1} = \frac{\sqrt{2}\sigma_m}{2\pi r C_{mem}} \qquad (5)$$

Using C_{mem} calculated from equation (5), permittivity of the membrane (ε_{mem}) can be obtained using the relation:

$$\varepsilon_{mem} = \frac{C_{mem}d}{4\pi r^2 \varepsilon_0} \quad (6)$$

where '*d*' is the thickness of the membrane, and ε_0 is the permittivity of the vaccum/free space – 8.854×10^{-12} F/m . In order to estimate the dielectric properties of the cell interior i.e., cytoplasm, the following relation is used as given by Gimsa *et al.* [42].

$$f_{x2}^2 = \frac{1}{4\pi^2}\frac{1}{\varepsilon_o^2}\frac{(\sigma_m-\sigma_{cyto})(\sigma_{cyto}+2\sigma_m)}{(\varepsilon_{cyto}-\varepsilon_m)(\varepsilon_{cyto}+2\varepsilon_m)} \quad (7)$$

Using the above mentioned equations, dielectric properties of membrane and cytoplasm can be estimated using the experimentally determined crossover frequencies. However, further optimization of these estimated dielectric parameters is required which is achieved through curve fitting and non-linear regression, where initial estimates of dielectric properties are used to back-calculate the crossover frequency (labeled theoretical) and then optimizing by minimizing the sum of squares error using non-linear regression. The properties estimated can then be used to determine the DEP characteristic curve to determine optimum sorting region.

4.3 Materials & Methods

This study involves culturing of MSCs suiting the planned experimental design which involves Day 1, Day 3 and Day 7 undifferentiated and treated cells with TGFβ2 (6 cell groups in total, combing the undifferentiated and the treated) whose culturing in described in detail in section 4.3.1. Following the culturing process, comes the DEP experiments which involves DEP Solution to suspend the cells, and crossover frequency experiments as discussed in section 4.3.2 and 4.3.3. Experimental results are then statistically analyzed using GraphPad Prism 8, and radial changes in cells are also determined using Image J, whose methodology is discussed in sections 4.3.4 and 4.3.5 respectively. Curve fitting procedure in determining the best-fit estimates is also discussed in section 4.3.6.

4.3.1 Cell culture

Murine MSCs (C3H10T1/2, ATCC, Manassas, VA), a model MSC used in prior studies investigating tenogenesis [43, 44], are cultured and supplemented with transforming growth factor beta-2 (TGFβ2), a protein that is known to control various cellular functions by binding to the surface proteins of cell, which triggers transmission of signals within cell and is known to induce tenogenesis as

previously described [45]. Briefly, cells are expanded in standard growth medium (Dulbecco's Modified Eagle's Medium (DMEM), 10% fetal bovine serum (FBS), and 1% Penicillin/Streptomycin) until 70% confluent, and used between passage 3 and 9. MSCs are trypsinized, and are seeded into each well of a 6-well plate at 5000 cells/cm^2. Cells are incubated for 24 h to allow for initial cell attachment, and then washed with warm phosphate buffered saline (PBS) (Gibco, Grand Island, NY). The cells are now switched to low-serum medium (DMEM, 1% FBS, 1% Penicillin/Streptomycin), and allowed to equilibrate for 24 h. Following equilibration, cells are rinsed with warm PBS and cultured for 0, 3, or 7 days (d) in low-serum medium with the corresponding amount of sterile water (vehicle controls) or low-serum medium supplemented with 50 ng/mL recombinant human TGFβ2 (PeproTech, Rocky Hill, NJ). The medium is changed every third day. To collect the cells for DEP characterization experiments, cells are washed in warm PBS and trypsinized for 3 min to ensure cell detachment from the well. The trypsin is neutralized using low-serum medium, and cells are centrifuged at 1200 RPM for 8 min. The supernatant is discarded, and the cell pellet is resuspended to approximately 10^6 cells/mL in DEP solution (Section 4.3.2) of known standard which serves as medium for DEP experiments, estimated properties varies based on the standards of this medium and hence plays a major role in DEP experiments. The suspended cell pellet obtained is to be used for DEP experiments within 30 min of trypsinization. Experiments are repeated a minimum of 3 times for each sample of MSC.

4.3.2 DEP Solution

DEP suspending medium properties (conductivity) is one of the important parameters that affects the cell's response to the experimental first crossover frequency. It is necessary to maintain the medium ideally at isotonic conditions in order to avoid shrinking, swelling, or lysis of the cells being suspended. A standardized DEP suspending medium (50 g/L) is prepared by dissolving 1.25 g of D-glucose in 25 ml of DI water. The pH of the buffer is maintained between 6.5 – 7. Conductivity of the medium is adjusted to ~0.060 S/m using sodium chloride crystals. Conductivity of the DEP solution is maintained consistent throughout the experiments. All experiments are performed at room temperature of 70^0 F.

4.3.3 DEP Experiment Setup

Physical DEP experimental setup involves a microscope to monitor changes in motion of the cells as frequency is tuned, a DEP microwell to suspend the cells and a function generator to tune the frequency. Experimental setup for this study is shown in Figure 4.3. The most primary step towards DEP experiments is fabrication of the microwell, using soft-lithography technique. This technique is termed 'soft' owning to the usage of elastomeric polymers in fabricating the microwell, post fabrication

steps involves electrode setup, and sealing with appropriate spacing. This process is discussed in detail in Section 4.3.3a below.

a) Microwell fabrication

~30 g of Sylgard 184 silicone elastomer (Dow Corning, Midland, MI, USA) is weighed using a weighing balance (XS204, Mettler Toledo) and mixed with the accompanying curing agent (~3 g) at 10:1 ratio. The mixture is degassed in a degassing chamber to ensure no air bubbles are trapped in the mixture, clear mixture is then poured into a petridish and is cured at 75 ºC in a sterile polystyrene petri dish (100 mm × 15 mm). The cured poly(dimethylsiloxane) (PDMS) is cooled and cut into ~6 X 6 mm^2 pieces followed by a microwell punched with a 3 mm Miltex biopsy punch. The PDMS piece with microwell is plasma cleaned using our in-house plasma cleaner [46] and sealed onto a pre-cleaned microslide (25 mm × 75 mm, 1.0 mm thick). This process is a slightly modified version compared to the previously mentioned process [47, 48]. High grade platinum (Pt) wire (99.5%, 0.2 mm diameter) is cut into 15 mm pieces and are inserted perpendicularly into the microwell such that wires are approximately on the same plane as that of the microslide. These Pt wires serve as the electrodes delivering a non-uniform electric field gradient for the DEP crossover frequency experiments, a simple figure showing the electrode setup in included (Figure 4.2). Spacing between the electrodes is adjusted to ~75 µm by using a microscope (Olympus IX-71 inverted microscope) and the electrode wires are sealed using epoxy to permanently fix the distance between the two point and planar electrodes. However it was noticed that occasionally the spacing was altered due to the pipette's in and out motion from the microwell (i.e., when rinsing the microwell); the spacing was adjusted back to the initial spacing in such cases and care was taken at the beginning of every experiment to verify and re-measure the electrode distance.

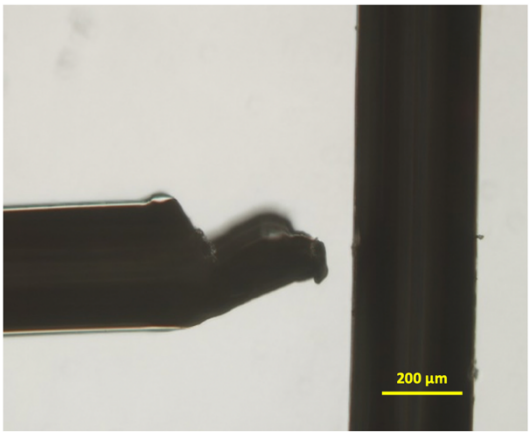

Figure 4.2: Sample Image showing sealed electrode setup of point and planar with ~75 µm electrode spacing in the DEP microwell.

b) DEP crossover frequency experiments

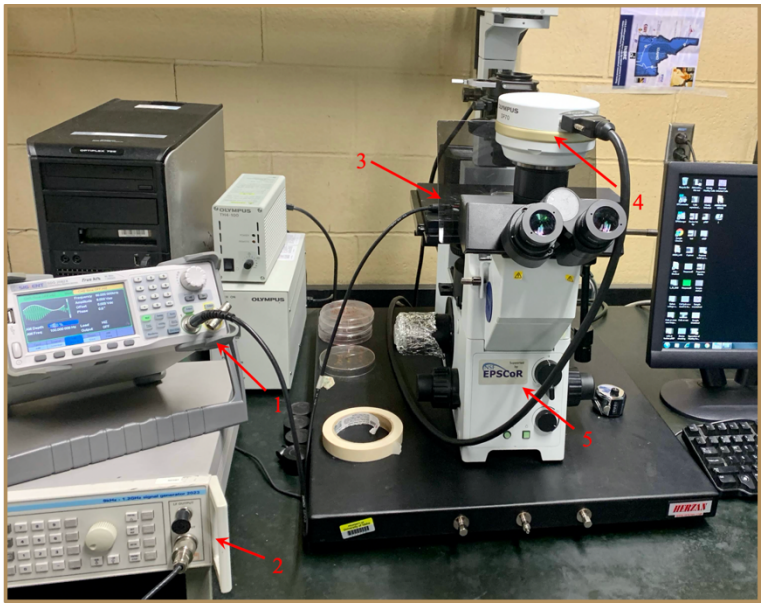

Figure 4.3: Image showing the experimental setup 1) Function Generator (Upto 80 MHz), f_{x1} experiments. 2) Function Generator (upto 1200 MHz), f_{x2} experiments. 3) Plane on which DEP microwell is placed. 4) Camera to record/visualize the experiments. 5) Olympus IX-71 Inverted Microscope.

The platinum electrodes in the microwell are connected to a waveform function generator (Siglent SDG 2082X) and electrical signals at a voltage of 8 $V_{p\text{-}p}$ are supplied to the microwell to create non-uniform electric field. Frequency is swept until the lower crossover frequency f_{x1}, is found where no noticeable motion is seen in the cells. The above used function generator, SDG 2082X cannot sweep frequencies higher than 80 MHz and hence the higher crossover frequency, f_{x2} experiments are done using a different function generator (Marconi Instruments, 9 kHz – 1.2 GHz signal generator 2023) at 13 decibel milliwatts (dBM) equivalent to ~2.825 $V_{p\text{-}p}$ voltage to experimentally determine the higher crossover frequency where second transition of pDEP to nDEP is noticed. Once after the frequency range of transition is determined, further frequency is fine-tuned to narrow down the range so as to determine the single frequency (integer) value. Experiments are repeated at least 6 times for all the stem cell groups, undifferentiated MSCs (controls), 3-day differentiated MSCs (treatment group), and 3-day aged undifferentiated MSCs (no treatment group) to determine the average crossover frequencies (f_{x1} and f_{x2}) at single DEP suspending medium conductivity (~0.06 S/m). Experiments are also done on Day 0 & Day 7 undifferentiated and differentiated cell groups.

4.3.4 Statistical Analysis

Obtained f_{x1} and f_{x2} through experiments are analyzed separately using one-way ANOVA and Welch's t-test (GraphPad Prism version 8.4.3 for Mac, GraphPad Software, San Diego, CA, USA) respectively. All the reported values in this study are expressed as mean± S.E (standard error).

4.3.5 Image Processing

Images captured during experiments are analyzed using ImageJ [49] to measure the stem cell size of all the different groups i.e., control, treatment, and no-treatment. Cell diameter is measured manually by setting up the scale and using straight segmented line. Further, area of the cells is also measured using 'Analyze Particle' tool and subsequently radius of each cell is obtained. At least six images corresponding to the crossover experiments are analyzed for each cell type to obtain the mean cell radius.

4.3.6 Curve-fitting procedure

Obtained experimental crossover frequencies, and the initial estimates for the parameters to be quantified, permittivity and conductivity are then used to theoretically estimate the crossover frequency using Equation and adjusted using non-linear regression to minimize the residual sum of squares error (difference between experimental and theoretical crossover frequencies) using Microsoft Excel. Initial estimates for the parameters are calculated using equations 5 and 6 for the membrane characteristics and for the cytoplasmic properties initial estimates are obtained from literature.

4.4 Results & Discussion

4.4.1 DEP crossover frequency response of stem cells

DEP crossover frequency response of the undifferentiated (baseline control), undifferentiated aged to day 3 (3d- no treatment) and differentiating cells at day 3 time point (3d- TGFβ2-treatment) were recorded after suspending the cells in the DEP suspending medium of conductivity 0.06 S/m. At a fixed voltage of 8 V_{pp}, frequency was swept from 0.01 MHz to 0.5 MHz in increments of 0.005 MHz and 2.83 Vpp, 1 MHz to 300 MHz in increments of 5 MHz to record f_{x1} and f_{x2} respectively. All experiments were completed within 30 min of suspending the stem cells in DEP suspending medium and the cells were not exposed to AC electric field for no longer than a minute at each frequency point. Post 1 min of cell exposure, the microwell is rinsed well with DEP suspending medium and 2 μL of fresh cell suspension from the same sample aliquot is pipetted into the microwell. This protocol is

followed for all the cell groups. Finally, after 30 min the samples are treated with 70 % EtOH solution followed by bleach and discarded. No change in cell viability and metabolic activity in human and mouse neural stem/progenitor cells is noticed at shorter exposure times of 30 s to 1 min [17, 31]. In general, mammalian cells exhibit nDEP at low frequencies and pDEP at higher frequencies, within the

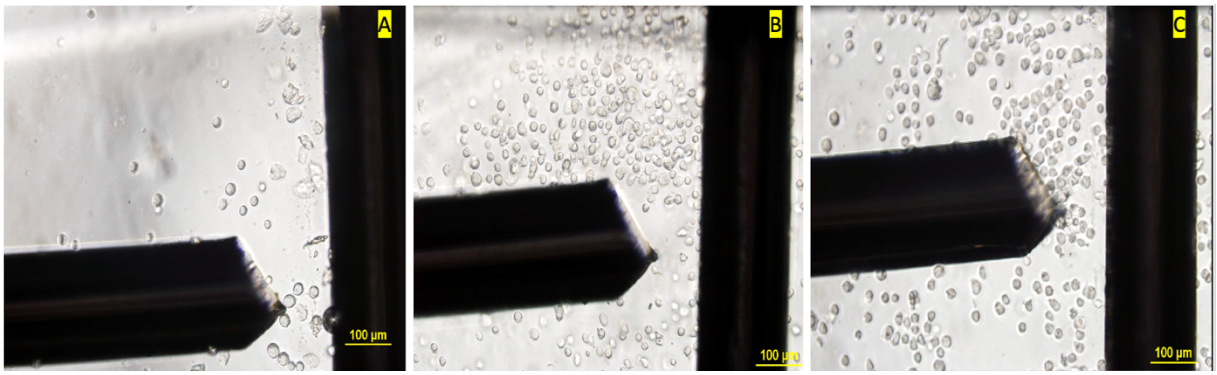

Figure 4.4: Images describing movement of cells away and towards the high electric field region i.e. nDEP and pDEP for cell groups. A) Baseline cells- control group experiencing pDEP at 105 kHz and 8 Vpp, B) 3 d-no treatment group experiencing nDEP.at 110 kHz and 8 Vpp C) 3 day treatment group with TGFβ2 i.e., differentiating into tenocytes experiencing pDEP at 200 kHz and 8 Vpp.

frequency range of 0.01 MHz -1 MHz [50] i.e., β-region. This similar trend is also observed while characterizing dielectric differences in murine cells under normal and cancerous condition [51]. Mean crossover frequencies are observed to be 0.0986 ± 0.0003 MHz, 0.134 ± 0.003MHz, and 0.175 ± 0.007 MHz for control, 3 d - no treatment, and 3d- treatment with TGFβ2 groups in this experimental study at 0.06 S/m medium conductivity and voltage of 8 Vpp. Day 0 and Day 7 untreated cells had crossover frequency ranging from 100-110 kHz and 135-150 kHz respectively at 0.06 S/m and 8 Vpp, no morphological changes are noticed for these cell groups. These reported frequencies were not repeatable and chosen not to be reported, since further experiments are needed to model these cell groups. For the day 1 and day 7 treated cells, day 1's experimental values were not repeatable, and day 7 cells appeared more elongated with crossover values of 110-130 kHz for smaller elongated cells while the large ones had values ranging between 50-70 kHz. It is expected that Day 1 treated and untreated will not significantly differ from the Day 0, which is statistically proven through their insignificance ($p > 0.1$). Day 7 crossover frequency for the treated cells groups failed in statistically significance as the values appeared close to the Day 0 cells. Hence these time points require further experiments. Day 7 will need to be modeled as ellipsoidal rather than spherical single shell model, which is complex.

4.4.2 Variance in cell size

Image analysis using ImageJ as discussed in Section 4.3.5, resulted in the following cell dimensions as provided in Table 4.1. Baseline cells are spherical in shape, and the sphericity is retained in both 3 day no treatment and 3 day- treatment with TGFβ2 cell groups as well, which is in agreement with the previously reported study where the cells remained spherical until 4 days of culturing [52].

Table 4.1: Various studies reporting sizes of MSCs derived from different sources.

Radius (in μm) of Mesenchymal stem cells					
		Baseline-control	**3d- no treatment**	**3d- treatment**	**Reference**
Current study (murine)		8.91± 0.09	10.10 ± 0.1914	10.11± 0.2109	
Adams *et al*. (human)		13.2			[17, 37]*
Velugotla *et al.* (human embryonic stem cells differentiating into MSCs)	H1-MSCs	7.5±1.55			[53]
	H9-MSCs	6.25±1.1			
Liu, L. *et al* (murine)		8.6 ± 0.95			[52]

*Adams *et al* 2014. does not cite size in the article, reported value was calculated and reported [32].

4.4.3 Quantification of dielectric properties

a) Statistical analysis of data

Analysis of categorical independent variables (three different cell groups for 3-day time period) and numerical dependent variable (f_{x1}) using One-way ANOVA resulted in significant different lower crossover frequencies for every group ($P < 0.05$). Unpaired t-test with Welch correction of f_{x2} data comparing undifferentiated cells with 3 day differentiated and 3 day undifferentiated resulted in a significant difference between the undifferentiated cells and the 3d differentiated ones ($P < 0.05$). However, undifferentiated cells and the 3d aged undifferentiated were not statistically significant, meaning that they had similar f_{x2} which signifies the electrophysiology of the cell's interior/cytoplasm.

b) Initial estimates for modeling

Initial estimates and their bounds effect the final estimated values. Hence, good initial guess reduces the time of estimating the final dielectric property values significantly. A bad guess my result in errors, such as negative R^2 or $R^2>1$, Inf or Imaginary values. It is also equally possible, to have the

final calculated values outside the bounds, which might not be true values. Hence fixing the bounds to large range for example cytoplasmic relative permittivity bounds can be fixed to 1-500 range, not fixing the range might result in values that doesn't comply with previous studies. Once a good close estimate is arrived, the sum of squares can be minimized using optimization algorithm by changing the estimated values, until the error is minimized. The values are considered to be final and best fit estimates, at the least possible sum of squares error, considering them to be optimized values. All the initial values are tabulated as shown in Table 4.2. In an effort to estimate the best fit values with minimal residual error, bounds are fixed to the initial values.

Table 4.2: Initial estimates of dielectric parameters used prior to non-linear regression for obtaining the best-fit parameters by minimizing the residual error; values for membrane are obtained from [17], cytoplasmic conductivity range is modified to 0.30-3.0 based on two different journal articles [40, 54].

Cell component	**Permittivity**	**Conductivity (S/m)**
Membrane	6.5 – 11	10^{-3} – 10^{-8}
Cytoplasm	50 – 100	0.30 – 1.5

c) Modeling of membrane properties

Membrane dielectric properties are initially estimated using equations 5 and 6 and are adjusted for best fit to obtain the mean values with the respective standard errors. A nominal membrane thickness of 7 nm is used in quantifying the dielectric properties of the membrane [37, 55].

The estimated electrical properties of the membrane are tabulated in Table 4.3 where a decreasing trend is observed for both the permittivity and capacitance of all the three groups. Though the 3d- no treatment and 3d-treatment with TGFβ2 radial changes are not significantly different from each other in terms of size and sphericity, 3 day- treatment group expressed higher f_{x1} values, resulting in lower permittivity and capacitance. This difference in membrane's capacitance and permittivity might be due to the onset of tenogenesis, or an increased rate of change in the membrane's protein expression due to the treatment of cells with a specific growth factor TGFβ2.

Table 4.3: Estimated membrane's electrical properties using DEP spherical single shell model, Mean ± S.E are reported for all the cell groups.

Property	Control	3d- no treatment	3d- treatment
Whole cell Capacitance (pF)	3.83 ± 0.012	3.19 ± 0.08	2.46 ± 0.1
Relative Permittivity	3.03 ± 0.01	1.97 ± 0.05	1.51 ± 0.06

d) Modeling of cytoplasmic parameters

Following the procedure described in Sec. 4.3.3b, cytoplasmic properties are quantified using the experimentally obtained f_{x2} as tabulated in Table 4.4.

Table 4.4: Cytoplasmic properties obtained through the fitting procedure described in Sec 4.3.6 using equation 7, where the 3d-TGFβ2 shows a decrease in cytoplasmic conductivity.

Type of cell	Conductivity(S/m)	Permittivity $(\varepsilon_{cell}/\varepsilon_0)$
Baseline- Control group	0.88 ± 0.01	55 ± 2
3 d- no treatment	0.88 ±0.02	55± 1
3-d TGFβ2	0.82± 0.02	62± 1

The second crossover frequency is highly sensitive to ion-leakage, and not so sensitive to permittivity of the cell's interior [37]. f_{x2} is also sensitive to temperature changes to the DEP solution[41] and lag time between experimenting and suspending the cells in the DEP suspending medium. Experimental values of f_{x2} are within ± 5 MHz, while the technical replicates (n=6) for each group did not change when the time lag between suspending cells in DEP media and experimenting was under 30 min along with shorter exposure times to electric fields at less than a minute. Statistical analysis of f_{x2} for control group and the 3 day- no treatment cells had no significant difference at $p<0.05$ which is also the trend observed for cytoplasmic conductivity. 3 day – treatment with TGFβ2 cell group exhibited higher f_{x2} than 3 day - no treatment and control cell groups. This is due to the fact that neither size nor shape affects f_{x2} [36]. Lower conductivity and increased permittivity of 3 day- treatment with

TGFβ2 cell group might be sign of the onset of tenogenesis associated with the cytoplasmic changes where these cells become more polarizable, also signifying cellular heterogeneity in cytoplasm.

4.4.4 Comparison of theoretical model to experimental frequencies

In order to graphically represent the theoretical model of single shell sphere (Equation 4) to the experimental frequencies, the following plots (Figure 4.5) is included plotting the theoretical curve to the experimental Re[K(ω)], which is determined by the different frequencies at which experiments are run for all the cell groups i.e. baseline, 3d untreated and 3d treated cell groups. The datapoints starts to skew as the frequency is increased due to a single conductivity experiment. For more accurate model, experiments at different conductivities should be done with subsequent curve-fitting to accurately determine the parameters to be used in the theoretical model. Since the f_{x2} experiments were run at a different voltage (2.83 Vpp) to that of the f_{x1} experiments (8 Vpp). This can be perhaps avoided by using mathematical approach of interpolating the properties at a particular voltage when two sets of experiments at two different voltages are conducted.

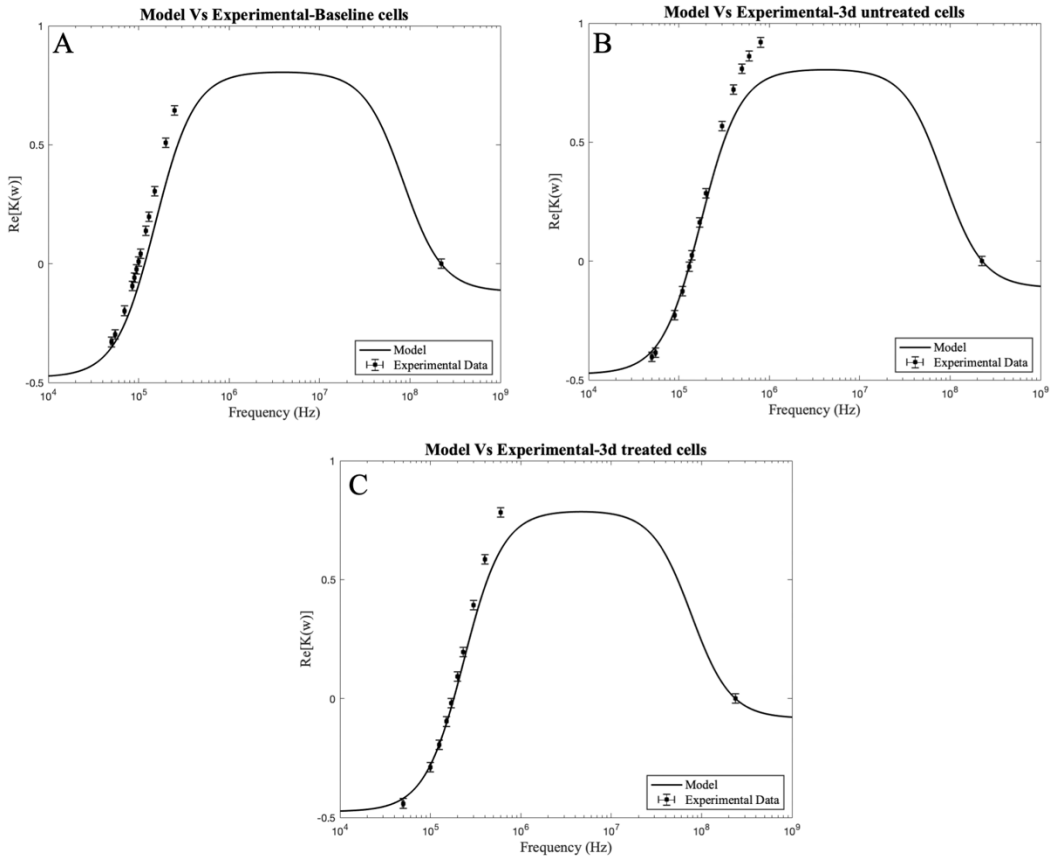

Figure 4.5: Plots comparing theoretical single shell spherical model to the experimentally determined Re[K(ω)], A) Baseline cells B) 3d untreated cells C) 3d treated cells. Horizontal error bar of ±5 kHz for f_{x1} is included and the respective error in Re[K(ω)] (y-axis) is represented.

4.4.5 Effect on Clausius-Mossotti factor as a function of frequency

A plot of Re[K(ω)] over frequency range, 10^4 Hz– 10^9 Hz (10 kHz – 1000 MHz) is generated to better understand the DEP characteristic behavior over the wide frequency range. All the positive y-axis

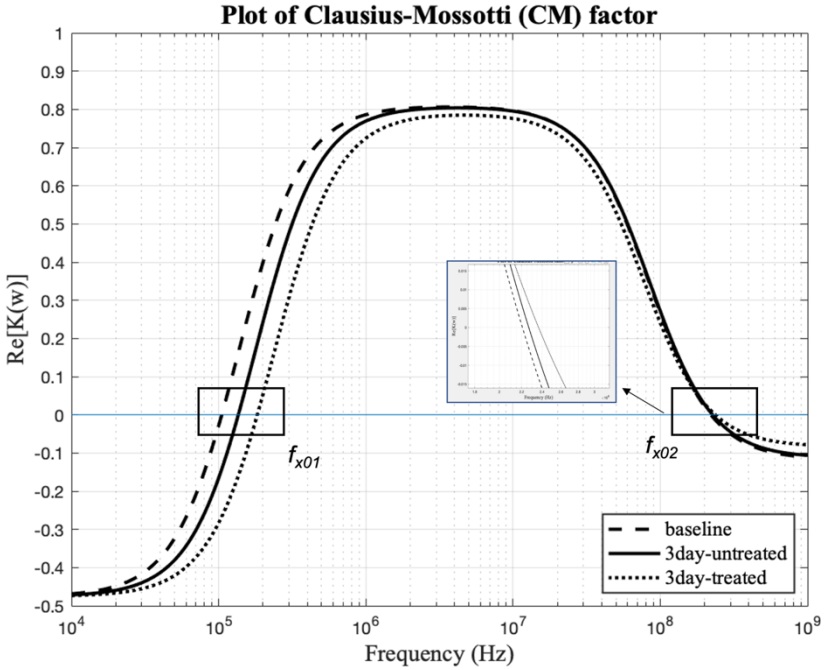

Figure 4.6: DEP characteristic plot of Re[K(ω)] vs. frequency identifying the first and second crossover frequency i.e., the co-ordinates at which the zero line intersects the curves provides the crossover frequency value.

values represent the pDEP behavior of the cells and all the negative y-axis values represent nDEP response of the cells. Crossover frequency values can also be estimated using the zero DEP line i.e., y-axis at 0, and there by estimating the dielectric properties. Dielectric properties can also be estimated using Re[K(ω)] values [56]. Figure 4.6 helps in determining sorting zone using AC fields to efficiently separate the cells based on their distinct size, shape and dielectric properties. Frequencies ranging close to first crossover frequency (f_{x1}) can be used to sort the cells based on figure 4.1, where the cell groups exhibit distinct behavior, which is indicated through distinctly non-intersecting curves. Inset image is a zoomed version at frequencies close to f_{x2}. The curves appear to be merging, which is not the actual case and hence an inset is used to describe the difference signifying the distinct characteristics of the cytoplasm. f_{x2} frequency can only be used to study the cells but not for sorting, as such high frequency as not easily accessible and damages membrane's structure.

4.5 Conclusion

Though using DEP based techniques in a clinical setting requires further multiple studies including different animal models with extensive investigation, it is seen to have the potential of being developed into modern day label free separation devices, that can enrich, isolate cells stem cells effectively to be used in treat injuries and diseases. Studies show that tendon like tissue is observed from MSCs after 21 days of treatment [57], further studies are required to characterize a complete tendon cell to better understand the electrophysiology associated with cytoplasm as a cell grows from an MSC to a complete tendon (21 days time point). This study hypothesizes that 3 day- no treatment and control groups did not exhibit variance in their cytoplasmic properties, which also needs further experiments and modeling to firmly state this especially since f_{x2} values account for temperature, ion leakage, changes of nucleaus volume This study progresses cytoplasmic characterization to a step ahead, since there not a lot of studies using DEP ultra high frequency characterization, as the higher frequency ranges are not easily accesible. The DEP second crossover regime still remains largely unexplored. The distinct properties of MSCs reveal their biophysical identity which can be used to separate cells based on the difference in their intrinsic electrical properties . It can be concluded that baseline cells are smaller in size than the 3 day treatment and no treatment groups. However, the treatment group of cells did not exhibit large variance in their radius on day 3, though the cells remained similar in size and shape, exhibited different crossover frequencies, signifying a change in membrane and cytoplasmic expressions. Smaller cells usually exhibit lower-first crossover frequency, which when applied to this scenario, 3d-control and 3d-TGFβ2 should have had lower first crossover frequency due to their large cell radii if their dielectric properties had remained similar. This also describes a difference in the membrane nature between Day 3 no treatment undifferentiated cells and Day 3 differentiating tenocytes. Understanding cellular level changes during differentiation is complex and requires sophisticated techniques. However, using DEP higher crossover frequency, cytoplasmic changes can be studied to better understand changes within nucleus and its content. This study characterized MSCs and their differentiating progeny (tenocytes) to obtain the dielectric properties, which can be extended to develop a stem cell sorter to efficiently filter differentiating/differentiated MSCs from non-viable cells and undifferentiated cells in a label free way at low cost which can be taken to transplantation scale through further studies.

References

[1] E. O. Adekanmbi and S. K. Srivastava, "Dielectrophoretic applications for disease diagnostics using lab-on-a-chip platforms," *Lab Chip,* vol. 16, p. 2148, 2016.

[2] M.-q. Du *et al.*, "Characterization and Differentiation into Adipocytes and Myocytes of Porcine Bone Marrow Mesenchymal Stem Cells," *Journal of Integrative Agriculture,* vol. 13, no. 4, pp. 837-848, 2014/04/01/ 2014, doi: https://doi.org/10.1016/S2095-3119(13)60497-9.

[3] R. A. Somoza, J. F. Welter, D. Correa, and A. I. Caplan, "Chondrogenic differentiation of mesenchymal stem cells: challenges and unfulfilled expectations," (in eng), *Tissue Eng Part B Rev,* vol. 20, no. 6, pp. 596-608, Dec 2014, doi: 10.1089/ten.TEB.2013.0771.

[4] H. Hanna, L. M. Mir, and F. M. Andre, "In vitro osteoblastic differentiation of mesenchymal stem cells generates cell layers with distinct properties," (in eng), *Stem cell research & therapy,* vol. 9, no. 1, p. 203, Jul 27 2018, doi: 10.1186/s13287-018-0942-x.

[5] C. Hildebrandt, H. Büth, S. Cho, n. Impidjati, and H. Thielecke, "Detection of the osteogenic differentiation of mesenchymal stem cells in 2D and 3D cultures by electrochemical impedance spectroscopy," *J. Biotechnol.,* vol. 148, p. 83, 2010.

[6] X. Guo *et al.*, "Cardiomyocyte differentiation of mesenchymal stem cells from bone marrow: new regulators and its implications," (in eng), *Stem cell research & therapy,* vol. 9, no. 1, p. 44, Feb 26 2018, doi: 10.1186/s13287-018-0773-9.

[7] Q. W. Wang, Z. L. Chen, and Y. J. Piao, "Mesenchymal stem cells differentiate into tenocytes by bone morphogenetic protein (BMP) 12 gene transfer," (in eng), *J Biosci Bioeng,* vol. 100, no. 4, pp. 418-22, Oct 2005, doi: 10.1263/jbb.100.418.

[8] A. J. Friedenstein, K. V. Petrakova, A. I. Kurolesova, and G. P. Frolova, "Heterotopic of bone marrow. Analysis of precursor cells for osteogenic and hematopoietic tissues," (in eng), *Transplantation,* vol. 6, no. 2, pp. 230-247, 1968/03// 1968. [Online]. Available: http://europepmc.org/abstract/MED/5654088.

[9] A. Bajek, N. Gurtowska, J. Olkowska, L. Kazmierski, M. Maj, and T. Drewa, "Adipose-Derived Stem Cells as a Tool in Cell-Based Therapies," (in eng), *Arch. Immunol. Ther. Exp. (Warsz.),* vol. 64, no. 6, pp. 443-454, 2016/12// 2016, doi: 10.1007/s00005-016-0394-x.

[10] J. Yoshioka, Y. Ohsugi, T. Yoshitomi, T. Yasukawa, N. Sasaki, and K. Yoshimoto, "Label-Free Rapid Separation and Enrichment of Bone Marrow-Derived Mesenchymal Stem Cells from a Heterogeneous Cell Mixture Using a Dielectrophoresis Device," (in eng), *Sensors (Basel),* vol. 18, no. 9, 2018/09/08/ 2018, doi: 10.3390/s18093007.

[11] K. S. Shin *et al.*, "Characterization of Fetal Tissue-derived Mesenchymal Stem Cells," (in eng), *Int J Stem Cells,* vol. 2, no. 1, pp. 51-8, May 2009, doi: 10.15283/ijsc.2009.2.1.51.

[12] M. Soncini *et al.*, "Isolation and characterization of mesenchymal cells from human fetal membranes," (in eng), *J Tissue Eng Regen Med,* vol. 1, no. 4, pp. 296-305, Jul-Aug 2007, doi: 10.1002/term.40.

[13] M. J. Łos, A. Skubis, and S. Ghavami, "Chapter 2 - Stem Cells," in *Stem Cells and Biomaterials for Regenerative Medicine*, M. J. Łos, A. Hudecki, and E. Wiecheć Eds.: Academic Press, 2019, pp. 5-16.

[14] Y. Guo, Y. Yu, S. Hu, Y. Chen, and Z. Shen, "The therapeutic potential of mesenchymal stem cells for cardiovascular diseases," *Cell Death & Disease,* vol. 11, no. 5, p. 349, 2020/05/11 2020, doi: 10.1038/s41419-020-2542-9.

[15] M. F. Pittenger and B. J. Martin, "Mesenchymal Stem Cells and Their Potential as Cardiac Therapeutics," *Circulation Research,* vol. 95, no. 1, pp. 9-20, 2004, doi: doi:10.1161/01.RES.0000135902.99383.6f.

[16] H. Shen, Y. Wang, Z. Zhang, J. Yang, S. Hu, and Z. Shen, "Mesenchymal Stem Cells for Cardiac Regenerative Therapy: Optimization of Cell Differentiation Strategy," *Stem Cells International,* vol. 2015, p. 524756, 2015/08/03 2015, doi: 10.1155/2015/524756.

[17] T. N. G. Adams, P. A. Turner, A. V. Janorkar, F. Zhao, and A. R. Minerick, "Characterizing the dielectric properties of human mesenchymal stem cells and the effects of charged elastin-like polypeptide copolymer treatment," (in eng), *Biomicrofluidics,* vol. 8, no. 5, p. 054109, 2014/09// 2014, doi: 10.1063/1.4895756.

[18] T. Squillaro, G. Peluso, and U. Galderisi, "Clinical Trials With Mesenchymal Stem Cells: An Update," (in eng), *Cell Transplant,* vol. 25, no. 5, pp. 829-48, 2016, doi: 10.3727/096368915x689622.

[19] M. Pevsner-Fischer, S. Levin, and D. Zipori, "The origins of mesenchymal stromal cell heterogeneity," (in eng), *Stem Cell Rev Rep,* vol. 7, no. 3, pp. 560-8, Sep 2011, doi: 10.1007/s12015-011-9229-7.

[20] J. Ge *et al.*, "The size of mesenchymal stem cells is a significant cause of vascular obstructions and stroke," (in eng), *Stem Cell Rev Rep,* vol. 10, no. 2, pp. 295-303, Apr 2014, doi: 10.1007/s12015-013-9492-x.

[21] E. Schmelzer, D. T. McKeel, and J. C. Gerlach, "Characterization of Human Mesenchymal Stem Cells from Different Tissues and Their Membrane Encasement for Prospective Transplantation Therapies," *BioMed Research International,* vol. 2019, 2019.

[22] Z. Hewitt, N. R. Forsyth, M. Waterfall, D. Wojtacha, A. J. Thomson, and J. McWhir, "Fluorescence-activated single cell sorting of human embryonic stem cells," (in eng), *Cloning Stem Cells,* vol. 8, no. 3, pp. 225-34, Fall 2006, doi: 10.1089/clo.2006.8.225.

[23] B. A. Sutermaster and E. M. Darling, "Considerations for high-yield, high-throughput cell enrichment: fluorescence versus magnetic sorting," *Sci Rep,* vol. 9, no. 1, p. 227, 2019/01/18 2019, doi: 10.1038/s41598-018-36698-1.

[24] B. Zhu and S. K. Murthy, "Stem Cell Separation Technologies," *Curr Opin Chem Eng,* vol. 2, no. 1, pp. 3-7, 2014, doi: 10.1016/j.coche.2012.11.002.

[25] A. Castagnola, S. Eda, and J. L. Jurat-Fuentes, "Monitoring stem cell proliferation and differentiation in primary midgut cell cultures from Heliothis virescens larvae using flow cytometry," *Differentiation,* vol. 81, no. 3, pp. 192-198, 2011/03/01/ 2011, doi: https://doi.org/10.1016/j.diff.2010.12.001.

[26] N. Abd Rahman, F. Ibrahim, and B. Yafouz, "Dielectrophoresis for Biomedical Sciences Applications: A Review," *Sensors (Basel),* vol. 17, no. 3, 2017/02/24/ 2017, doi: 10.3390/s17030449.

[27] Y. Huang, J. Yang, X. B. Wang, F. F. Becker, and P. R. Gascoyne, "The removal of human breast cancer cells from hematopoietic CD34+ stem cells by dielectrophoretic field-flow-fractionation," (in eng), *J Hematother Stem Cell Res,* vol. 8, no. 5, pp. 481-490, 1999, doi: 10.1089/152581699319939.

[28] M. Stephens, M. S. Talary, R. Pethig, A. K. Burnett, and K. I. Mills, "The dielectrophoresis enrichment of CD34+ cells from peripheral blood stem cell harvests," (in eng), *Bone Marrow Transplant,* vol. 18, no. 4, pp. 777-82, Oct 1996.

[29] M. S. Talary, K. I. Mills, T. Hoy, A. K. Burnett, and R. Pethig, "Dielectrophoretic separation and enrichment of CD34+cell subpopulation from bone marrow and peripheral blood stem cells," *Medical and Biological Engineering and Computing,* vol. 33, no. 2, pp. 235-237, 1995/03/01 1995, doi: 10.1007/BF02523050.

[30] L. A. Flanagan *et al.*, "Unique dielectric properties distinguish stem cells and their differentiated progeny," (in eng), *Stem Cells,* vol. 26, no. 3, pp. 656-665, 2008/03// 2008, doi: 10.1634/stemcells.2007-0810.

[31] J. Lu, C. A. Barrios, A. R. Dickson, J. L. Nourse, A. P. Lee, and L. A. Flanagan, "Advancing practical usage of microtechnology: a study of the functional consequences of dielectrophoresis on neural stem cells," (in eng), *Integr Biol (Camb),* vol. 4, no. 10, pp. 1223-1236, 2012, doi: 10.1039/c2ib20171b.

[32] M. G. Simon, Y. Li, J. Arulmoli, L. P. McDonnell, and A. Akil, "Increasing label-free stem cell sorting capacity to reach transplantation-scale throughput," *Biomicrofluidics,* vol. 8, p. 064106, 2014.

[33] A. Y. Wu and D. M. Morrow, "Clinical use of Dieletrophoresis separation for live Adipose derived stem cells," *J Transl Med,* vol. 10, no. 1, p. 99, 2012/05/17 2012, doi: 10.1186/1479-5876-10-99.

[34] B. Yafouz, N. A. Kadri, and F. Ibrahim, "Dielectrophoretic Manipulation and Separation of Microparticles Using Microarray Dot Electrodes," *Sensors (Basel),* vol. 14, no. 4, pp. 6356-6369, 2014/04/03/ 2014, doi: 10.3390/s140406356.

[35] P.-Y. Weng, I. A. Chen, C.-K. Yeh, P.-Y. Chen, and J.-Y. Juang, "Size-dependent dielectrophoretic crossover frequency of spherical particles," *Biomicrofluidics,* vol. 10, no. 1, 2016/02/11/ 2016, doi: 10.1063/1.4941853.

[36] R. Pethig, A. Menachery, S. Pells, and P. DeSousa, "Dielectrophoresis: A Review of Applications for Stem Cell Research," *J Biomed Biotechnol,* vol. 2010, no. 182581, pp. 1-7, 2010, doi: 10.1155/2010/182581.

[37] R. R. Pethig, *Dielectrophoresis: Theory, Methodology and Biological Applications*. 2017.

[38] E. O. Adekanmbi and S. K. Srivastava, "Dielectric characterization of bioparticles via electrokinetics: The past, present, and the future," *Applied Physics Reviews,* vol. 6, no. 4, p. 041313, 2019, doi: 10.1063/1.5113709.

[39] G. N. Morgan H, "Dielectrophoresis," in *Encyclopedia of Microfluidics and Nanofluids*. New York: Springer Science, 2014, pp. 1-11.

[40] J. Gimsa, P. Marszalek, U. Loewe, and T. Y. Tsong, "Dielectrophoresis and electrorotation of neurospora slime and murine myeloma cells," (in eng), *Biophysical journal,* vol. 60, no. 4, pp. 749-760, 1991, doi: 10.1016/S0006-3495(91)82109-9.

[41] C. Chung, M. Waterfall, S. Pells, A. Menachery, S. Smith, and R. Pethig, "Dielectrophoretic Characterisation of Mammalian Cells above 100 MHz," (in English), *Journal of Electrical Bioimpedance,* vol. 2, no. 1, p. 64, 2011, doi: https://doi.org/10.5617/jeb.196.

[42] J. Gimsa, P. Marszalek, U. Loewe, and T. Y. Tsong, "Dielectrophoresis and electrorotation of neurospora slime and murine myeloma cells," *Biophys. J.,* vol. 60, p. 749, 1991.

[43] B. A. Pryce, S. S. Watson, N. D. Murchison, J. A. Staverosky, N. Dünker, and R. Schweitzer, "Recruitment and maintenance of tendon progenitors by TGFβ signaling are essential for tendon formation," *Development,* vol. 136, no. 8, pp. 1351-1361, 2009, doi: 10.1242/dev.027342.

[44] A. Scott, P. Danielson, T. Abraham, G. Fong, A. V. Sampaio, and T. M. Underhill, "Mechanical force modulates scleraxis expression in bioartificial tendons," (in eng), *J Musculoskelet Neuronal Interact,* vol. 11, no. 2, pp. 124-32, Jun 2011.

[45] S. K. Theodossiou, J. Tokle, and N. R. Schiele, "TGFβ2-induced tenogenesis impacts cadherin and connexin cell-cell junction proteins in mesenchymal stem cells," *Biochemical and biophysical research communications,* vol. 508, no. 3, pp. 889-893, 2019/01/15/ 2019, doi: https://doi.org/10.1016/j.bbrc.2018.12.023.

[46] E. O. Adekanmbi, J. Dustin, and S. K. Srivastava, "Electro-osmotic surface effects generation in an electrokinetic-based transport device: A comparison of RF and MW plasma generating sources," *Electrophoresis,* vol. 40, no. 11, pp. 1573-1579, Jun 2019, doi: 10.1002/elps.201800464.

[47] K. L. Chiok, N. C. Paul, E. O. Adekanmbi, S. K. Srivastava, and D. H. Shah, "Dimethyl adenosine transferase (KsgA) contributes to cell-envelope fitness in Salmonella Enteritidis," (in eng), *Microbiol Res,* vol. 216, pp. 108-119, 2018, doi: 10.1016/j.micres.2018.08.009.

[48] E. O. Adekanmbi, M. W. Ueti, B. Rinaldi, C. E. Suarez, and S. K. Srivastava, "Insulator-based dielectrophoretic diagnostic tool for babesiosis," (in eng), *Biomicrofluidics,* vol. 10, no. 3, pp. 033108-033108, 2016, doi: 10.1063/1.4954196.

[49] C. A. Schneider, W. S. Rasband, and K. W. Eliceiri, "NIH Image to ImageJ: 25 years of image analysis," *Nature Methods,* vol. 9, no. 7, pp. 671-675, 2012/07/01 2012, doi: 10.1038/nmeth.2089.

[50] D. M. Vykoukal, P. R. Gascoyne, and J. Vykoukal, "Dielectric characterization of complete mononuclear and polymorphonuclear blood cell subpopulations for label-free discrimination," (in eng), *Integr Biol (Camb),* vol. 1, no. 7, pp. 477-84, Jul 2009, doi: 10.1039/b906137a.

[51] P. R. C. Gascoyne, J. Noshari, F. F. Becker, and R. Pethig, "Use of dielectrophoretic collection spectra for characterizing differences between normal and cancerous cells," *IEEE Trans. Industry Appl.,* vol. 30, p. 829, 1994.

[52] L. Liu, L. Tseng, Q. Ye, Y. L. Wu, D. J. Bain, and C. Ho, "A New Method for Preparing Mesenchymal Stem Cells and Labeling with Ferumoxytol for Cell Tracking by MRI," *Sci Rep,* vol. 6, no. 1, p. 26271, 2016/05/18 2016, doi: 10.1038/srep26271.

[53] S. Velugotla, S. Pells, H. K. Mjoseng, C. R. E. Duffy, and S. Smith, "Dielectrophoresis based discrimination of human embryonic stem cells from differentiating derivatives," *Biomicrofluidics,* vol. 6, p. 44113, 2012.

[54] Y. Zhao *et al.*, "Electrical Property Characterization of Neural Stem Cells in Differentiation," *PLOS ONE,* vol. 11, no. 6, p. e0158044, 2016, doi: 10.1371/journal.pone.0158044.

[55] T. N. G. Adams, A. Y. L. Jiang, P. D. Vyas, and L. A. Flanagan, "Separation of neural stem cells by whole cell membrane capacitance using dielectrophoresis," (in en), *Methods,* vol. 133, pp. 91-103, 2018/01/15/ 2018, doi: 10.1016/j.ymeth.2017.08.016.

[56] Y. J. Lo *et al.*, "Derivation of the cell dielectric properties based on Clausius-Mossotti factor," *Applied Physics Letters,* vol. 104, no. 11, p. 113702, 2014, doi: 10.1063/1.4869480.

[57] J. Y. Lee *et al.*, "BMP-12 treatment of adult mesenchymal stem cells in vitro augments tendon-like tissue formation and defect repair in vivo," *PloS one,* vol. 6, no. 3, pp. e17531-e17531, 12/10/received 02/03/accepted 3/18/entrez 3/18/pubmed7/6/medline 2011.

Chapter 5: Dielectrophoretic ultrahigh frequency characterization and *in-silico* sorting on uptake of rare earth elements by *Cupriavidus necator*

Anthony T. Giduthuri[1], Ezekiel O. Adeknambi[1], James G. Moberly[1], Soumya K. Srivastava[1*]

[1]Department of Chemical & Materials Engineering, University of Idaho, Moscow, ID. 83843.

(Submitted to *Electrophoresis* Journal for publication under Special Issue)

Abstract

Rare earth elements (REEs) are widely used across different industries due to their exceptional magnetic and electrical properties. In this work *Cupriavidus necator (C. necator)* is characterized using dielectrophoretic ultra-high frequency measurements, typically in MHz range to quantify the properties of cytoplasm in *C. necator* for its metal accumulation capacity. *C. necator,* a gram-negative bacteria strain is exposed to REEs like europium, samarium, and neodymium in this study. Dielectrophoretic crossover frequency experiments were performed on the native *C. necator* species pre- and post-exposure to the REEs at MHz frequency range. The net conductivity of native *C. necator*, *C-europium, C-samarium, and C-neodymium* are 16.56 µS/cm, 16.78 µS/cm, 16.67 µS/cm, and 16.20 µS/cm respectively. The estimated properties of the membrane in our previous study are used to develop a microfluidic sorter by modeling and simulation to separate REE absorbed *C. necator* from the unabsorbed native *C. nec*ator species using COMSOL Multiphysics commercial software package v5.5. The optimal AC potential was obtained to be 9.5 V at fixed AC frequency of 100 kHz.

5.1 Introduction

Rare earth elements (REEs) are lanthanide group elements (Atomic number 57- 71) along with Scandium, Sc (Atomic number 21) and Yttrium, Y (Atomic number 39). These are sub classified into three categories as light REEs (La, Ce, Pr, and Nd), medium REEs (Sm, Eu, Gd), and heavy REEs (rest of the lanthanide group and Y) [1]. These elements are widely used across technology industry due to their distinct electrical, magnetic, chemical, and optical properties [2] with applications in metallurgy industry as metal alloys [3], catalysts [4], biomedical devices [5], etc. Hence recovery of REEs from waste streams and end of the life products is an attractive technology. Recovery of REEs was studied previously using extraction [6, 7] but possess environmental concerns. This proves the need for developing greener methods of REE extraction. Several research studies have been published to extract REEs through different biological mechanisms, especially using bacteria as discussed elsewhere [8, 9].

Sorption of these REE ions by the microorganism can occur through two possible ways: bioaccumulation (active) and/or biosorption (passive). Bioaccumulation is absorption of the metal ions into the living organism and is regulated by its metabolic activity while passive biosorption can occur on the surface of both living and dead organisms independent of the organism's metabolic activity [9].

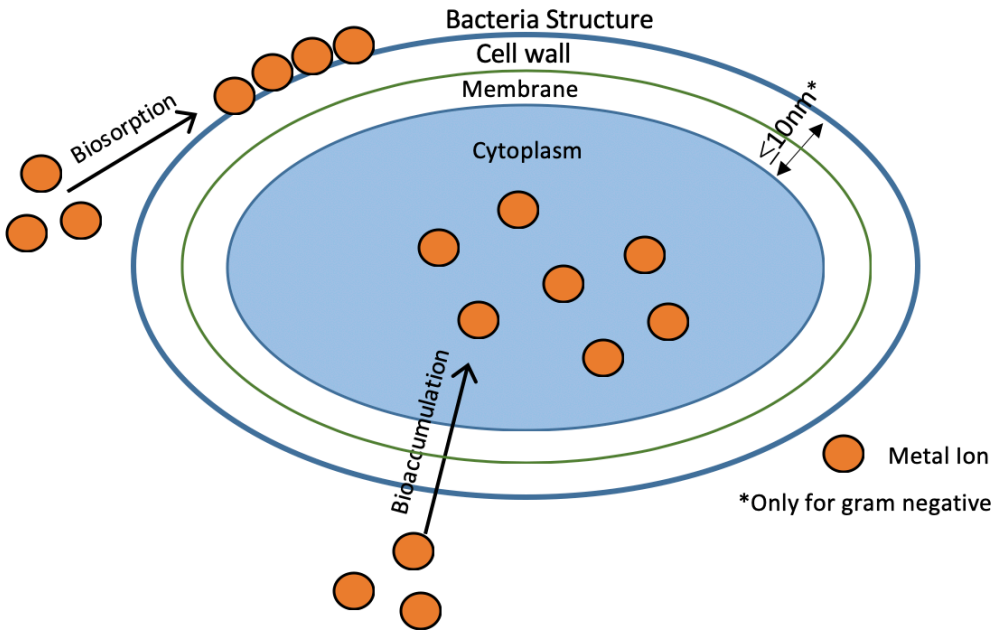

Figure 5.1: Bacteria model demonstrating the phenomena of bioaccumulation and biosorption, where bioaccumulation results in metal ions migrating into the cytoplasm passing through the cell wall and biosorption is an accumulation of metal ions on the surface of bacteria. i.e. membrane.

Bioaccumulation results in the change of the organisms's electrical properties and biosorption will change both the membrane and cytoplasm electrical properties. Both bioaccumulation and biosorption explained above are demonstrated in Figure 5.1, for reader's understanding.

In this work dielectrophoresis (DEP) is utilized to characterize the bacteria's cytoplasmic (interior) conductivity linking to the genomic variation observed due to the REE uptake by them. DEP dates back to the 1950's [10] but has gained popularity during the last decade for its potential in biomedical applications [11, 12]. Recently, DEP is explored for its applicability in non-biomedical fields like in separation of minerals [13]. This study is the first report that utilizes DEP to characterize a gram-negative bacterium in both its native and REE exposed states at high frequency. This paper determines the net conductivity of the organism, and also provides an *in-silico* model to sort the native and REE

exposed bacteria from a heterogenous population of *C. necator*. Until now, DEP was used to quantify the REE adsorbed by the *Cupriavidus necator (C. necator)* on its surface by quantifying the DEP first crossover frequency to obtain properties related to the cell-wall [14].

5.2 Dielectrophoresis Theory

Dielectrophoresis (DEP) is the induced motion on dielectric particles due to non-homogenous (non-uniform) electric field gradient using alternating current (AC) [15]. DEP has been used in particle separation [16], enrichment [17], manipulation [18], quantification [14] and several other biomedical applications [12]. It's a non-destructive and label/marker free electrokinetic technique to determine the electrical signatures. Some of the popular methods which employ DEP to characterize and quantify the dielectric signatures of the cells are electrorotation, zero force method (also termed as crossover frequency method), DEP spectra, capture voltage spectra, traveling wave which were well discussed in a recent review article by our research group [19].

The technique used in this current work is the DEP crossover frequency quantification at ultrahigh frequency ranges to characterize the cytoplasmic properties (genotypic information) of the *C. necator*. The transition from negative DEP (nDEP) to positive DEP (pDEP) and vice versa is termed as the first and second crossover frequency respectively which is described in detail [19, 20]. Positive dielectrophoresis occurs when the particles move towards the high electric field gradient, if the particle is more polarizable than the medium. Negative dielectrophoresis occurs when the particle is less polarizable than the suspending medium where it moves away from the high electric field maxima to a low field minima [21, 22].

Broche *et al*. in 2005 [23] obtained an expression to quantify the second crossover frequency as given below

$$f_{co2} = \frac{1}{2\pi}\sqrt{\frac{\sigma_{cyto}^2 - \sigma_{cyto}\sigma_m - 2\sigma_m^2}{2\varepsilon_m^2 - \varepsilon_{cyto}\varepsilon_m - \varepsilon_{cyto}^2}} \qquad (1)$$

The subscript *cyto* and *m* refers to the properties of the cytoplasm and suspending medium respectively, whereas σ denotes the conductivity and ε denotes the permittivity of the particle i.e. *C. necator* here. To obtain the dielectric properties (conductivity & permittivity) of the *C. necator* interior (cytoplasm), the above equation (1) can be used to fit the experimental data to the appropriate biological shell model i.e. single or double shell model [19].

A slightly modified version of equation (1) was reported by Gimsa *et al*. [24] represented as below:

$$f_{co2}^2 = \frac{1}{4\pi^2}\frac{1}{\varepsilon_o^2}\frac{(\sigma_m-\sigma_{cyto})(\sigma_{cyto}+2\sigma_m)}{(\varepsilon_{int}-\varepsilon_m)(\varepsilon_{int}+2\varepsilon_m)} \quad (2)$$

which was further simplified on the basis of medium conductivity i.e. when the conductivity of the media is < 0.2 S/m, which is required such that $\sigma_{cyto} > \sigma_m$, this condition makes the roots of equation (2) to be real, which is usually the case in all our DEP based studies (refer Sec 4.1) [25], equation (2) can be simplified in this situation as below:

$$f_{co2} = \frac{\sigma_{cyto}}{2\pi}\frac{1}{\varepsilon_o}\sqrt{\frac{1}{(\varepsilon_{int}-\varepsilon_m)(\varepsilon_{int}+2\varepsilon_m)}} \quad (3)$$

At frequencies higher than first crossover (f_{co1}), the effective resistance of the membrane which acts as an insulating shell around the bacteria's cytoplasm is zero, therefore the non-uniform electric field applied penetrates the outer membrane and effectively can be used to characterize the electrical properties of intracellular of any biological entity. This frequency is known as DEP second crossover frequency (f_{co2}) that can be used to determine the particle's net or whole conductivity, which can be combined with the shell properties to develop a real-time separation device via simulation and fabrication.

5.3 Materials & Methods

5.3.1 C. necator culturing & biosorption assay

C. necator (ATCC # 17697) used for biosorption assay was grown in culturing media prepared as described previously [14]. For all assays, *C. necator* was grown in culture bottles placed on an orbital shaker at 135-rpm and 35ºC. Parent solutions of *C. necator* were inoculated (2% v/v) from freezer stocks into culturing media prepared, grown to early stationary phase, (~12 h) prior to use in biosorption assays. Biosorption assay used Acetic acid/acetate buffer solution (AABS) to minimize the potential of complexation or precipitation induced by the culturing medium component along with the additional growth of *C. necator* cells. AABS is prepared as described in our previous article [14].

C. necator cells were rinsed three times with AABS prior to exposing them to the REE containing solution. After the final wash, the supernatant was decanted, and the pellet was vortexed with 1.5 ml of ~400 µM single element REE solution) in a centrifuge tube and incubated at 35ºC for one hour to allow biosorption of REEs. Incubated *C. necator* cells were sequentially centrifuged for 10 min at 10,000 RCF

to form a pellet of the dispersed cells. The supernatant REE solution is removed and the DEP suspending medium is added to the *C. necator* cell pellet in the tube for further experiments.

5.3.2 REE metal solutions preparation

Europium(III) nitrate hexahydrate (Strem Chemicals, Newburyport, MA, USA) molecular weight – 337.98 g/mol, Neodymium(III) nitrate hexahydrate (Strem Chemicals, Newburyport, MA, USA) molecular weight – 438.35 g/mol, and Samarium(III) nitrate hexahydrate (Strem Chemicals, Newburyport, MA, USA) molecular weight – 444.47 g/mol are used in the making of REE solutions. Eu(III), Nd(III), and Sm(III) were weighed at ~0.0338 g, ~0.0438 g, and ~0.044 g respectively and dissolved in 250 ml of deionized (DI) water to make 400 µM of the respective REE solutions.

5.3.3 DEP experiments

a) DEP suspending medium

A standard suspending medium is required for DEP experiments to suspend the biological cells in the medium whose properties (conductivity) are adjusted. D-glucose is used, which serves as the nutrient for the *C. necator* cells to be alive by maintaining the osmolarity. DEP suspending medium (50 g/L) is prepared by dissolving 1.25 g of D-glucose in 25 ml of DI water. The pH of the buffer is maintained between 6.5 – 7 to avoid any *C. necator* lysis and to preserve the uniform conditions and osmolarity of the microorganism. This pH is necessary to maintain the pH of the culture media and AABS that the cells were suspended in initially. Conductivity of the medium is adjusted to ~0.050 S/m using phosphate buffer saline (PBS) solution for initial experiments and subsequently conductivity was varied to 0.072 S/m, 0.095 S/m, and 0.190 S/m for further experiments.

b) Microwell fabrication

Sylgard 184 Silicone Elastomer (Dow Corning, Midland, MI, USA) was weighed at ~30 g using a weighing balance (XS204, Mettler Toledo) and mixed with the accompanying curing agent (~3 g) at 10:1 ratio. The mixture is degassed in a degassing chamber and is cured at 75^0 C in a sterile polystyrene petridish (100 mm × 15 mm) . The resulting poly(dimethylsiloxane) (PDMS) is cooled and cut into ~6 X 6 mm2 square pieces, punched with a 3 mm Miltex biopsy punch, plasma cleaned (Harrick plasma cleaner – PDC-32g), and sealed onto a pre-cleaned microslide (25 mm × 75 mm, 1.0 mm thick). This process is a slightly modified version compared to the previously mentioned process [26, 27]. High grade platinum (Pt) wire (99.5%, 0.2 mm diameter) is cut into 15 mm pieces and are inserted perpendicularly into the microwell such that wires are approximately on the same plane as that of the

microslide. These Pt wires serve as the electrodes delivering a non-uniform electric field gradient for the DEP crossover frequency quantification experiments. Spacing between the electrodes is adjusted to ~100 μm by using a microscope (Olympus IX-71 Inverted Microscope) and the electrode wires are sealed using epoxy to permanently fix the distance between the electrodes. However it was noticed that occasionally the spacing was altered due to the pipette's motion in and out of the microwell (rinsing the microwell), the spacing was adjusted back to initial spacing in such cases and care was taken at the beginning of every experiment to verify the electrode distance.

c) DEP crossover frequency experiments

Post the biosorption, centrifugation, and removal of REE supernatant (Sec 3.1), DEP suspending medium is added to the *C. necator* pellet and vortexed for better dispersion. 2 μL of this suspension is pipetted into the DEP microwell and AC frequency is swept using function generator (Siglent SDG 2082X) at a sinusoidal amplitude of 8 V_{pp}. Frequency is manually swept in the range of 0 - 80 MHz to determine the second crossover frequency i.e. transition from pDEP (moving towards pin electrode) to nDEP (moving away from electrode). Technical replicate experiments to determine the average crossover frequency are done using the same sample for at least six times. Biological replicate experiments are performed for three times with different *C. necator* samples. Both the biological and technical replicate experiments were performed at four different conductivities in the range of 0.02 - 0.2 S/m to suspend the REE exposed and native *C. necator*.

5.4 Results & Discussion

5.4.1 Experimental results

The second crossover frequency i.e. zero DEP force obtained for native *C. necator*, *C-Eu*, *C-Sm*, and *C-Nd* are approximately around 43 MHz, with ± 1 MHz differences in some cases as shown in the Table 5.1 below.

Table 5.1: Second crossover frequency data obtained for C. necator (native) and REE exposed C. necator (C-Eu, C-Sm, and C-Nd). Experiments conducted at four (4) different conductivities of the DEP suspending medium, values below are averaged for six (6) technical replicates and three (3) biological replicates at each conductivity for all the groups.

Conductivity (S/m)	**DEP Crossover frequency (in MHz)**			
	Native	**Metal exposed**		
	C. necator	***C-Eu***	***C-Sm***	***C-Nd***
0.050	43	43	43	42
0.072	43	43	43	42
0.095	42	44	43	42
0.190	44	44	44	42

Equation (3) for the second crossover frequency signifies that it is independent of the conductivity of the suspending medium, largely depends on the conductivity of the cytoplasm, and to a lesser extent on the permittivity [25].

The DEP crossover frequencies were averaged over three biological and six technical replicates for fitting the data to a single shell model using curve fitting (Excel, MATLAB, PRISM) and equation (3) that relates the permittivity and conductivity of the cytoplasm with the second crossover frequency; thus quantifying the properties of the *C. necator's* interior.

5.4.2 Statistical data analysis

The obtained experimental data is categorized into three (3) variables (independent variable 1 – suspending medium conductivity, independent variable 2 – *C. necator* native and REE exposed cells, and dependent variable – DEP crossover frequency) were analyzed using a two-way ANOVA in GraphPad PRISM. The data analyzed is found to be significant for the *C. necator* groups (p-value = 0.0079) and with no significance in the row factor (i.e. variation in the suspending medium conductivity; p-value = 0.1298). This signifies that the second crossover frequencies are significantly different for the native C. necator and the REE exposed C. necator i.e. C-Eu, C-Nd, and C-Sm.

5.4.3 Dielectric properties of C. necator

The physical characteristics of the *C. necator* strain are 0.7 – 0.9 μm by 0.9 –1.3 μm short rods, and are gram-negative by nature [28]. *C. necator* is known to accumulate polyhydroxyalkanoates (PHAs) up to 90% of its dry weight under extreme conditions [29] and also to synthesize these PHAs

[30, 31]. There are very few studies reported in literature who have correlated or quantified the dielectric constant i.e. cytoplasmic properties. Some of the gram-negative bacteria like *S. Typhimurium and E. coli* and gram-positive bacteria like L. innocua and L. sakei has been well studied. Under ambient conditions i.e. at room temperature & > 30 relative humidity (R.H) , the dielectric constants of different bacteria were reported by Esteban-Ferrer *et al.* in 2014 [32] as tabulated in Table 5.2 below.

Table 5.2: Effective dielectric constants for gram negative and gram positive bacteria calculated using electrostatic force microscopy under ambient conditions, it is observed that the net effective dielectric constant for the gram negative bacteria is less than the gram positive bacteria. (Adapted with permission from [32]).

Bacteria type	**Effective dielectric constant**	**Mean geometric parameters**	
		Height (nm)	**Mean effective equatorial radius (µm)**
Gram negative '-' *S. typhimurium* and *E. coli*	6-7	212 ± 26 *(S.typhi)* 348 ± 34 *(E. Coli)*	0.75 ± 0.06 (*S.typhi)* 0.9 ± 0.1 (*(E. Coli)*
Gram positive '+' *L. sakei* and *L. innocua*	15-20	636 ± 40 (*L. sakei*) 260 ± 33 (*L. innocua*)	1.1 ± 0.1 (*L. sakei*) 0.7 ± 0.1 (*L. innocua*)

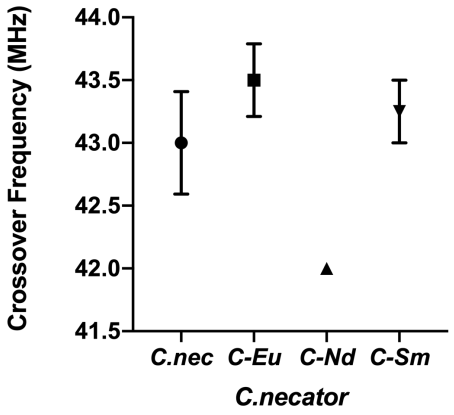

Figure 5.2: Plot of mean DEP crossover frequencies for different C. necator groups with the standard error mean (SEM). Experimental crossover frequency remained the same for all the replicates for C-Nd species, hence so error bar.

All the physical properties discussed related to *C. necator* morphology and the suspending medium are combinedly used in quantifying the cytoplasmic dielectric properties of *C. necator* i.e. the interior of the microorganism.

DEP second crossover frequency is highly sensitive to the conductivity of the cytoplasm and not so sensitive to the changes in permittivity [25]. The microorganism, *C. necator* is known to accumulate PHA's which acts as insulators. Due to the accumulation of PHA's a decrease in conductivity of the cytoplasm is observed. Hence it is more accurate to term the cytoplasmic conductivity obtained as the 'net conductivity' of *C. necator* as shown below:

$$\sigma_p = \sigma_{cyt} + k \qquad (4)$$

where σ_{cyt} – conductivity of cytoplasm, σ_p – net conductivity of the microorganism *C. necator*, and k contributes for the observed decrease in conductivity due to the presence of PHAs, REE bioaccumulation, and other predominant mechanisms affecting the cytoplasm e.g. ion leakage. The term k is usually negative when insulating PHAs are predominant and is positive when conducting REEs are bioaccumulated.

In this present study, k is hypothesized to be negative due to the presence of PHAs in the cytoplasm of *C. necator* to a large extent despite the fact that some amount of REE bioaccumulation is observed in the microorganism's interior. To quantify accurately the extent of REE accumulation vs. PHAs requires complicated techniques such as ICP-MS [33]. Presence of indirect carbon sources used in preparing growth media for biosorption like citric acid and 1,4-Piperazinediethanesulfonic acid (PIPES) can induce the production of PHAs by the microorganism [14] . Some of the prime important factors that will affect the cytoplasmic properties of the *C-Eu, C-Sm, and C-Nd* are: ion leakage, presence of PHAs, and REE bioaccumulation. Nevertheless, the presence of PHAs and ion leakage will also induce effects on the cytoplasmic properties of the native *C. necator* microorganisms in this study. The difference in conductivities between both the groups can be possibly utilized to quantify the REE bioaccumulated in these microorganisms.

TEM images of *C-Nd* shown in Figure 5.3, also supports the presence of PHAs inside the *C. necator* (shown in lighter areas), while the darker regions are electron rich areas indicating higher concentration of Neodymium (III) [Nd] inside them.

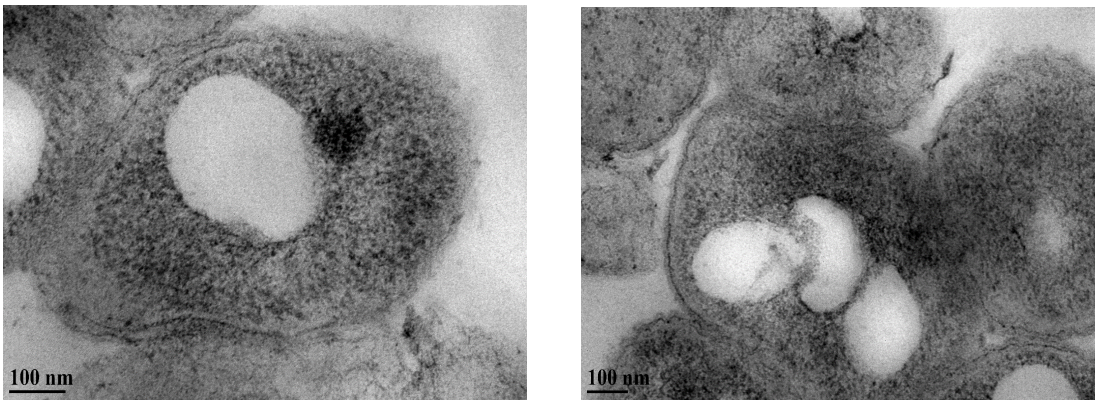

Figure 5.3: (A) TEM SA27500x Magnification of C. necator thin section at 50 µM initial [Nd] and pH 4.53 with an hour of incubation time. (B) TEM SA 20000× Magnification of C. necator thin section @ 50 µM Initial [Nd] and pH 4.53 with an hour of incubation time. The darker areas are electron dense areas (likely heavy metals), while lighter areas are electron deficient (likely PHAs).

This study is the first one to report electric signatures of *Cupriavidus necator*, specially related to the cytoplasm. Not many studies are reported on the cytoplasmic signatures due to the involvement of ultrahigh frequency regime. Few reports in literature as summarized in Table 5.3 have characterized and quantified the net conductivity of different gram-negative bacteria [34].

Table 5.3: Literature reported values of the net conductivities of different gram-negative bacteria strains. *Acinetobater calcoaceticus* closely resembles Cupriavidus necator with respect to the shape and dimensions. (Adapted with permission from [34]).

Species	**Gram stain**	**Net conductivity σ_p (µS /cm)**	**Shape**	**Dimensions (µm)**
Acinetobater calcoaceticus	-	< 20	Cocci, rod	1.5×2.5
Agrobacterium tumefaciens	-	452 ± 50	Rod	3.0×1.0
Erwinia carotovora	-	20 ± 9	Rod	3.0×1.0
Escherichia coli	-	412 ± 25	Rod	2.0×0.5
Pseudomonas putida	-	195 ± 14	Rod	5.0×1.0
Rhodobacter sphaeroides	-	967 ± 53	Rod	1.3×0.9

As discussed previously, permittivity is not a major contributor affecting the DEP second crossover frequency, the bounds were fixed between 6 – 15 based on previously reported values in Table 5.2 by other research reports [32]. The net conductivities were estimated using equation (3), and was optimized by the sum of squares of residual error technique between the measured and the fitted value. The net conductivities reported in Table 5.4 are evaluated using the mean crossover frequency for 6 technical and 3 biological replicates. Evaluation of properties for each experimental data point, resulted in a change of ± 0.10, hence mean crossover frequency is a better way to evaluate these properties.

Table 5.4: Net particle conductivities calculated using the DEP second crossover frequency experimental data over 6 technical and 3 biological replicates obtained for native C. necator and REE exposed bacteria (*C-Eu, C-Nd, C-Sm*).

Native & REE uptake	***Native C. necator***	***C-Eu***	***C-Sm***	***C-Nd***
Net conductivity (μS/cm)	16.56	16.78	16.67	16.20

5.5 Simulation study

The overall goal behind this simulation is to separate the REE exposed cells and native cells from a heterogenous mixture of cells. While there are several microfluidic techniques available to manipulate cells [35], DEP has been proved by several researchers to separate cells utilizing the minute differences in their electrical properties [36, 37]. In this simulation study, the principle of separating the *C. necator* REE exposed cells by DEP has been employed, utilizing the electrical properties of the membrane.

5.5.1 Design of microdevice & setup of simulation

The evaluated properties of the membrane of native *C. necator* and REE absorbed *C. necator* cells which is currently under consideration in another journal is utilized in simulating a DEP platform for sorting. COMSOL Multiphysics simulation package v5.5 (COMSOL, Inc., Burlington, MA, USA) that uses finite element analysis approach was utilized to develop the microscale sorting device.

The design of the device is adapted from Piacentini *et al.* 2011 [38], who used this platform to dielectrophoretically separate platelets from red blood cells (RBCs) employing electrical properties of platelets [39] and RBCs [40]. Detailed device design with dimensions is shown in Figure 5.4.

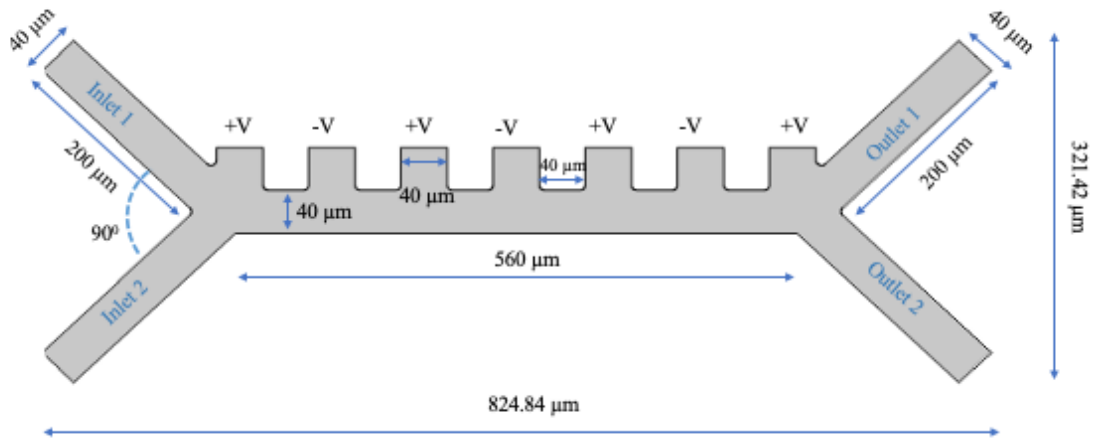

Figure 5.4: Design of the microdevice showing the dimensions, where voltage remains the same at every boundary and vary in magnitude by + and – alternatively.

Simulation studies utilized creeping flow physics to model the fluid flow, and electric currents physics under AC/DC module to study the electric field and particle tracing for fluid flow physics to compute the trajectories of native *C. necator* and REE exposed *C. necator* to determine the sorting voltage under the influence of dielectrophoretic and drag forces.

Simulation is modeled using two studies, where Study 1 comprised of two sub steps i.e., (1) stationary that solves for the fluid profile and (2) frequency domain solving for the AC electric potential (100 kHz). Study 2 is a time-dependent study that accounts for the computation of the particle trajectories using the particle tracing for fluid flow module while accounting for the DEP force.

The boundary wall of the geometry is assumed to be insulated, with creeping flow condition at inlet ports 1 and 2. A heterogenous mixture of *C. necator* in its native and REE absorbed states is introduced into the device at 134 µm/s through the inlet 1 and the suspending medium is introduced into the device at 853 µm/s through inlet 2. Particle tracing physics assumes the following conditions while solving for the trajectories: the particles bounce (wall condition) and freeze at the outlets. Simulation also employs using the fluid medium parameters as discussed in Table 5.5. A user controlled meshing calibrated for fluid dynamics using the pre-defined element size parameters for coarser mesh is used. Thickness of the device (out of plane) of 10 µm is fixed in this study.

Table 5.5: Table of parameters used in the simulation study.

Parameters	Value
Fluid viscosity	0.001 Pa-s
Fluid medium conductivity	0.055 S/m
Channel depth	10 µm
Fluid density	1000 kg/m^3
Dielectric permittivity of the medium	80

The dielectric constant assumed in this study i.e. 80 as mentioned in Table 5.5 was previously reported for aqueous dextrose (5% wt) at 25^0 C as 77.37 [41].

Equations associated with the physics and the boundary conditions employed for the DEP sorting of REE exposed *C. necator* from a heterogenous mixture of both native and REE exposed *C. necator* using COMSOL are listed in Table 5.6. Zeta potential for PDMS is assumed to be -0.1 V [42]. A frequency domain study is used to solve for the physics contributing to electric currents at 100 kHz frequency. While the *C. necator* cells and the fluid medium is introduced into the sorting device (Figure 5.4) at the velocities in the creeping flow regime (i.e. Reynolds number << 1), a stationary study followed by particle tracing are solved to obtain particle trajectories by taking into account the drag and the dielectrophoretic forces using the boundary conditions described in Table 5.6.

Calculating the effect of DEP force requires the electrical properties of particles of interest that are to be sorted i.e. *C. necator* native and REE exposed in the current study. Two important electrical parameters that are required to calculate the DEP force are conductivity and permittivity. While the former one signifies the ease at which electricity passes through and the later one signifies the ability to transmit (or permit) electric field [43]. While bacterial cells possess insulating outer shell (membrane) and conducting interior (cytoplasm), for this simulation study sorting is based on membrane properties as summarized in Table 5.7.

Table 5.6: List of physics involved with respect to the dependent variables and the study type. Equations associated with each of the physics along with the boundary conditions that were incorporated into COMSOL 5.5a for sorting study are also provided.

Physics	**Dependent variable**	**Study type**	**Equations & conditions**
Electric currents	V	Frequency Domain	$\nabla \cdot J = Q_{j,V}$ $J = \sigma E + J_e$ $E = -\nabla \mathrm{V}$ Out of plane thickness = 10 μm Insulated wall boundary $n \cdot J = 0$
Fluid flow (creeping)	*u*	Stationary	$0 = \nabla \cdot [-\rho I + \mathrm{K}] + F$ $\rho \nabla \cdot u = 0$ $\mathrm{K} = \mu(\nabla u + (\nabla u)^T)$ Reference Temp = 293.15 K Reference Pressure = 1 atm Wall boundary – electroosmotic velocity $u = \mu_{eo} E_t$ $\mu_{eo} = \frac{\epsilon_r \varepsilon_0 \zeta}{\mu}$, $E_t = E - (E \cdot n)n$ where ζ is the Zeta potential of the polymer PDMS. Boundary conditions: Normal inflow velocity (Inlet 1) – 134 μm/s Normal inflow velocity (Inlet 2) – 853 μm/s Pressure (Outlet) – 0 (relative), suppressing back flow.
Particle Tracing for fluid flow	*q*, *v* *q* – particle position *v* – particle velocity	Time dependent	$\frac{\mathrm{d}(m_\mathrm{v}\mathbf{v})}{\mathrm{d}t} = \mathbf{F}_\mathrm{t} \frac{d(m_v v)}{dt} = F_t$ (Newtonian Formulation) Wall condition: Bounce $v = v_c - 2(n \cdot v_c)n$ (v_c is particle velocity when striking the wall) Outlet condition: Freeze; $v = v_c$ $F_D = \frac{1}{\tau_p} m_p (u - v); \ \tau_p = \frac{\rho_p d_p^2}{18\mu}$ $F_{DEP} = 2\pi r_p^3 \varepsilon_0 \Re e(K) \nabla \lvert E \rvert^2$ $K = \frac{\varepsilon_{r,p}^* - \varepsilon_r^*}{\varepsilon_{r,p}^* + 2\varepsilon_r^*}$ $\varepsilon_r^* = \varepsilon_r - \frac{i\sigma}{\omega \varepsilon_0}$ for time harmonic fields $\varepsilon_r^* = \varepsilon_r$ for stationary fields

Table 5.7: Electrical properties of the membrane for both native and REE exposed *C. necator* used in the simulation study for separation.

Bacteria membrane properties	**Conductivity (μS/m)**	**Permitivity**
Native *C. necator*	0.05	12
REE exposed *C. necator* (Mean of *C.Eu, C.Nd, and C.Sm*)	0.03	14.3

5.5.2 Voltage optimization

The device design illustrated in Figure 5.4 is used for the optimization study that has seven (7) fixed voltage terminals. The terminals are varied in polarity between + and – alternatively while the magnitude remains constant for all the seven (7) terminals. As known from prior knowledge, DEP force is dependent on cell size, cell's electrical properties, medium conductivity (fixed at 0.055 S/m), and the non-uniform electric field gradient. While all the dependent parameters mentioned above are determined experimentally, except the non-uniform electric field gradient which is a function of applied voltage. Hence a parametric study is performed varying the applied voltage potential between 2 and 15 V, while the polarity is altered between the arrangement of the electrode terminals as explained above. The frequency is fixed at 100 kHz for the entire simulation. It is observed that a voltage range of 9 – 9.5 V enabled separation of both the variants of *C. necator* (i.e., native and REE exposed) by generating the desired electric field required to experience the DEP force. The voltage is further narrowed to obtain optimal separation maintaining the specificity. Separation is observed at 9.5 V which is the optimal voltage where the bacteria experiences desired DEP force to sort into different outlet ports i.e. the observed particle trajectories are different. The observed trajectory of both native and REE exposed *C. necator* remains same until the cells reach the vertex close to the division of outlet channels. This behavior is due to the similarity of cell sizes and a narrow dielectric property differences observed for both native and REE exposed *C. necator*. Electric field strength at an applied voltage potential of 9.5 V is plotted using a 2D plot group across the surface as illustrated in Figure 5.5. Electric field or electric field strength can be written as:

$$E = -\nabla \mathrm{V} \qquad (5)$$

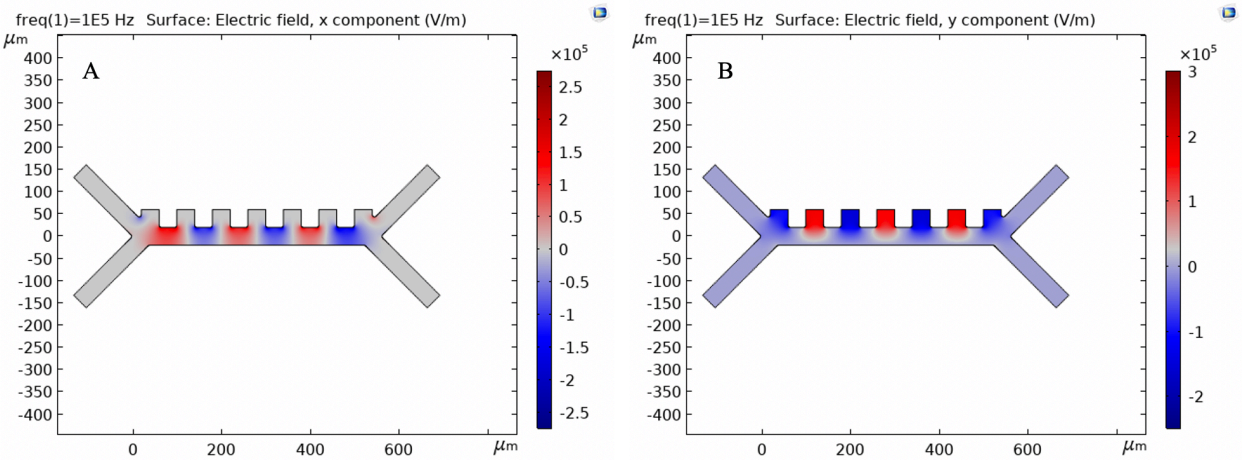

Figure 5.5: Electric field strength plotted across the surface of the device at an applied voltage of 9.5 V. The red and blue regions indicate the high and low electric field strength respectively. Electric field strength is resolved into components for rectangular co-ordinates where A) x-component of the electric field strength - $Ex = \partial V/\partial x$ and B) y-component of the electric field strength - $Ey = \partial V/\partial y$.

where V denotes the voltage potential and ∇ is the gradient which is a collection of partial derivatives. Electric field strength is resolved into components for rectangular co-ordinates and are individually plotted as A & B in Figure 5.5 for better understanding.

A detailed schematic of the particle trajectories of the native and the REE exposed *C. necator* for voltages at the vicinity of the optimal voltage i.e., 9.5 V is illustrated in Figure 5.6. Electric field strength, a function of applied voltage potential whose gradient generates necessary DEP force required at the terminals, yield the separation. Applied voltage potential is varied between 9.3 – 10 V (i.e., 9.3 V, 9.4 V, 9.5 V and 10 V), to determine the change in the trajectories of the native and REE exposed *C. necator* based on the non-uniform gradient in the electric field strength. In this study, the particle tracing physics module for fluid flow condition has both the bacteria's (native and REE exposed) initial position set to be uniformly distributed and release one particle of each kind per release over a range of 0 – 3 s at a interval step of 0.05 s. Hence, same number of the native and the REE exposed bacteria is released into the channel through inlet 1. At a voltage potential of 9.3 V, the DEP force experienced by both the native and REE exposed *C. necator*, is not sufficient to result in separation and hence follows the same trajectory into outlet channel 1 as shown in Figure 5.6A. This motion of both the bacteria types into outlet channel 1, is also due to the higher velocity of the medium introduced into the device through inlet 2 (853 μm/s) compared to the velocity of the bacteria release (134 μm/s) through inlet 1. This higher velocity of the medium through inlet 2 – left lower channel, tends to push all the particles to outlet 1 (right upper channel) by virtue of the velocity profile only i.e., drag forces dominate and DEP

force generated is low to observe any separation. This profile of particle trajectories remained the same for voltages below 9.3 V. While in Figure 5.6B, partial sorting is observed i.e., the native *C. necator* species (particles in red) enter both outlet channels 1 and 2, and the REE exposed *C. necator* (particles in blue) remain in outlet 1, as in Figure 5.6A. Hence no change was noticed in the trajectory of the REE exposed *C. necator* but the native *C. necator* enters both the outlet channels.

It is also observed from Table 5.7, that the conductivity of native *C. necator* is higher than the REE exposed, while the permittivity follows a reversed pattern of REE exposed *C. necator* permittivity being higher than that of the native *C. necator*. As permittivity signifies the ease of polarizability of the particle to the electric field and conductivity signifies ease of penetration of the electric field i.e. particles of higher conductivity are sensitive to lower strength and vice versa, these electrical properties play an important role in deciding the particle trajectories for the bacteria on separation (whether native/ REE exposed should enter outlet 1/outlet 2 is based on their electrical properties). Figure 5.6C, demonstrates the case of perfect separation at 9.5 V (based on the electrical properties of the particles). Separation is also observed to occur at voltage of 9.6 V and 9.7 V, but since optimum voltage (lower value) is better towards making it portable, the lower value of 9.5 V is being reported as optimal voltage yielding separation. At all the higher voltages i.e., >9.9 V, both the *C. necator* forms changes the trajectory to outlet 2 yielding no separation.

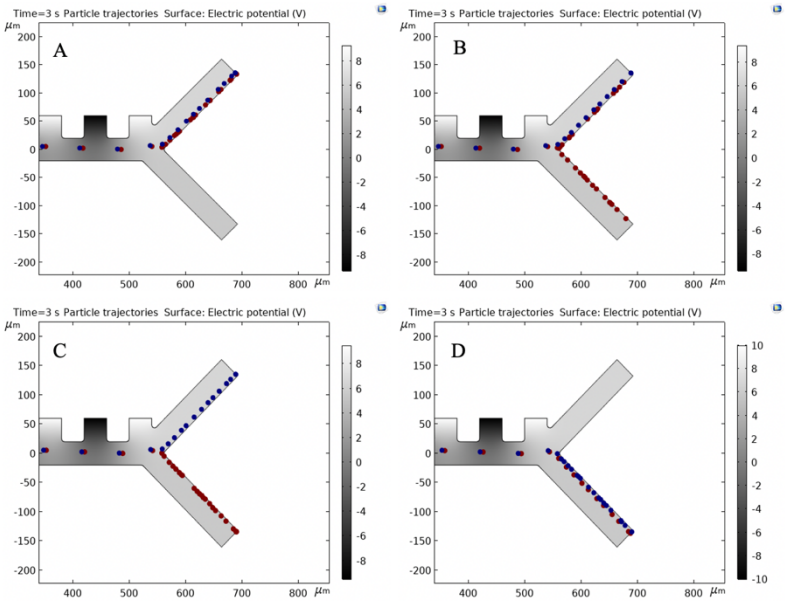

Figure 5.6: The red particles are native *C. necator* and the blue are the REE exposed. The frequency is maintained at 100 kHz for all cases. A) Computed particle trajectories at 9.3 V where both the forms of *C. necator* move to outlet 1; B) computed particle trajectories of the particles at 9.4 V, where the native *C. necator* enters outlet 1 and the REE exposed enters both outlet 1 and outlet 2, indicating partial separation; C) computed particle trajectories of the particles at 9.5 V, where complete separation occurs; D) computed particle trajectories of the particles at 10 V, where the trajectory changes to outlet 2 contrary to A for both the *C. necator* forms.

The study is optimized to obtain the lowest AC potential for separation, i.e., 9.5 V and 100 kHz in this case, which can be further expanded to future work by experimentally validating the simulation study.

5.6 Conclusions

This study characterizes the *Cupriavidus necator* bacteria for changes in the properties induced by bioaccumulation of rare earth elements using dielectrophoresis. Measuring the second crossover frequency for REE exposed and the native species is a novel approach since DEP, by virtue, is known to detect subtle changes within the cell or any changes in the membrane. In the present research, based on the obtained conductivities of the *C. necator*, there are minute changes in the net conductivity of both the native and the REE exposed species that suggests that there is potential to quantify the REE bioaccumulated and the volume of the PHA's present. The significant low conductivity of the cytoplasm obtained might be due to the PHA's that are typically insulators adding to the decrease in the net conductivity of REE absorbed *C. necator* species. Further, a possible device design is proposed by utilizing COMSOL Multiphysics v5.5 and electrokinetics based on the estimated properties of the membrane. The device is about 1-mm long and 0.5 mm wide containing rectangular obstacles ~5 rectangular obstacles of 40 μm wide. The distance between the obstacles in also maintained at 40 μm. Low frequency AC field is utilized to manipulate the articles with frequency being fixed at 100 kHz. The optimized AC voltage of separation was found to be 9.5 V that yielded different particle trajectories of native *C. necator* and REE absorbed species. Overall, this device could be applicable to different biosorbent species and other rare earth elements to maximize biosorption efficiency. This promising new application in dielectrophoresis can be utilized in treating wastewater streams from nuclear reactors and also to obtain knowledge about the geothermal water streams that occur naturally throughout the world.

References

[1] Y. Xiao, L. Huang, Z. Long, Z. Feng, and L. Wang, "Adsorption ability of rare earth elements on clay minerals and its practical performance," *Journal of Rare Earths,* vol. 34, no. 5, pp. 543-548, 2016/05/01/ 2016, doi: https://doi.org/10.1016/S1002-0721(16)60060-1.

[2] F. Zhao, E. Repo, Y. Meng, X. Wang, D. Yin, and M. Sillanpää, "An EDTA-β-cyclodextrin material for the adsorption of rare earth elements and its application in preconcentration of rare earth elements in seawater," *Journal of Colloid and Interface Science,* vol. 465, pp. 215-224, 2016/03/01/ 2016, doi: https://doi.org/10.1016/j.jcis.2015.11.069.

[3] G. Charalampides, K. I. Vatalis, B. Apostoplos, and B. Ploutarch-Nikolas, "Rare Earth Elements: Industrial Applications and Economic Dependency of Europe," *Procedia Economics and Finance,* vol. 24, pp. 126-135, 2015/01/01/ 2015, doi: https://doi.org/10.1016/S2212-5671(15)00630-9.

[4] Ó. Barros *et al.*, "Recovery of Rare Earth Elements from Wastewater Towards a Circular Economy," (in eng), *Molecules,* vol. 24, no. 6, p. 1005, 2019, doi: 10.3390/molecules24061005.

[5] E. Willbold *et al.*, "Effect of the addition of low rare earth elements (lanthanum, neodymium, cerium) on the biodegradation and biocompatibility of magnesium," *Acta Biomaterialia,* vol. 11, pp. 554-562, 2015/01/01/ 2015, doi: https://doi.org/10.1016/j.actbio.2014.09.041.

[6] P. Josso, S. Roberts, D. A. H. Teagle, O. Pourret, R. Herrington, and C. Ponce de Leon Albarran, "Extraction and separation of rare earth elements from hydrothermal metalliferous sediments," *Minerals Engineering,* vol. 118, pp. 106-121, 2018/03/15/ 2018, doi: https://doi.org/10.1016/j.mineng.2017.12.014.

[7] F. Xie, T. A. Zhang, D. Dreisinger, and F. Doyle, "A critical review on solvent extraction of rare earths from aqueous solutions," *Minerals Engineering,* vol. 56, pp. 10-28, 2014/02/01/ 2014, doi: https://doi.org/10.1016/j.mineng.2013.10.021.

[8] W. D. Bonificio and D. R. Clarke, "Rare-Earth Separation Using Bacteria," *Environmental Science & Technology Letters,* vol. 3, no. 4, pp. 180-184, 2016/04/12 2016, doi: 10.1021/acs.estlett.6b00064.

[9] E. S. Kazak, E. G. Kalitina, N. A. Kharitonova, G. A. Chelnokov, E. V. Elovskii, and I. V. Bragin, "Biosorption of Rare-Earth Elements and Yttrium by Heterotrophic Bacteria in an Aqueous Environment," *Moscow University Geology Bulletin,* vol. 73, no. 3, pp. 287-294, 2018/05/01 2018, doi: 10.3103/S0145875218030043.

[10] H. A. Pohl, "The Motion and Precipitation of Suspensoids in Divergent Electric Fields," *Journal of Applied Physics,* vol. 22, no. 7, pp. 869-871, 1951/07/01 1951, doi: 10.1063/1.1700065.

[11] R. Pethig, "Review article-dielectrophoresis: status of the theory, technology, and applications," (in eng), *Biomicrofluidics,* vol. 4, no. 2, p. 022811, 2010, doi: 10.1063/1.3456626.

[12] N. Abd Rahman, F. Ibrahim, and B. Yafouz, "Dielectrophoresis for Biomedical Sciences Applications: A Review," *Sensors (Basel),* vol. 17, no. 3, 2017/02/24/ 2017, doi: 10.3390/s17030449.

[13] G. R. Ballantyne and P. N. Holtham, "Application of dielectrophoresis for the separation of minerals," *Minerals Engineering,* vol. 23, no. 4, pp. 350-358, 2010/03/01/ 2010, doi: https://doi.org/10.1016/j.mineng.2009.09.001.

[14] E. O. Adekanmbi, A. T. Giduthuri, S. Waymire, and S. K. Srivastava, "Utilization of Dielectrophoresis for the Quantification of Rare Earth Elements Adsorbed on Cupriavidus necator," *ACS Sustainable Chemistry & Engineering,* vol. 8, no. 3, pp. 1353-1361, 2020/01/27 2020, doi: 10.1021/acssuschemeng.9b03878.

[15] A. Ramos, H. Morgan, N. G. Green, and A. Castellanos, "Ac electrokinetics: a review of forces in microelectrode structures," (in en), *Journal of Physics D: Applied Physics,* Text vol. 31, no. 18, pp. 2338-2353, 21 September 1998 1998, doi: 10.1088/0022-3727/31/18/021.

[16] P. R. Gascoyne and J. Vykoukal, "Particle separation by dielectrophoresis," *Electrophoresis,* vol. 23, p. 1973, 2002.

[17] A. P. Brown, A. B. Harrison, W. B. Betts, and J. G. O'Neill, "Measurement of the dielectrophoretic enrichment of yeast on grid electrodes using image analysis," (in eng), *Microbios,* vol. 91, no. 366, pp. 55-65, 1997.

[18] B. H. Lapizco-Encinas and M. Rito-Palomares, "Dielectrophoresis for the manipulation of nanobioparticles," *Electrophoresis,* vol. 28, p. 4521, 2007.

[19] E. O. Adekanmbi and S. K. Srivastava, "Dielectric characterization of bioparticles via electrokinetics: The past, present, and the future," *Applied Physics Reviews,* vol. 6, no. 4, p. 041313, 2019/12/01/ 2019, doi: 10.1063/1.5113709.

[20] E. O. Adekanmbi and S. K. Srivastava, "Applications of electrokinetics and dielectrophoresis on designing Chip-Based disease diagnostic platforms," in *Bio-Inspired Technology*: IntechOpen, 2019.

[21] P.-Y. Weng, I. A. Chen, C.-K. Yeh, P.-Y. Chen, and J.-Y. Juang, "Size-dependent dielectrophoretic crossover frequency of spherical particles," *Biomicrofluidics,* vol. 10, no. 1, 2016/02/11/ 2016, doi: 10.1063/1.4941853.

[22] H. Morgan, M. P. Hughes, and N. G. Green, "Separation of Submicron Bioparticles by Dielectrophoresis," *Biophys J,* vol. 77, no. 1, pp. 516-525, 1999/07/01/ 1999, doi: https://doi.org/10.1016/S0006-3495(99)76908-0.

[23] L. M. Broche, F. H. Labeed, and M. P. Hughes, "Extraction of dielectric properties of multiple populations from dielectrophoretic collection spectrum data," (in en), *Phys Med Biol,* Text vol. 50, no. 10, pp. 2267-74, May 21 2005, doi: 10.1088/0031-9155/50/10/006.

[24] J. Gimsa, P. Marszalek, U. Loewe, and T. Y. Tsong, "Dielectrophoresis and electrorotation of neurospora slime and murine myeloma cells," *Biophys. J.,* vol. 60, p. 749, 1991.

[25] R. R. Pethig, *Dielectrophoresis: Theory, Methodology and Biological Applications*. Wiley, 2017.

[26] K. L. Chiok, N. C. Paul, E. O. Adekanmbi, S. K. Srivastava, and D. H. Shah, "Dimethyl adenosine transferase (KsgA) contributes to cell-envelope fitness in Salmonella Enteritidis," (in eng), *Microbiological research,* vol. 216, pp. 108-119, 2018, doi: 10.1016/j.micres.2018.08.009.

[27] E. O. Adekanmbi, M. W. Ueti, B. Rinaldi, C. E. Suarez, and S. K. Srivastava, "Insulator-based dielectrophoretic diagnostic tool for babesiosis," (in eng), *Biomicrofluidics,* vol. 10, no. 3, pp. 033108-033108, 2016, doi: 10.1063/1.4954196.

[28] N. S. Makkar and L.E.Casida, "Cupriavidus necator gen.nov., sp. nov.;a Nonobligate Bacterial Predator of Bacteria in Soil," *International Journal of Systematic Biology,* vol. 37, no. 4, pp. 323-326, 1987. [Online]. Available: https://www.microbiologyresearch.org/docserver/fulltext/ijsem/37/4/ijs-37-4-323.pdf?expires=1582823097&id=id&accname=guest&checksum=9A699925460123272B06BCEC18AEB107.

[29] F. Mravec *et al.*, "Accumulation of PHA granules in Cupriavidus necator as seen by confocal fluorescence microscopy," *FEMS Microbiology Letters,* vol. 363, no. 10, 2016, doi: 10.1093/femsle/fnw094.

[30] N. Berezina, "Novel approach for productivity enhancement of polyhydroxyalkanoates (PHA) production by Cupriavidus necator DSM 545," (in eng), *N Biotechnol,* vol. 30, no. 2, pp. 192-5, Jan 25 2013, doi: 10.1016/j.nbt.2012.05.002.

[31] A. Flores-Sánchez, M. d. R. López-Cuellar, F. Pérez-Guevara, U. Figueroa López, J. M. Martín-Bufájer, and B. Vergara-Porras, "Synthesis of Poly-(R-hydroxyalkanoates) by Cupriavidus necator ATCC 17699 Using Mexican Avocado (Persea americana) Oil as a Carbon Source," (in en), *International Journal of Polymer Science,* Research Article vol. 2017, 2017/08/21 2017, doi: https://doi.org/10.1155/2017/6942950.

[32] D. Esteban-Ferrer, M. A. Edwards, L. Fumagalli, A. Juárez, and G. Gomila, "Electric Polarization Properties of Single Bacteria Measured with Electrostatic Force Microscopy," *ACS Nano,* vol. 8, no. 10, pp. 9843-9849, 2014/10/28 2014, doi: 10.1021/nn5041476.

[33] R. C. Merrifield, C. Stephan, and J. R. Lead, "Quantification of Au Nanoparticle Biouptake and Distribution to Freshwater Algae Using Single Cell - ICP-MS," (in eng), *Environ Sci Technol,* vol. 52, no. 4, pp. 2271-2277, Feb 20 2018, doi: 10.1021/acs.est.7b04968.

[34] R. E. Fernandez, A. Rohani, V. Farmehini, and N. S. Swami, "Review: Microbial analysis in dielectrophoretic microfluidic systems," (in eng), *Analytica chimica acta,* vol. 966, pp. 11-33, 2017, doi: 10.1016/j.aca.2017.02.024.

[35] T. Luo, L. Fan, R. Zhu, and D. Sun, "Microfluidic Single-Cell Manipulation and Analysis: Methods and Applications," (in eng), *Micromachines,* vol. 10, no. 2, p. 104, 2019, doi: 10.3390/mi10020104.

[36] S. K. Srivastava, J. L. Baylon-Cardiel, B. H. Lapizco-Encinas, and A. R. Minerick, "A continuous DC-insulator dielectrophoretic sorter of microparticles," *Journal of Chromatography A,* vol. 1218, no. 13, pp. 1780-1789, 2011/04/01/ 2011, doi: https://doi.org/10.1016/j.chroma.2011.01.082.

[37] S. K. Srivastava, A. Gencoglu, and A. R. Minerick, "DC insulator dielectrophoretic applications in microdevice technology: a review," *Analytical and Bioanalytical Chemistry,* vol. 399, no. 1, pp. 301-321, 2011/01/01 2011, doi: 10.1007/s00216-010-4222-6.

[38] N. Piacentini, G. Mernier, R. Tornay, and P. Renaud, "Separation of platelets from other blood cells in continuous-flow by dielectrophoresis field-flow-fractionation," *Biomicrofluidics,* vol. 5, no. 3, pp. 34122-341228, Sep 2011, doi: 10.1063/1.3640045.

[39] M. Egger and E. Donath, "Electrorotation measurements of diamide-induced platelet activation changes," (in eng), *Biophys J,* vol. 68, no. 1, pp. 364-72, Jan 1995, doi: 10.1016/s0006-3495(95)80197-9.

[40] S. Park, Y. Zhang, T. H. Wang, and S. Yang, "Continuous dielectrophoretic bacterial separation and concentration from physiological media of high conductivity," (in eng), *Lab Chip,* vol. 11, no. 17, pp. 2893-900, Sep 7 2011, doi: 10.1039/c1lc20307j.

[41] C. G. M. Maryott and A. Arthur, "Dielectric Constants of Aqueous Solutions of Dextrose and Sucrose," *Journal of Research of the National Bureau of Standards,* vol. 45, no. 4, p. 299, 1950. [Online]. Available: https://pdfs.semanticscholar.org/956c/22b394d931ad4c1cf9856460419468abb821.pdf.

[42] E. O. Adekanmbi, A. T. Giduthuri, and S. K. Srivastava, "Dielectric Characterization and Separation Optimization of Infiltrating Ductal Adenocarcinoma via Insulator-Dielectrophoresis," (in eng), *Micromachines (Basel),* vol. 11, no. 4, Mar 25 2020, doi: 10.3390/mi11040340.

[43] R. Taherian, "4 - Application of Conducting Composite in Dielectrics**Hereby, from Shodhganga 4 is appreciated due to the valuable content used in this chapter," in *Electrical Conductivity in Polymer-Based Composites*, R. Taherian and A. Kausar Eds.: William Andrew Publishing, 2019, pp. 73-90.

Chapter 6: Challenges, Conclusions, and Future Scope

In this thesis, a comprehensive work on characterization of mesenchymal stem cells (MSCs) and their differentiated progeny towards tenocytes has been discussed and accomplished via dielectrophoresis. DEP as a technique that has become popular due to its growing potential to open up an era of economical, rapid, and efficient medical lab-on-a-chip platforms revolutionizing the field of medicine. Soon, stem cell-based therapies which are still at a nascent stage due to their limitations associated with heterogeneity can be addressed and be made into a reality. Ultra-high frequency characterization of cell's cytoplasm remains relatively an unexplored area, as most characterization research studies via DEP are based on the lower or first crossover frequency which signifies the biophysics of the membrane. Advancing to ultra-high frequency (UHF) characterization is a significant step towards understanding the biophysical changes associated with cytoplasm once these MSCs undergo differentiation. To this date, based on a thorough literature search via google scholar and web of science resulted in no research study characterizing the MSCs cytoplasm or the interior of the cell. Hence this is the first work being reported to our best knowledge.

While experimenting with MSCs, several unavoidable challenges occurred that had to be addressed in order to successfully narrow down the DEP crossover frequency range maintaining repeatability and reproducibility of the experiments while being statistically significant. Challenges pertaining to the DEP characterization experiments of MSCs and their differentiating tenocyte progenitors focusing on the effects of morphology is discussed below.

6.1 Challenges

6.1.1 Cell Adherence

The adherent nature of MSCs to plastic aids tendon healing [1] is a primary and major concern in DEP characterization experiments utilizing polymeric microfluidic platforms. In order to avoid this adherence, experiments are rapidly performed within 1-2 min and the device is flushed with 70 % ethanol and with the DEP suspending medium twice before adding fresh cell suspension to flush the cells adhered to the bottom of the micro well. To better avoid this, addition of Bovine serum albumin or Tween 20 can be helpful, though they could affect the cells' outer structure which should be accounted while calculating the electrical properties. Hence, this study preferred having no additional agents to the buffer and advanced the protocol of flushing the microwell multiple times with DEP suspending medium, Care should be taken to avoid adding cell suspension to the microwell, with flushing after 70

% ethanol alone which will result in death of cells. At least two flushes with DEP suspending medium post 70% ethanol flush is preferred to flush out all the alcohol before adding cells to the microwell.

6.1.2 Effect of trypsinization

Cultured cells from flasks are dissociated by trypsinization ,which digests protein and mechanically disrupts cells from their natural culturing habitat [2]. It is noticed that longer treatment with trypsin affected the values of the first crossover frequency during experiments, while shorter times made cells adhere in the microwell. In order to better address this problem, trypsin treatment time periods should be kept constant, so as to not affect DEP frequency values drastically since trypsin is known to affect the cell membrane that is detectable using the DEP first crossover frequency.

6.1.3 Heterogeneity of MSC samples

This thesis studies MSCs, which are known to vary widely in their size representing a heterogenous population. As it is known that DEP first crossover frequency is affected by the size and shape of these cells and passive electrical nature of the membrane as discussed in Chapter 3(Section 3.4), including the number of cells in the microwell. Density of cell suspension and volume being added to micro-well is kept constant throughout the study. Studying at a single cell level, helps is understanding the cell better but does not aid in clinical setting since it is typically impossible to study one cell at instance for transplantation scale. Hence DEP, based characterization based on average cell population might aid in characterization, using which sorting regions can be better understood. As the shape remained spherical until day 3 time point, only size-based variance is accounted here to estimate the dielectric properties.

6.1.4 Differentiation time period

At the day 7 period, MSCs undergoing tenogenesis appeared to be elongated, which requires complex modeling of the shape in order to determine the electrical properties though experiments are performed on this time point using single shell model[3]. Statistical analysis on the dielectric properties obtained by curve fitting at the day 7 time point via students' t-test for the three groups of cells i.e., baseline and day 7 treatment and no treatment groups failed with no significance. This is partly due to the lack of homogenous shaped cells (as discussed in sec 6.1.3) and varying sizes from 15 - 30 μm in diameter. It is also noticed that the day 7 stem cell suspension after treatment with trypsin appeared cloudier and were present in the form of clusters once they are suspended in the DEP medium. To break those clusters and overcome issues of clogging the channels in the microdevice, cells should be well-dispersed using a cell vortexer at low speed for 2-3 seconds prior to DEP experiments. Centrifuging

time and force to settle the cells before removing trypsin and addition of DEP suspending medium should be kept minimal at 300 RCF or less as mammalian cells are sensitive to centrifugal forces to avoid lysis, death of cells. In addition, day 1 into treatment with growth factor, the cells are spherical in shape with no noticeable changes in their size. They also had similar dielectric properties as the no treatment undifferentiated cells. statistical tests on the day 1 time period also reported no significant differences between the undifferentiated no treatment MSCs and day 1 into treatment with TGFβ2. Hence, we can conclude that day 3 time period provided the best results to further this research towards developing a DEP sorting platform.

6.1.5 DEP suspending medium

Maintaining the standards of DEP suspending medium is essential to accurately determine the crossover frequency and to test the repeatability. Change of standards, affect the first crossover frequency values. While it is a preferred way, to linearly change the conductivity of suspending medium to and determine the first crossover frequency at respective medium conductivities, to estimate the membrane properties more accurately, care should be taken to maintain the conductivity standard of medium constant for every experiment trial, when experiment is being repeated at a certain conductivity. pH of the buffer should be kept close to neutrality as to the cell culture media, to avoid unwanted stress induced to wide changes in pH. Iso-tonicity of the suspending medium is necessary to maintain cells' viability and membrane's integrity throughout the experiments to avoid cell shrinkage, breakage of outer membrane etc.

6.2 Simulation study

The simulation demonstrated in Chapter 5, is a separation study based on the dielectric properties of the cell's outer membrane of the bacteria *Cupriavidus necator*, a gram-negative bacteria strain which is rod shaped with dimensions ranging 0.7 – 0.9 µm by 0.9 –1.3 µm. These bacteria's shape and dimensions are very different from the mesenchymal stem cells. Simulation study also employs device design that has been adapted from a different study and has been optimized with parametric studies to achieve optimum separation of the native and REE exposed bacteria groups. This simulation is only included in this thesis, to be seen as an example of designing and optimizing a sorting device suitable to separate undifferentiated and tenogenically differentiating MSCs. However, with changing dimensions and shape the physics employed such as stokes drag force for submicron particles for bacteria dimensions <10 µm will no longer be valid for stem cells and should be accounted and re-modeled completely to develop a stem cell sorter.

6.3 Conclusions and Future work

In this study, both low (first) and high (second) DEP crossover frequency technique is used to quantify the electrical properties of MSCs and their differentiating progenitors (tenocytes) at several time points viz. Day 1, Day 3, and Day 7. Results suggest that, Day 1 ($p > 0.05$), Day 3 ($p < 0.05$) and Day 7 ($p < 0.05$) during the course of differentiation, cells express distinct passive electrical properties, using which the differentiated and undifferentiated cells can be sorted for their application in regenerative medicine. Day 1 and Day 7 as indicated above are not statistically significant, while it is expected that Day 1 should be resembling Day 0 cells in electrical behavior and hence not significant. Day 7 timepoint being not significant from Day 0 needs further modeling as a ellipsoid owing to their elongated shape. Since first crossover frequency correlates size, shape and electrical properties of membrane, accurate modeling of shape and size will help in estimating the electrical properties for this time point, which will be distinct. In order to better understand cytoplasmic changes within the cell from the development of an MSC to tenocyte, which usually takes 21 days [4], further ultra-high frequency characterization can be performed, though experiments may not be required until 21 day time point to sort the cells. With the results reported in this these, we are able to cut down the time taken to detect these differentiation changes to as early as 3 days. However, with more rigorous testing, we will be able to completely support our hypothesis of measuring early differentiation changes without the need of extensive labeling and expensive instrumentation. This research will advance both the fields of electrokinetic cell manipulation and regenerative therapies. In order to study, physiological functions at cellular level, single cell characterization techniques such as electrorotation have been emerging even though the single cell analyses is sophisticated with analysis rate of one cell at any instance. DEP is now being exploited at single cell level [5, 6], and is proven to be successful than other complex single cell techniques like electrorotation, impedance flow cytometry though the application of DEP is largely towards developing lab-on-a-chip platforms for cell manipulation and separation.

In order to understand the design of a sorting platform, a scenario is presented in Chapter 5 included in this thesis where in sorting of cells based on the electrical properties evaluated using DEP crossover technique platform (point and planar microwell platform) developed in MESA Lab at University of Idaho. The simulation study is developed using COMSOL Multiphysics software where in different physical mechanisms like creeping flow, frequency dependent electric field and particle tracing for fluid flow are applied to study the cell trajectory under non-uniform electric fields. Further extension of this characterization study to simulating a microfluidic stem cell sorter employing DEP and

experimental validation of the simulation study is seen in future, along with detailed modeling of the MSCs cytoplasm to study relative cell to nucleus volume changes during differentiation.

References

[1] S. Chaudhury, "Mesenchymal stem cell applications to tendon healing," (in eng), *Muscles Ligaments Tendons J,* vol. 2, no. 3, pp. 222-9, Jul 2012.

[2] C. Miersch, K. Stange, and M. Röntgen, "Effects of trypsinization and of a combined trypsin, collagenase, and DNase digestion on liberation and in vitro function of satellite cells isolated from juvenile porcine muscles," (in eng), *In Vitro Cell Dev Biol Anim,* vol. 54, no. 6, pp. 406-412, 2018, doi: 10.1007/s11626-018-0263-5.

[3] E. O. Adekanmbi and S. K. Srivastava, "Dielectrophoretic applications for disease diagnostics using lab-on-a-chip platforms," *Lab Chip,* vol. 16, p. 2148, 2016.

[4] J. Y. Lee *et al.*, "BMP-12 treatment of adult mesenchymal stem cells in vitro augments tendon-like tissue formation and defect repair in vivo," (in eng), *PLoS One,* vol. 6, no. 3, p. e17531, Mar 11 2011, doi: 10.1371/journal.pone.0017531.

[5] M. Elitas *et al.*, "Dielectrophoresis as a single cell characterization method for bacteria," *Biomedical Physics & Engineering Express,* vol. 3, no. 1, p. 015005, 2017/01/06 2017, doi: 10.1088/2057-1976/3/1/015005.

[6] A. Fazelkhah *et al.*, "Parallel single-cell optical transit dielectrophoresis cytometer," *ELECTROPHORESIS,* vol. 41, no. 9, pp. 720-728, 2020, doi: 10.1002/elps.201900393.